General response to Reviews

David Mair[1], Alessandro Lechmann[1], Romain Delunel[1], Serdar Yeşilyurt[1], Dmitry Tikhomirov[1,2], Christof Vockenhuber[3], Marcus Christl[3], Naki Akçar[1], and Fritz Schlunegger[1]

[1]Institute of Geological Sciences, University of Bern, Bern, 3012, Switzerland
[2]Department of Geography, University of Zurich, Zurich, 8057, Switzerland
[3]Laboratory of Ion Beam Physics, ETH Zurich, Zurich, 8093, Switzerland
[4]Department of Geography, Ankara University, Ankara, 06100, Turkey

Correspondence to: David Mair (david.mair@geo.unibe.ch)

General response

We thank the reviewers for the constructive and insightful comments. We found the reviews very helpful in improving the manuscripts clarity, for adjusting the focus and in increasing the overall quality. We did prepare a revised version of the manuscript implementing the changes outlined in the author responses to reviewer comments 1 and 2. For the detailed point-by-point response please see the author comments in the responses to the reviewer comments below. There we addressed all main points raised by the reviewers and their more specific in-line comments.

Minor changes made in addition to reviewer's requests

Former Table 2/now Table A1: Concentrations of samples EW-01-4, -5, -6 were previously incorrectly reported, which we have corrected.

Former Fig. 7 becomes the new Fig.3 to better illustrate morphology of the Eiger mountain.

Response to reviewer comment 1 (RC1):

David Mair[1], Alessandro Lechmann[1], Romain Delunel[1], Serdar Yeşilyurt[1,4], Dmitry Tikhomirov[1,2], Christof Vockenhuber[3], Marcus Christl[3], Naki Akçar[1], and Fritz Schlunegger[1]

[1]Institute of Geological Sciences, University of Bern, Bern, 3012, Switzerland
[2]Department of Geography, University of Zurich, Zurich, 8057, Switzerland
[3]Laboratory of Ion Beam Physics, ETH Zurich, Zurich, 8093, Switzerland
[4]Department of Geography, Ankara University, Ankara, 06100, Turkey

Correspondence to: David Mair (david.mair@geo.unibe.ch)

General response

We thank the anonymous Referee for the constructive, insightful and detailed comments, which we consider very helpful to increase the quality and focus of the manuscript. The reviewer raises 6 major points, which we will address in the same order:

1) *The manuscript is poorly structured. The authors use a range of unclear terms such as headwall, flank, side, footwall, foothill that make it difficult to understand the text. […]*

We restructure the paper following the reviewer's recommendation. The major changes include a better-structured and more detailed introduction of the topic. This also includes a more careful use of the terms the reviewer has outlined. We thus will change, update and improve the terminology following the reviewer's recommendations (see also line by line responses).

[…] The introduction section lacks of clear objectives or aims of the study. […]

We acknowledge that the aims of the study needed a clarification, which we will be done in the revised manuscript (please see lines 62 to 68).

[…] This section is mixed with results. […]

We change this particular paragraph of the introduction, and we make sure not include any results so that introduction, methods, results and discussion are now better separated from each other, which admittedly increases the transparency.

[…] The glacial history of the Eiger is missing in the study site section, however, glacial history is necessary to understand the maximum age of CN samples and the time scales that are integrated in the denudation rates. […]

This is improved. We expand the introduction to include the glacial history (line 74 ff.).

[…] The method section is incomplete and lacks of conducted geotechnical measurements. The reconstructed temperature time series is difficult to understand and used input parameters are insufficiently introduced.

We update the method section accordingly and introduce the input parameters more carefully . We also clarify and justify the selection of the time series of temperature data that we employ in our paper, which will additionally be featured in the new Fig. 2.

Unfortunately, no geotechnical measurements are available for the sample sites due to the poor accessibility of the sites. The Eiger north face is too steep to be accessible for non-professional alpinists; therefore, it was not possible to collect bedrock samples and to conduct geotechnical analyses on them. However, geotechnical parameters would rather quantify the short-term bedrock conditions and thus be only of limited use for our understanding of the long-term average denudation pattern.

2) This paper uses five denudation rates, one derived from a new10Be measurement (EW-1) and four already published in a previous study (Mair et al.,2019). The one measurement, the method and the results are described in very detail, however, the resulting denudation rate is very similar to already published EW-2, which is only located 41 m above EW-1. Rock temperature is adapted by altitudinal temperature lapse rates and the close altitudinal location of EW-1 and EW-2 results in the use of the same frost cracking model. The title and the objectives suggest that frost cracking is the main topic of this paper, however, more than half of the length of this paper focuses on one 10Be sample that at the end produce similar results that the previous study. I recommend to omit this sample and the cosmogenic nuclide technique from the method and result sections and just use your published data from Mair et al. (2019) for your analysis of frost cracking results. This would significantly reduce the manuscript length and the author can address comments 3 and 4 in more detail.

We note here, that the 10Be-based denudation rate estimates is based on one depth profile that includes the ^{10}Be concentrations from 5 samples and not from one alone as inferred above. The decay of the ^{10}Be concentrations with depth thus records a long-term memory of exposure and denudation, which makes this methodology very powerful (please see also Mair et al., 2019). However, we acknowledge that the part of the paper where we describe the application of the cosmogenic nuclide technique is too long for the manuscript. Contrastingly, available space is too limited to fully describe the method, as reviewer 2 points out (see also response to RC2). Therefore, we follow the reviewer's recommendation and shift the methodological description and results of the ^{10}Be analysis from the main manuscript to the new Appendix A. We see this as the best compromise because we think that the measured data should be available to the reader and the public. We seize this opportunity to clarify and expand the methods part where we fully describe the way of how we use the cosmogenic nuclide technology (as suggested by reviewer 2; see also Response to RC2).

3) The authors reconstructed a rock temperature series based on rock temperature logger data by Gruber et al. (2004) and PERMOS data from the years 2001-2014. The authors should produce a figure showing the original data and the generated time series they use as input data. They use only 7 complete years from the data to generate the time series for their sample locations. Which years are used are unknown and it remains unknown how representative the time series is. […]

We acknowledge the need for a more detailed description of the temperature dataset that we use in this paper. We design a new plot (new Fig. 2) where we illustrate the temperature data that we use to estimate the temperature quantities and the resulting input curves for the frost cracking modelling. We further clarify the source and the nature of the data (e.g., years for which data is available) more carefully along with a better justification. All information is there, and we acknowledge that we could have done a better job explaining the material that we use for our paper.

[…] The rock temperature data could be compared to a longer air temperature time series. There will be a thermal offset, however, this offset should be similar for all the years. Furthermore, the authors shift the temperature data to back to LIA and Medieval climatic optimum based on published temperature offsets. This can be suited for EW-3 and EM-samples, however, EW-2 is exposed to atmospheric conditions more than 1.73 ± 0.26 ky (Mair et al., 2019). […]

We are not aware of air temperature data for the studied sites, therefore suitable records would be close-by weather stations. However, we refrain from comparing temperature data with such records since we expect a strong influence of local microclimatic conditions, on rock temperatures (Noetzli et al., 2019). Therefore, we consider such a comparison not helpful for understanding the local temperature regime. Nevertheless, we compare temperature offsets with the climate conditions during the Roman warm period and during the migration period when paleoclimate was cooler. This is based on a different record (Büntgen et al., 2011), which we use to enclose the exposure of EW-02.

[…] Differences in temperatures between logger locations are explained by an insolation model and there is no information how this model is derived in the entire manuscript.

We describe, along with references, the maximum insolation GIS tool that we employ to estimate the maximum annual insolation in section 2.

4) The authors used the frost cracking model by Andersen et al, 2015. They use a rock porosity of 2 % and provide no basis why they use this value. […]

We use a rock porosity value of 2% for the local limestone because it is in excellent agreement with the porosity of 1.8 ± 0.5 that we measured for a previous article (Mair et al., 2019; Supplementary Notes S4) and because it is the default value of Andersen et al. (2015), therefore allowing a better comparison to other studies. We clarify this point in the revised manuscript.

[…] The model requires more than 15 more variables such as flow restrictions, conductivities, heat capacities and so on that are not introduced in the method section. Therefore, it is impossible to understand the model set up. […]

We introduce the variables of the model in the method section. However, we refrain from discussing all of them in detail, as this would be a repetition of the work of Andersen et al. (2015).

[…] There are different limestones at Eiger, which could results in differences of variables such as conductivities of rock. Different conductivities can result in different model results. The authors should test the sensitivity of their model in terms of their chosen input parameters. In addition, they use a fixed frost cracking window (FCW) of -8 to -3_C. Andersen et al. (2015) already demonstrated the consequences of different FCWs in their study and the authors should address this in the discussion. […]

We update our paper accordingly and complement our results with model runs for different conductivities and different FCWs, and we discuss how the results depend on the selection of the input parameters.

[…] FCWs are lithology and strength dependent which is currently reflected by the model by Rempel et al. (2016) and the lab study by Draebing and Krautblatter (2019). […]

We use the most commonly referenced approach due to a lack of empirical data for our setting. Andersen et al. (2015) already evaluated different windows for their model and find similar patterns of FCI intensity in response to different MAT windows. They found that despite differences in the absolute FCI values the relative pattern remains the same. Thus, we expect a similar behaviour for our setting (see also comment above). Nevertheless, we test the effects of different FCW in additional model runs and evaluate potential effects for our setting. We have will thus update our paper accordingly.

[…] In addition, the model assumes water availability in rock when temperatures are above 0°C. […]

We address this point by clearly stating the model assumption in the method section and by discussing potential effects in the discussion section. However, we note that the main reason for the assumption is that water availability is governed by the thermal conditions, where the thermal gradient has to be positive. Temperatures do not necessarily need to exceed 0°C; a reservoir for liquid water, however, is required (see also related in-line responses).

[…] The length of rock the water needs to travel to the freezing front is penalized following Anderson et al. (2013). The authors should discuss the penalization thus water flow can be increased by fractures and therefore increase the FCI. […]

We provide now an expanded discussion on these mechanisms within the method section and discuss its potential effects in the discussion section.

[…] The assumption of water availability decreases frost cracking in permafrost, which is the major argument of the authors for the difference in the denudation rates between North and South and upper and lower locations. However, this assumption is contrary to the findings of Murton et al. (2006) that find higher frost cracking in permafrost due to water release of the active layer during thawing and refreezing of water at the permafrost table. Physical frost cracking models by Walder and Hallet (1985) and Rempel et al. (2016) would show contrary results thus these models integrate mechanical parameters such as ice pressure and rock strength. The authors should be more careful in their discussion and discuss the influence of model assumptions on their results. […]

We recognize that there is a misconception of one of our main arguments here. We infer that permafrost might reduce water availability from below for the scenario where (i) the surface is frozen, (ii) no significant thawing occurs at the permafrost table and (iii) no regolith reservoir for water is present (Andersen et al. 2015). In these scenarios water would need to reach the freezing front from below, which would limit the permafrost conditions (Andersen et al. 2015), while in general permafrost occurrence would promote the occurrence of cracking, as the reviewer points out. We acknowledge that this argument needs a clarification, which we present through expanding the method section to better document, and justify the model's assumptions and through amending the discussion section to reflect these issues (see also corresponding in-line responses).

5-6) The denudation rates reflect different time scales ranging from 0.29 ± 0.05 to 1.73 ± 0.26 ky (Mair et al., 2019). These are quite large differences where climatic conditions and therefore frost cracking will change. The scaling issue is not addressed at all by the authors. […]

We seize the opportunity to address this point more clearly in the method and discussion sections. We do find comparatively little change in climatic conditions throughout the last millennium in near sedimentary records. We add additional temperature data set for the Roman climatic optimum conditions from Büntgen et al. (2011). These data indicate that the temperature changes over time are smaller than between the studied sites.

[…] Other studies observed a paraglacial adjustment of rockwalls and increased denudation rates directly after deglaciation or with a response time up to millennia after deglaciation (Grämiger et al., 2017).

Different glacial history between North and South rockwall could result in differential paraglacial adjustment between North and South rockwall and different denudation rates. […]

Following the works cited in the manuscript, it is reasonable to assume that in the NW the last glaciation occurred during the alpine LGM, while in the SE the rock faces were covered by ice during the Younger Dryas. Our denudation rates, however, are valid for times < 2 ka and thus for a shorter period. Therefore, the time in-between is most likely too long (> 9 kyr) for a paraglacial adjustment to be considered. The numerical models and field evidence predict that the main damages of rock faces occurred during deglaciation (Grämiger et al., 2017). Furthermore, the response time of stress release through sheeting depends to the rock quality (McColl 2012). In highly fractured rock, as is case for the limestone at Mt Eiger, stress release should occur shortly after or during the deglaciation (McColl 2012). Finally, the likeliness of sheeting joints to form also depends on the pre-existing fracture density, where a high fracture density (as is the case at Mt. Eiger) accommodates stresses during glaciation and deglaciation quite fast, which therefore hinders sheeting joints to form (McColl 2012). However, a reconfiguration of paraglacial stress might have been an important factor during the deglaciation and sometime thereafter. Thus, we follow the reviewer's recommendations and add the corresponding argument to the discussion section.

[…] The authors also use the APIM model to analyze the effect of permafrost. The APIM models permafrost on a regional scale of the European Alps and logger data used by the authors in this study demonstrate that the APIM model fails to model permafrost distribution on the South rockwall. Model results from APIM cannot be used on smaller scale and the use is contradictive to the logger data due to scale issues. In addition the APIM suggest a current permafrost distribution (for a period around 2012) due to the used data input (logger data and rock glacier inventories) and provide no insights into past permafrost distribution. […]

We concede that the APIM model resolution is not high enough to reliably predict the occurrence of permafrost. We therefore eliminate the corresponding sentences from the manuscript. Instead, we discuss possible permafrost occurrence on the basis of the temperature data that we use in our paper

[…] In summary, the authors focus too much on frost weathering, discuss a bit thermal stresses and permafrost, however, completely ignore alternative explanation of the observed denudation rates. McColl and Draebing (2019) recently reviewed rock slope adjustment and describe how paraglacial processes, permafrost and weathering processes jointly influence rock slope stability. Therefore, I recommend to discuss the denudation rates more openly and not only focused on frost weathering. […]

We follow the reviewer's recommendation and restructure the discussion accordingly. We now discuss the potential influence of alternative paraglacial processes on the local denudation rates.

Line by line responses

2: *What are headwalls? Steep rockwalls or rockslopes? You use rockwall, headwall, face, flank and side. I recommend to stick to a clear geomorphic term such as rockwall or rockslope.*

We now use 'rockwall' instead of 'headwall' and 'flank', and we use 'face' instead of 'side' for clarity.

9: *Maybe use headwalls to clarify it.*

Done.

10: *Rockfalls are preconditioned by fractures which can be also from tectonic origin. Thermo-cryogenic processes prepare and can also trigger rockfalls (cf. McColl, 2012 and McColl and Draebing, 2017).*

We rephrase the text; the point is now clarified in the introduction.

11: *What controls and conditions do you mean? Controls by fractures and influence by thermo-cryogenic processes. Please clarify.*

Clarified.

12: *What you mean with debated? What are the positions of this debate?*

Poorly phrased, now improved to better explain the original idea.

12: *What do you mean with new? You present results from your measurements and compare them to published denudation rates?*

"new and published" removed to better comply with the new structure of the manuscript.

13: *reconstructed temperature conditions*

Suggestion is followed.

15: Suggestion is followed.

16: *I never heard the term footwall before. Better use "foot of the rockslope or rockwall".*

Corrected

19: *Better use the term rockslope, rockwall or rock face. Otherwise, what is the difference between a flank and a face?*

Recommendation followed to avoid unclear terminology.

19: *"and resulting"*

Implemented.

34: *Hallet et al. tested Berea Sandstone and Murton et al. Tuffeau Limestone which are both abundant in the Arctic or South UK and possess porosities between 20 and 40% which are not existing* *rockwalls. Better cite Draebing & Krautblatter (2019) who tested recently frost cracking on samples from Alpine rockwalls or Murton et al. (2016) which used Wetterstein Limestone.*

We follow the suggestion and cite both publications now.

38: *Have a look at Draebing & Krautblatter (2019). They compared the efficacy of volumetric expansion and ice segregation.*

This work is now referenced and its findings are presented in the introduction.

39: *These studies by Matsuoka refer more to volumetric expansion.*

True, not cited at this point any more.

40: *The efficacy of which processes? Thermal processes are higher near the surface when diurnal temperature variations are occuring (cf. Collins & Stock, 2016 or Draebing et al., 2017) and propagate to greater rock depth when they occur seasonally (cf. Gischig et al. 2011 a, b).*

I would suggest to refer to frost cracking processes only and they are governed by diurnal processes for volumetric expansion (Cf. Matsuoka, 2008) and seasonal for ice segregation (Anderson, 1998) and temperature gradients.

We follow the reviewer's suggestion and adapt the statements to be more precise.

45: *Draebing and Krautblatter (2019) simulated the influence of water in their ice segregation tests and show how water is driven to a frozen crack.*

Suggested work is now referenced at this point.

47: *also Draebing and Krautblatter (2019)*

Now referenced.

52: *also Draebing and Krautblatter (2019)*

Now referenced.

64: *microclimatic conditions.*

Changed.

64: *Try to keep terms for rockwall small. You use rockwall, face, flank and side. I recommend to stick to a clear geomorphic term such as rockwall or rockslope.*

We follow the recommendation (see also response to major points).

65: *This section presents results. In the end of the introduction you should present the aims of your study. Please clarify what you are doing without presenting results.*

You could write: Our study aims 1) to quantify rockwall denudation in different rockwall locations experiencing differnt climatic conditions using CN, 2) model frost cracking and 3) compare denudation rates with potential preparing and triggering factors.

Or something similar. Than it is clear what you will present in this manuscript.

We rewrite the paragraph accordingly.

65: *What is a foothill? You mean foot of the rockslope or rockwall? I am not sure that you took samples at the foot of the rockwall. These location I would expect in Interlaken not at 2500 m altitude. I recommend to rename the location and define the term before you use it to clarify it for the reader.*

We follow the recommendation (see corresponding comments above).

67: *Contains results*.

Rewritten (see comment above).

75: *Can you present the glacial history of the Eiger. This is necessary to understand if there is a glacial history at your sampling location. Have they been covered by ice? Since when the locations are ice-free? In addition, a glacial history is necessary to understand potential paraglacial processes (cf. McColl 2012 or McColl and Draebing, 2019).*

We follow the suggestion and briefly discuss the glacial history at this point.

76: *strikethrough*

Changed.

76: *Oversteepened by what? Glacier erosion?*

Changed to steep.

78: *Can you be more quantitative and calculate a slope angle range based on your DEM.*

We expand on this issue and now provide slope distributions in Fig. 1b. The results are now incorporated in the text.

79: *Please be more quantitative and provide a slope angle or slope angle range.*

We follow the recommendation (see also previous comment).

80: *what are "active glaciers". Depending on definition glaciers need to have moving ice to be glaciers. Do you mean by small "cirque glaciers"? Be more precise.*

Clarified.

82: *five but four are identical with this study.*

Five were sampled, but only four could be interpreted. This is now clarified.

93: *Nice way to say it. In other words you add one 10Be profile to your already published results. You can shorten this section significantly.*

We shorten this section by moving some information to the new Appendix and by streamlining the remaining text.

101: *How do you know this? If there are small rock ledges a significant snow cover can accumulate (cf. Haberkorn et al. 2015 or Draebing et al. 2017a).*

There is a misconception – 'snow cover significant for TCN analysis' was the intended statement. As we shorten the text, we remove the misleading statement.

106: *Fig. 2 shows that EW-2 and EW-3 are located in rockwalls where the model shows. permafrost in nearly all conditions. However, there is no difference to EM1 and EM2. There is maybe a very slight decrease in permafrost probability but this difference is too low to come to the conclusion that the rockwall is "less likely" affected by permafrost. The aim of the APIM is to model permafrost on a regional scale (European Alps). It provides the probability of permafrost and should not be over-interpreted on mountain scale. The resolution is pretty coarse. If high-resolution models are available such as Noetzli et al., (2007), you can draw conclusion on differences in permafrost distribution but you cannot do this based on a coarse regional permafrost model which only provides very slight differences between your measurement locations.*

You should focus on the PERMOS data and interpret the MAT in your results. Positive MAT at EM-sampling sites indicate non-permafrost conditions, however, the regional model by Boeckli et al. (2012) shows permafrost occurrence in arrange somewhere between nearly and mostly cold conditions. The APIM contradicts the temperature data and I would suggest to omit the model and focus on the PEMOS data thus the model is not accurate enough for your scale.

We concede that the results of the APIM model should not be interpreted in this context. Thus, we follow the recommendation and focus now on the PERMOS data. We seize this opportunity to display the reconstructed MAT data in new Fig. 2 (see also response to major point 3).

109: *Thes are results of this study. You should move the data to the result section, describe the mapping approach in the method section and compare it with the general geological data (all references incl. Mair et al. 2018) in the discussuion section.*

We follow the recommendation.

113: *therein*

Changed.

130: *Be more precise and include a subsection on your mapping approach. Describe also how you analyse your data, which software you use to produce the stereonets.*

We follow the recommendation and provide the requested information in the new section 3.1.

191: *You mean you need a time series of rock temperature data to run your model. You use data from Permos (2019) which is based on loggers installed oirginally by Gruber et al. (2004b). Please rephrase and simplify your text.*

Simplified.

203: *Which years you used? Be more precise. Can you please add the data to this paper in form of a figure. Please highlight the logger locations in Figure 1.*

We display the used temperature data now in new Fig. 2. and provide the complete data series in the supplement.

206: *Why this lapse rate? Is the PERMOS data supporting this lapse rate?*

We provide references for this lapse rate in the revised manuscript. The PERMOS data allow no estimation of a lapse rate due to the differences in the microclimatic conditions between NW and SE rockwall.

207: *Can You provide a figure of your modelled rock surface temperature that you used as input for your frost cracking. Please clarify which years are the basis of these modelled rock surface temperature data. Do you omit extreme warm years such as 2003?*

We provide the data series in the supplement and display the years we have considered and the modelled temperature curve that we have used in new Fig. 2.

214: *You assume that there is no response time between climatic warming of air temperature and rock surface temperature. This is a fair assumption but you should highlight it.*

Highlighted.

217: *This model is not a mechanistic model. It incorporates no information on rock properties such as the model of Walder and Hallet (1985). Better use numerical model.*

Changed.

219: *Please simplify the sentence.*

Simplified.

224: *This is highly questionable and a pure assumption. The model by Walder and Hallet (1985) shows that the frost cracking window depends on lithology. A recent study by Draebing and Krautblatter (2019) show that there can be significant differences. You should highlight that this is an assumption based on current knowledge and other studies exist which show alternative frost cracking windows.*

We thank for the comment and follow the recommendation.

229: *This penalty function is suggested by Anderson et al. (2013) and there is no data supporting it. Please highlight that this is an assumption due to lack of available studies that could provide data.*

We follow the recommendation.

232: *Why 2 %? Do you have rock property data that confirm this range. By using your model you assume that heat transport only occurs by conduction, that no fractures are in your rockwalls which produce anisotropy and are preferred path of water and advective heat transport. Please add these assumptions.*

We now reference porosity calculations from density measurements to support the inferred value of 2%, and we discuss the mentioned assumptions now in the text.

257: *strikethrough*

Changed.

336: *Why is this so? Can there be a paraglacial signal such as sheeting joints (cf. McColl 2012) or can you exclude these?*

Indeed, we now discuss this possibility. We consider sheeting joints in response to deglaciation as unlikely to explain the differences in the denudation pattern because: 1) Suitable rockwall parallel joints are only present in the NW (C2; former Fig. 5), where they show a spacing of m to tens of meters. 2) The last possible glaciation was the LGM deglaciation period in the NW and the Younger Dryas in the SW, which would imply a response time for sheeting joints to form of 9 ka or more. 3) Furthermore, the response time of stress release through sheeting is related to the rock quality (McColl 2012). In highly fractured rock, as is the case for the limestone at Mt. Eiger, stress release should occur shortly after or during the deglaciation (McColl 2012). The general likeliness of sheeting joints to form also depends on the pre-existing fracture density, where a high fracture density (as is the case at Mt. Eiger) better accommodates stresses during glaciation and deglaciation, which in turn hinders sheeting joints to form (McColl 2012). However, reconfiguration of paraglacial stress might have been an important factor during the deglaciation and sometime thereafter.

365: *Same scaling problem mentioned above. You should stick to the PERMOS and Gruber data and omit a regional model that is too coarse to show actual permafrost. In addition, the model by Boeckli et al. (2012) is based on current temperature conditions and give no indications if there was permafrost in the past at the Eiger.*

We follow the recommendation and change the sentence accordingly (see response to related comment above).

369: *That's true, however, Murton et al. (2006) demonstrated an increase frost cracking due to permafrost conditions when the active-layer thaws and refreezes at the permafrost table. You cannot exclude this. […]*

We think that this point is due to a misunderstanding (smiliar to the major point 4). We do not want to contradict the findings of Murton et al. (2006); active layer thawing should increase water availability and the FCI. Permafrost might hinder water availability only during times when no thawing occurs. We clarify the argument to avoid confusion.

[…] The frost cracking model you used a priori assumes that water is only available when rock temperature is positive. There is supercooled water that can exist below th freezing point and these assumptions are maybe wrong.

We address this point by clearly listing all model assumptions in the method part. We change the corresponding sentence accordingly (see also major point 4 above).

376: *How you calculate this? It is not described in the method section nor are the results presented in the result section.*

We use the hemispherical viewshed algorithm to calculate maximum annual solar radiation in ESRIS's ArcGis, which was developed by Fu and Rich (2002). We describe this now in the method section, and present the results briefly in the corresponding section.

377: *You should have a look at Draebing and Krautblatter (2019) who quantified the efficacy of frost cracking processes.*

We include the recent findings of Draebing and Krautblatter (2019) in the section.

380: *See also Rode et al. you cited.*

Now also referenced here.

384: *See Draebing and Krautblatter (2019) that quantified stresses.*

We include the recent findings of Draebing and Krautblatter (2019) in the section.

386: *SeeDraebing and Krautblatter (2019) and Walder and Hallet (1985)*

Text amended and works referenced.

388: *Why? This depends on fracture toughness, crack geometry and other lithological properties such as Walder and Hallet (1985) and more recently Rempel et al. (2016) showed.*

Changed, as this admittedly was too simplistic. We expand the literature discussion and now discuss the effect of different windows in our used model.

396: *You don't have regolith cover. Omit this sentence.*

Omitted.

402: *The reason for lower efficacy are the assumptions of water availability only during positive rock temperatures. Water can also be available at negative MATs. Different models such as Walder and Hallet (1985) or Rempel et al. (2016) will result in different results. You should be more careful with your interpretation.*

We concede this argument needs a better clarification (see also responses to major point 4 and comment in line 369). We do not exclude the possibility of water being present at negative MATs as the model also predicts that the FCI on the NW sites increases for colder MATs (see modified former Fig. 6). The model assumes that a liquid water reservoir is essential for an effective ice segregation, which is supported by experimental findings (Walder and Hallet 1985, Matsuoka 2001; and references therein). The model of Rempel et al. (2016) indeed predicts different results, but employs a set of assumptions as well (e.g. cracking is directly correlated to porosity and to constant water availability at the lower boundary). We now discuss that different models would predict different cracking behavior. However, we note that the alternative models would not be able to explain the difference in denudation pattern.

414: *On what basis you draw this conclusion?*

The conclusion is based on the lack of suitable deposits in any geological maps. We clarify this now and refer to some maps.

415: *Why is that so? You referring to a bergsturz event (>1 M m^3).*

We clarify the sentence accordingly.

416: *You can also have paraglacial stress release joints (sheeting joints) that responding to former glaciation and can have large response times (cf. Grämiger et al., 2017).*

Paraglacial stress has indeed the potential to release joints. We address this point now more prominent in the introduction and discussion (see response to major points 5 and 8). We modify the statement accordingly.

417: *What do you mean? If you shift the MAT to adapt to past climates then the mean will always be smaller than the max? Do you mean mean MAT based on current conditions? Please rephrase.*

Rephrased and clarified.

418: *That is based on the model assumptions Lower temperatures will reduce water availability. However, this is contrary to the findings of Murton et al. (2006) which observed increased frost cracking during active-layer thaw.*

We address this argument now clearly in the introduction, method and discussion section (see response to major point 4 and related in-line comments. We rephrase the sentence accordingly.

419: *You modelled these scenarios? It is missing in the method section.*

We do not model the scenarios; we use the result of the modelling study, which we reference (cf. CH2018).

425: *To which graph you are referring to?*

Changed reference to table 1, which is more appropriate.

References

Andersen, J. L., Egholm, D. L., Knudsen, M. F., Jansen, J. D. and Nielsen, S. B.: The periglacial engine of mountain erosion – Part 1: Rates of frost cracking and frost creep, Earth Surf. Dyn., 3, 447–462, doi:10.5194/esurf-3-447-2015, 2015.

Anderson, R. S.: Near-Surface Thermal Profiles in Alpine Bedrock: Implications for the Frost Weathering of Rock, Arct. Alp. Res., 30, 362, doi:10.2307/1552008, 1998.

Anderson, R. S., Anderson, S. P. and Tucker, G. E.: Rock damage and regolith transport by frost: An example of climate modulation of the geomorphology of the critical zone, Earth Surf. Process. Landforms, 38, 299–316, doi:10.1002/esp.3330, 2013.

Boeckli, L., Brenning, A., Gruber, S. and Noetzli, J.: Permafrost distribution in the European Alps: Calculation and evaluation of an index map and summary statistics, Cryosphere, 6, 807–820, doi:10.5194/tc-6-807-2012, 2012.

Büntgen, U., Tegel, W., Nicolussi, K., McCormick, M., Frank, D., Trouet, V., Kaplan, J. O., Herzig, F., Heussner, K.-U., Wanner, H., Luterbacher, J. and Esper, J.: 2500 Years of European Climate Variability and Human Susceptibility, Science (80-.)., 331, 578–582, doi:10.1126/science.1197175, 2011.

CH2018 (2018), CH2018 – Climate Scenarios for Switzerland, Technical Report, National Centre for Climate Services, Zurich, 271 pp. ISBN: 978-3-9525031-4-0.

Collins, B. D. and Stock, G. M.: Rockfall triggering by cyclic thermal stressing of exfoliation fractures, Nat. Geosci., 9, 395–400, doi:10.1038/ngeo2686, 2016.

Draebing, D. and Krautblatter, M.: The Efficacy of Frost Weathering Processes in Alpine Rockwalls, Geophys. Res. Lett., 46, 6516–6524, doi:10.1029/2019GL081981, 2019.

Draebing, D., Haberkorn, A., Krautblatter, M., Kenner, R. and Phillips, M.: Thermal and Mechanical Responses Resulting From Spatial and Temporal Snow Cover Variability in Permafrost Rock Slopes, Steintaelli, Swiss Alps, Permafr. Periglac. Process., 28, 140–157, doi:10.1002/ppp.1921, 2017a.

Draebing, D., Krautblatter, M. and Hoffmann, T.: Thermo-cryogenic controls of fracture kinematics in permafrost rockwalls, Geophys. Res. Lett., 44, 3535–3544, doi:10.1002/2016GL072050, 2017b.

Fu, P. and Rich, P. M.: A geometric solar radiation model with applications in agriculture and forestry, Comput. Electron. Agric., 37, 25–35, doi:10.1016/S0168-1699(02)00115-1, 2002.

Gischig, V. S., Moore, J. R., Evans, K. F., Amann, F. and Loew, S.: Thermomechanical forcing of deep rock slope deformation: 1. Conceptual study of a simplified slope, J. Geophys. Res. Earth Surf., 116, 1–18, doi:10.1029/2011JF002006, 2011a.

Gischig, V. S., Moore, J. R., Evans, K. F., Amann, F. and Loew, S.: Thermomechanical forcing of deep rock slope deformation: 1. Conceptual study of a simplified slope, J. Geophys. Res. Earth Surf., 116, 1–18, doi:10.1029/2011JF002006, 2011b.

Grämiger, L. M., Moore, J. R., Gischig, V. S., Ivy-Ochs, S. and Loew, S.: Beyond debuttressing: Mechanics of paraglacial rock slope damage during repeat glacial cycles, J. Geophys. Res. Earth Surf., 122, 1004–1036, doi:10.1002/2016JF003967, 2017.

Gruber, S., Hoelzle, M. and Haeberli, W.: Rock-wall temperatures in the Alps: Modelling their topographic distribution and regional differences, Permafr. Periglac. Process., 15, 299–307, doi:10.1002/ppp.501, 2004.

Haberkorn, A., Phillips, M., Kenner, R., Rhyner, H., Bavay, M., Galos, S. P. and Hoelzle, M.: Thermal Regime of Rock and its Relation to Snow Cover in Steep Alpine Rock Walls: Gemsstock, Central Swiss Alps, Geogr. Ann. Ser. A Phys. Geogr., 97, 579–597, doi:10.1111/geoa.12101, 2015.

Mair, D., Lechmann, A., Herwegh, M., Nibourel, L. and Schlunegger, F.: Linking Alpine deformation in the Aar Massif basement and its cover units - The case of the Jungfrau-Eiger mountains (Central Alps, Switzerland), Solid Earth, 9, 1099–1122, doi:10.5194/se-9-1099-2018, 2018.

Mair, D., Lechmann, A., Yesilyurt, S., Tikhomirov, D., Delunel, R., Vockenhuber, C., Akçar, N. and Schlunegger, F.: Fast long-term denudation rate of steep alpine headwalls inferred from cosmogenic 36Cl depth profiles, Sci. Rep., 9, 11023, doi:10.1038/s41598-019-46969-0, 2019.

Matsuoka, N.: Microgelivation versus macrogelivation: towards bridging the gap between laboratory and field frost weathering, Permafr. Periglac. Process., 12, 299–313, doi:10.1002/ppp.393, 2001.

Matsuoka, N.: Frost weathering and rockwall erosion in the southeastern Swiss Alps: Long-term (1994-2006) observations, Geomorphology, 99, 353–368, doi:10.1016/j.geomorph.2007.11.013, 2008.

McColl, S. T.: Paraglacial rock-slope stability, Geomorphology, 153–154, 1–16, doi:10.1016/j.geomorph.2012.02.015, 2012.

McColl, S. T. and Draebing, D.: Rock Slope Instability in the Proglacial Zone: State of the Art, , 119–141, doi:10.1007/978-3-319-94184-4_8, 2019.

Murton, J. B., Peterson, R. and Ozouf, J. C.: Bedrock fracture by ice segregation in cold regions, Science (80-.)., 314, 1127–1129, doi:10.1126/science.1132127, 2006.

Murton, J. B., Ozouf, J. C. and Peterson, R.: Heave, settlement and fracture of chalk during physical modelling experiments with temperature cycling above and below 0 °C, Geomorphology, 270, 71–87, doi:10.1016/j.geomorph.2016.07.016, 2016.

Noetzli, J., Gruber, S., Kohl, T., Salzmann, N. and Haeberli, W.: Three-dimensional distribution and evolution of permafrost temperatures in idealized high-mountain topography, J. Geophys. Res., 112, F02S13, doi:10.1029/2006JF000545, 2007.

Noetzli, J., Pellet, C., and Staub, B. (eds.), Glaciological Report (Permafrost) No. 16-19 of the Cryospheric Commission of the Swiss Academy of Sciences, 104 pp, doi:10.13093/permos-rep-2019-16-19, 2019.

PERMOS 2019. PERMOS Database. Swiss Permafrost Monitoring Network, Fribourg and Davos, Switzerland. DOI:10.13093/permos-2019-01.

Rempel, A. W., Marshall, J. A. and Roering, J. J.: Modeling relative frost weathering rates at geomorphic scales, Earth Planet. Sci. Lett., 453, 87–95, doi:10.1016/j.epsl.2016.08.019, 2016.

Walder, J. S. and Hallet, B.: Geological Society of America Bulletin A theoretical model of the fracture of rock during freezin, GSA Bull., 96, 336–346, doi:10.1130/0016-7606(1985)96<336, 1985.

Response to reviewer comment 2 (RC2):

David Mair[1], Alessandro Lechmann[1], Romain Delunel[1], Serdar Yeşilyurt[1,4], Dmitry Tikhomirov[1,2], Christof Vockenhuber[3], Marcus Christl[3], Naki Akçar[1], and Fritz Schlunegger[1]

[1]Institute of Geological Sciences, University of Bern, Bern, 3012, Switzerland
[2]Department of Geography, University of Zurich, Zurich, 8057, Switzerland
[3]Laboratory of Ion Beam Physics, ETH Zurich, Zurich, 8093, Switzerland
[4]Department of Geography, Ankara University, Ankara, 06100, Turkey

Correspondence to: David Mair (david.mair@geo.unibe.ch)

General response

We thank the anonymous Referee for the constructive comments regarding the cosmogenic nuclide application, which help us to improve the quality and clarity of our work significantly. We address the main concerns in the light of the comments by referee #1, who suggested to restructure the manuscript and to focus on the pre-conditions leading to rock fall processes. This is a recommendation, which we follow (see also response to reviewer comment 1; RC1). As a consequence, we move the cosmogenic nuclide part to the new Appendix A. This allows us to address the 2 main concerns of reviewer #2:

1) The methodological concerns (see detailed responses below): "*One concern is that there is little new data offered here and what is presented is close to the limits of what might be considered acceptable in terms of noise-to-signal. […]*" We concede that the measured ^{10}Be concentrations are low and close to the detection limit. Thus, we agree that it is essential to assess the blank correction (see detailed responses below). Accordingly, we present our arguments for using the long-term variance weighted average blank correction, for which we provide statistics on its variability (Table 1). However, we also provide the results of the in-batch blank measurements, which is approximately 2x higher than the weighted long-term average value. We concede that using the higher value for blank correction, several samples would not show acceptable signal-to-noise ratios in 3 samples, with the consequence that that these ^{10}Be concentrations would not be interpretable. We discuss these points in Appendix A, mark the denudation rate value for EW-01 in the main manuscript as potentially non-interpretable (due to ^{10}Be concentrations at the detection limit), and point to the discussion in Appendix A. However, we think that the ^{10}Be data is worth being reported in the Appendix; especially in the

context for understanding the challenges that are associated with the modelling of the *in situ* denudation rates in such settings (see also detailed response below).

2) The reliance on a previous publication, as referee #2 points out: *"[…] While the paper reads well, necessary information is often lacking to properly assess what is being done and there is too much reliance on a previous publication (Mair et al., 2019), which the reader is essentially forced to read if they want to understand this paper. […]"*.

The new Appendix A provides a concise summary on the denudation rate modelling. Furthermore, we understand that there is a need to clarify why the consideration of inherited ^{10}Be concentrations is important upon modelling. We also realize that it is relevant to discuss the consideration of a model scenario where denudation rates are uniform (see responses below). Both aspects are provided and discussed in Appendix A.

From here on, we will address each point individually and in the same order, as the reviewer raised them.

One concern is that there is little new data offered here and what is presented is close to the limits of what might be considered acceptable in terms of noise-to-signal. This leads me to be unconvinced that what data is presented support the findings. I do not agree with the authors that the relative analytical uncertainties of 11-69% at 1 simga are small (as is claimed in Line 296), instead they are hampering a sound interpretation of a small set of data.

We concede that relative uncertainties of up to 69% at 1 sigma are not small. We now discuss the ^{10}Be data in more depth in the new Appendix A (see also response to related comments below). We clearly point out the limitation of the small data set and the effect of the large uncertainty. We also rewrite the corresponding section 5.1 to comply with the reviewer's comments and the new structure of the entire paper.

Modelling of the limited dataset is valid to try and extend the approach and investigate erosion in a more general sense, but the profile modelling is either missing crucial information, or is inappropriately used. The authors apply a published model (Hidy et al. 2010) that to my knowledge has been mostly used in order to extricate age/erosion information in situations where variable pre-exposure could be a concern. This has been suitable for sedimentary deposits, where samples have a pre-depositional exposure history (inheritance). In the case of bedrock, as sampled here, any inheritance must have other origins. […]

We acknowledge the need for clarification here. As the reviewer correctly points out, inheritance in bedrock samples could not stem from a pre-exposure history. We thus refrain from using the term ‘inheritance’ to avoid any confusion with the concept established in the cosmogenic community and based on work on sediments. For bedrock profiles, we explain the occurrence of inherited nuclides with a history where bedrock was previously exposed, and our samples were shallow enough to start accumulating cosmogenic nuclides. A scenario, which could have achieved this, would be a mass wasting event that was too small to completely reset the TCN clock. Alternatively, inherited nuclides at depth can build up through a prolonged exposure period during which the surface has experienced a low denudation rate, followed by a period of higher denudation (which translates to the current exposure). Such scenarios would allow for the accumulation of “excess nuclides” at depth. We expand the corresponding section in Appendix A accordingly to explain these mechanisms and to clarify this point (see also the following 2 responses below).

[…] I’m confused as to why the authors consider production by muons to be an inherited component in a study of erosion (e.g. L176). Muon production at depth as the rock erodes is not ‘previous exposure’, as the authors state, but part of the ongoing exposure that is being used to constrain the erosion rate. […]

There is a misconception here, due to previously ambiguous phrasing in the manuscript. We calculate muogenic production at depth in the generally accepted way (e.g., Balco et al., 2008; Hidy et al., 2010; Marrero et al., 2016). We use the inference that inherited nuclides would only be produced by muogenic production to define a boundary condition for the model (see responses below). In case where inherited nuclides are present, an initial landslide would remove some meters of bedrock, with the consequence that all nuclides from spallogenic production would have mostly been removed. If the rockfall was much larger and removed several tens of meters of bedrock, then nuclides from muogenic production could also have been removed. For the alternative scenario of a prolonged exposure (see previous response above), the jump to higher denudation rates would result in a situation where near-surface bedrock with nuclides from spallation would be removed after the shift towards high denudation rates. Thus, we can use the site-specific muon attenuation length as parameter to model the contribution of inherited ^{10}Be in samples collected at greater depth, and we can compare these concentrations with those from surface samples. We elaborate a corresponding statement in Appendix A together with the underlying assumption and a justification thereof.

[…] Assuming inheritance values equivocal to the concentration of the surface sample and relating this to muons (L168 and L180) would seem to suppose a large enough landslide occurred to entirely remove the spallogenic component. This, however, would go against what is claimed on L305, that the 'inheritance' is too large to support the notion of a deep landslide, and instead they mention multiple dm thick rockfall events (see also below on this point). […]

The statement in question describes the boundary conditions for the model setup. We consider an uppermost limit in our model where in the surface sample the inherited nuclides make up 100% of the total TCN concentration. This would correspond to a large and recent rockfall event, and the contribution of inheritance with depth should then follow the muon attenuation curve. This is the case because until the rockfall event, the rocks would have resided at depths where only muogenic production occurs (see also previous response). We rephrased the mentioned passages for clarification purposes.

[…] On L300 it is mentioned that the inherited component likely comes from greater exposure at depth, before the current exposure period. Unless the authors are arguing for some kind of intervening burial, which I'm pretty sure is not the case, these would not be different periods of exposure, but one period perhaps separated by a hiatus (i.e. non-steady-state erosion). […]

The reviewer raises a point here which we have not carefully addressed yet, but which we will do in the revised manuscript. The inherited nuclides could potentially stem from a rock fall event prior to the current exposure history, or from a change in the denudation rate (see previous responses). The latter would correspond to the scenario in discussion here. However, it would represent a shift from a mechanism where continuous erosion occurs first at low rates and then at higher rates. We clarify the statement in question in the revised manuscript

[…] If non-steady-state erosion is the case it would go against a model that tries to fit a smooth production profile with depth; though erosion via stochastic mass wasting would arguably better explain why there is difficulty fitting a smooth profile through the data than some notion of inheritance.

The reviewer touches a point, which we will certainly consider. One assumption of the model is that erosion occurs in a uniform and steady way (Lal, 1991; Hidy et al., 2010). We have to assume that small-scale stochastic erosion events over a very short timescale (< 1 yr) could correspond to a continuous erosional mechanism if longer time scales are considered (> 10 yr). The validity of this assumption can to some extend be tested by comparing the modelling results with the ^{10}Be concentrations in the depth profile, where reasonably low reduced chi square values can be interpreted as indication of a smooth profile. However, we adapt the text in Appendix A to explicitly state and discuss these assumptions.

[…] Perhaps I'm missing something fundamental here but if so the authors need to do a better job of explaining why they are including inheritance in the first place, and then why they are relating it to muogenic production.

We seize the opportunity to expand on the cosmogenic nuclide method part in the Appendix to clarify the unclear points raised by the reviewer (see responses above).

The authors claim dm sized rockfall erosion. I suspect with dm size erosion events one could sample a metre or so away and get different results (i.e. these blocks fall from a specific site stochastically). Whether this is an issue depends on what is meant by dm; 10cm, 90cm? I don't see the support for this claim of erosion thickness other than the jointing would suggest it. […]

We infer that the occurrence of rock falls at the scale between 1 cm and 10 cm, averaging on a temporal scale of > 10 yrs, could be considered as a steady state denudation scenario, which we employ for TCN applications (see related response above).

[…] That is, the bedrock structure data would be better used as a parameter constraining possible mass loss depth in an erosion rate modelling exercise, rather than being an assumed outcome of the cosmo profile analysis that it would likely be causing trouble for anyway (see above RE fitting a smooth profile to stochastic erosion events). Approximate fits to the data can be gotten by assuming the simplest case of a large rockslide 2.2 kyr ago setting surface concentrations to zero. Admittedly the fit is not as good as shown by the authors as I use a much simplified approach but my point is the claims based on the cosmo data are weak (non-unique outcomes are clearly possible), not fully explained and are specific to certain sites.

We thank the reviewer for the suggestion, but we refrain from such an approach, as it would require several assumptions, as pointed out by the reviewer. In particular, this infers that the rockfall event would have to be large enough to remove all previous nuclide concentrations, which is contradicted by the "truncated" shape of the TCN depth profiles (Mair et al., 2019). The underlying assumptions for the interpretation presented in this work (and also in Mair et al., 2019) are justified as outlined above. Furthermore, the model would allow us to actually test such a hypothesis. It should return a result with an inheritance close to zero, a low denudation rate and a minimum age close to 2.2 kyr.

The results are sensitive to the blank correction due to the low 10Be concentrations. Blank corrections as high as 19% could be acceptable if the authors can show the subtraction is robust. This probably *requires several in-batch blanks, rather than a longterm lab background average, which needs to be justified here. The vague nature of the blank subtraction as it's reported lessens the confidence in such low concentration data, i.e. what is the uncertainty in this long-term blank value (not given on L140 or in table 3); was a blank/s measured in the batch, or at the same time in the lab, and if so what of the results? If the authors are forced to use a long-term average as no in-batch measurements were made I would expect to see some discussion of how variable this value has been over time (long-term averages would mask occasionally high/low values which is a problem when it comes to measurements close to the lab background). Is there any idea of what inter-batch background variability is?*

We thank for bringing this point up. We actually use the long-term, variance-weighted average blank value of 2.44×10^{-15}, which is calculated from several in-batch blanks for each bottle of Be spike (Table 1). However, the long-term, variance-weighted average ratio should be 2.48×10^{-15} with an uncertainty of 18.8 % that is based on 28 blank measurements (see Table 1 for all measured in-batch blank values from the corresponding Be spike batch). We apologize for initially reporting an incorrect value and for erroneously calling it 'long-term average' instead of 'long-term, variance-weighted average', which makes a difference. We justify the use of the 'long-term, variance-weighted average' because the main contribution of contamination is likely to stem from the impurity of the used carrier (Scharlau Beryllium standard solution 1000 mg/l BE03450100 by Scharlab S.L.). We justify this by having established high standard clean lab protocol, e.g., by using only supra-pure acids for dissolving, which in general leads to very stable and low blank ratios, even across several spike batches (we are happy to provide more data here, if needed). However, the in-batch measured blank ratio for the EW-01 samples is 4.81×10^{-15}, almost 2x times higher than the long-term, variance-weighted average ratio. Using this value for blank subtraction would amount to a 29 - 35% relative correction for samples EW-01-4,-5,-6, a level at which we would not consider the measured concentrations as much different to the blank. Hence, we agree that this needs a transparent discussion, which we now provide in Appendix A. We indicate the result of EW-01 in the main manuscript as potentially non-interpretable, due to the low concentrations at the detection limit, and we refer to the Appendix.

Line by line responses

L61- *The way this is written makes it appear as though new 36Cl data will be presented, rather than the inclusion of previously published data in the discussion. Same goes for the conclusion section L433.*

Clarified.

L64- *Saying the long-term denudation of the mountain will be quantified sounds a bit too grand and is incorrect, as the rates reported are pretty short term and for a few specific locations only.*

We recognize that there is a difference in the definition of long-term between the rockfall and cosmogenic nuclide community. We clarify it by relating it to the millennial timescale.

L100- *Some discussion of the issues that might relate to sampling a constructed tunnel would be appropriate. How pristine were the surfaces sampled, especially for the zero depth sample, was it near the lip of the tunnel?*

We provide now a brief description of how and were we collected the samples, and we indicate that the zero depth sample was taken at the present bedrock surface.

L158- *The shielding correction is high (0.55), so sensitivity of the results to the exponent used in the topographic shielding correction ('m' in Dunne et al 1999) should be considered.*

We use a coefficient of m = 2.3 ± 0.5 for the angular flux dependence, following Nishiizumi et al. (1989). In a general case, a variation in the exponent m would have only a small effect on the shielding factor as the dependence on the angular flux varies only slightly (Gosse and Phillips, 2001; Fig 5). The shielding is commonly defined as ratio between open sky flux and blocked out flux (Dunne et al. 1999; Gosse and Phillips, 2001), thus flux variations from changes in m should amount to a ~ 5% difference in shielding factor and/or attenuation length for values between 1.8 and 3.5 (Heidbreder et al., 1971), depending on the parametrization. This would cause a corresponding increase/decrease in the absolute exposure age. The denudation rate values would vary by a few percent only, but the overall results would not systematically change.

L168- *If the maximum likely age is 20 kyr why then use 75 kyr?*

We select a broad range of model constraint values in an effort not to predetermine the solution space and thus not to bias the interpretation. We particularly test if, hypothetically, the sites were above or below the LGM glaciation.

L207- *Applying values that are 'slightly higher' is vague and seems arbitrary.*

Specified and justified.

L298- *The 'clear minimum' for denudation in the different simulations is zero. I'm not sure this suggests a clear minimum, or a problem, as it implies the model wants to go below zero. […]*

The clear minimum refers to the reduced chi square space, which coincides with the mean and median denudation rates and thereby indicating a Gaussian distribution of the denudation rate histogram. We clarify the text accordingly.

[…] I also see no justification for using these 3 values?

We think that the reviewer refers to the total allowed denudation values of 12, 15 and 20 m. These values are used as constraints for our model to work. We try to realistically estimate the maximum amount of removable bedrock during the exposure, and run three setups to test the independence of the result from this boundary condition. The values are obtained following these arguments:

We use these 3 values because the deepest samples were taken at depths close to or exceeding 3 m and consequently, the production of TCN has almost exclusively occurred by muon pathways. Muon attenuation scales exponentially, with reported muon attenuation lengths between ~4000 and $5300 \pm 950\ \mathrm{g\,cm^{-2}}$ for $2.7\ \mathrm{g\,cm^{-3}}$ rock density (e.g., Braucher et al., 2013). This translates to muon attenuation depths of ~15 m to ~19 m for 1 attenuation length, and ~30 to ~38 m for 2 attenuation lengths, which accounts for a reduction of muogenic production by ~63% and ~87%, respectively. This means that independent of the attenuation length, our deepest samples would have been located at a depth of > 23 m at the start of the exposure to allow for more than 20 m of total erosion to occur (Mair et al., 2019). Any potential nuclides inherited from before would then have accumulated at this depth or even deeper at muon production rates < 2% of the surface production rate. These are the major arguments why we run 3 values ≤ 20m. We add a short justification in the Appendix.

L301- *I don't understand how the uniformity of the 'cut-off' depths suggests a robust measurement. Time simply extends by a proportional amount to allow for the greater amount of denudation (i.e. Table 4)?*

We relate this question to a misunderstanding. The agreement of the modelled denudation rates show that the results are independent on the selection of a maximum for the total amount of denudation. We clarify the Appendix text accordingly.

L311- *This statement probably needs to cite the Mair et al 2019 study.*

Referenced now.

L304- *Define 'large' inheritance? The deepest sample is within zero at 2 sigma. I don't think these arguments about concentrations at depth are sound for such large uncertainties. Also, 'lower' should be 'higher', or the statement needs to be written more clearly.*

We rewrote the statement to focus on the shape of the depth profiles and correct for 'lower' to 'higher'.

L315 and L411- *If the argument is being made for steady-state erosion (though what steady-state means in relation to dm size chunks is unclear) the rate should persist for several multiples of the attenuation length (see the Lal 1991 paper cited). I'm not sure if it's appropriate to talk about the minimum age, based on assuming the sample concentrations represent exposure ages measurements, as being the time over which the measurements are appropriate. This point needs more explanation.*

We suggest an erosion mechanism at a scale between 1 cm and 10 cm, which occurs steadily over a temporal scale of < 10 yrs. This can be considered as a steady state denudation mechanism if TCN timescales are used as reference (see responses above). We further clarify that the reported minimum ages are the modelled minimum ages. This also accounts for the occurrence of inherited nuclides. Accordingly, we do not directly relate concentrations to exposure ages. The minimum ages refer to a minimum time span during which the modelled conditions are applicable (i.e., denudation scenario, nuclide production etc.).

Fig 1A could be the same orientation as the diagrams (i.e. it's currently a mirror image of 1B).

Changed accordingly.

L155/L158- *What are spallogenic particles?*

Corrected to spallogenic production.

#	10Be/9Be ratio	Rel. err. [%]	Ratio err.
1	9.00E-15	34.90	3.1410E-15
2	2.40E-15	82.90	1.9896E-15
3	2.40E-15	90.60	2.1744E-15
4	2.30E-15	103.20	2.3736E-15
5	9.50E-15	35.30	3.3535E-15
6	1.20E-15	180.10	2.1612E-15
7	1.30E-15	180.10	2.3413E-15
8	1.57E-14	23.20	3.6424E-15
9	5.84E-15	27.85	1.6259E-15
10	5.31E-15	20.04	1.0632E-15
11	4.70E-15	23.60	1.1104E-15
12	1.21E-15	65.13	7.8934E-16

13	2.35E-15	50.01	1.1745E-15
14	8.42E-15	18.94	1.5947E-15
15	8.51E-16	57.77	4.9154E-16
16	1.31E-14	15.08	1.9771E-15
17	1.17E-15	33.37	3.8897E-16
18	6.48E-15	27.76	1.8001E-15
19	5.79E-15	100.09	5.7961E-15
20	2.35E-15	103.91	2.4413E-15
21	5.75E-15	22.98	1.3222E-15
22	2.22E-15	29.54	6.5612E-16
23	4.81E-15	23.23	1.1182E-15
24	2.74E-15	32.04	8.7939E-16
25	4.23E-15	20.44	8.6576E-16
26	5.81E-15	19.44	1.1303E-15
27	1.27E-15	37.18	4.7128E-16
28	3.89E-15	32.60	1.2696E-15
Variance-Weighted Avg. Ratio			**2.478E-15**
Variance of the Var.-Weighted Avg. Ratio			**4.656E-16**
Standard error of the w. avg. Ratio			**1.831E-16**

Table 1. Measured blank ratios used for the long-term, variance-weighted blank correction for the used Be spike batch.

References

Balco, G., Stone, J. O., Lifton, N. A. and Dunai, T. J.: A complete and easily accessible means of calculating surface exposure ages or erosion rates from 10Be and 26Al measurements, Quat. Geochronol., 3, 174–195, doi:10.1016/j.quageo.2007.12.001, 2008.

Dunne, J., Elmore, D. and Muzikar, P.: Scaling factors for the rates of production of cosmogenic nuclides for geometric shielding and attenuation at depth on sloped surfaces, Geomorphology, 27, 3–11, doi:10.1016/S0169-555X(98)00086-5, 1999.

Gosse, J. C. and Phillips, F. M.: Terrestrial in situ cosmogenic nuclides: Theory and application, Quat. Sci. Rev., 20, 1475–1560, doi:10.1111/j.1755-0998.2010.02842.x, 2001.

Heidbreder, E., Pinkau, K., Reppin, C. and Schönfelder, V.: Measurements of the distribution in energy and angle of high-energy neutrons in the lower atmosphere, J. Geophys. Res., 76, 2905–2916, doi:10.1029/JA076i013p02905, 1971.

Hidy, A. J., Gosse, J. C., Pederson, J. L., Mattern, J. P. and Finkel, R. C.: A geologically constrained Monte Carlo approach to modeling exposure ages from profiles of cosmogenic nuclides: An example from Lees Ferry, Arizona, Geochemistry, Geophys. Geosystems, 11, doi:10.1029/2010GC003084, 2010.

Lal, D.: Cosmic ray labeling of erosion surfaces: in situ nuclide production rates and erosion models, Earth Planet. Sci. Lett., 104, 424–439, doi:10.1016/0012-821X(91)90220-C, 1991.

Mair, D., Lechmann, A., Yesilyurt, S., Tikhomirov, D., Delunel, R., Vockenhuber, C., Akçar, N. and Schlunegger, F.: Fast long-term denudation rate of steep alpine headwalls inferred from cosmogenic 36Cl depth profiles, Sci. Rep., 9, 11023, doi:10.1038/s41598-019-46969-0, 2019.

Marrero, S. M., Phillips, F. M., Borchers, B., Lifton, N., Aumer, R. and Balco, G.: Cosmogenic nuclide systematics and the CRONUScalc program, Quat. Geochronol., 31, 160–187, doi:10.1016/j.quageo.2015.09.005, 2016.

Nishiizumi, K., Winterer, E. L., Kohl, C. P., Klein, J., Middleton, R., Lal, D. and Arnold, J. R.: Cosmic ray production rates of 10 Be and 26 Al in quartz from glacially polished rocks, J. Geophys. Res., 94, 17907, doi:10.1029/JB094iB12p17907, 1989.

The role of frost cracking in local denudation of steep Alpine ~~headwalls~~ rockwalls over millennia (Mt. Eiger, Switzerland)

David Mair[1], Alessandro Lechmann[1], Romain Delunel[1], Serdar Yeşilyurt[1,4], Dmitry Tikhomirov[1,2], Christof Vockenhuber[3], Marcus Christl[3], Naki Akçar[1], and Fritz Schlunegger[1]

[1]Institute of Geological Sciences, University of Bern, Bern, 3012, Switzerland
[2]Department of Geography, University of Zurich, Zurich, 8057, Switzerland
[3]Laboratory of Ion Beam Physics, ETH Zurich, Zurich, 8093, Switzerland
[4]Department of Geography, Ankara University, Ankara, 06100, Turkey

Correspondence to: David Mair (david.mair@geo.unibe.ch)

Abstract. Denudation of steep rockwalls ~~headwalls~~ is driven by rock fall processes of various size and magnitude. ~~They~~ Rockwalls are sensitive to temperature changes mainly because thermo-cryogenic processes weaken bedrock through fracturing, ~~thus~~ which can pre-condition the occurrence of~~ing~~ rock fall. However, it is still unclear how ~~these controls~~ ~~s of the~~ fracturing of rock together with ~~and conditions~~ ~~and~~ cryogenic ~~influence~~ processes impact ~~— thereof on~~ the denudation processes operating on steep ~~headwalls~~ rockwalls ~~have remained debated~~ ~~are still unclear~~. In this study, we link data on ~~new and published~~ long-term ~~headwall~~ rockwall denudation rates ~~data for~~ at ~~the~~ Mt Eiger ~~Mountain in the~~ (Central Swiss Alps) with the local bedrock fabric and the reconstructed temperature conditions at these sites, which depend on the insolation pattern. We then estimate the ~~tendency~~ probability of bedrock for failure through the employment of a theoretical frost cracking model~~, which bases on the reconstructed temperature conditions~~. The results show that the denudation rates are low in the upper part of the NW rockwall, but they are ~~headwall compared to the~~ high ~~rates~~ both ~~on~~ in the lower part of the NW rockwall ~~footwall~~ and on the SE face, despite similar bedrock fabric conditions. ~~For these sites,~~ Th~~th~~e frost cracking model predicts a large difference in cracking intensity from ice segregation where the inferred efficiency is low in the upper part of the NW ~~headwall~~ rockwall, but relatively large on the lower ~~footwall~~ section of the NW wall and on the SE ~~flank~~ rock face of ~~the~~ Mt. Eiger. We explain this pattern by the differences in insolation and ~~local~~ temperature conditions at these sites. ~~These~~ ~~The contrasts might additionally be enhanced by permafrost occurrence in the upper NW wall, which would further reduce cracking efficiency.~~ Throughout the last millennium, temperatures in bedrock ~~conditions~~ have been very similar to the present ~~temperatures in bedrock~~. These data thus suggest the occurrence of large contrasts in microclimate between the NW and SE walls of ~~the~~ Mt. Eiger, conditioned by differences in insolation. We use these contrasts to~~,~~ ~~which~~ explain the relatively low denudation rates in the upper part of the NW ~~headwall~~ rockwall ~~of the Eiger~~, ~~but~~ and the rapid denudation in the SW ~~side~~ face and in the lower part of the NW ~~footwall foot of the Eiger~~ rock face where frost cracking is more efficient.

1 Introduction

~~Steep bedrock h~~Steep bare bedrock faces~~eadwalls, -~~are a common feature of alpine landscapes. ~~They These rockwalls~~They are situated at various elevations but are especially prominent in high altitude environments. These rock surfaces experience a variety of physical and chemical processes, that result in the formation of new fractures and in the enlargement of existing weakness zones (Krautblatter and Moore, 2014; and references therein), which ~~further~~ promote the denudation of these ~~headwall~~rockwalls. Previous research has resulted in the generally accepted notion that among the various mechanisms leading to ~~headwall~~rockwall denudation, rock fall and rockslide processes are the most important agents (e.g., Krautblatter et al., 2012; Moore et al., 2009), mainly because all loosened material is eventually removed by gravitational processes. In this context, laboratory experiments disclosed a close relationship between rock fracturing and temperature variations (e.g., Draebing and Krautblatter, 2019; Murton et al., 2016). In cold and permafrost areas, a set of three different, but closely related physical processes have been proposed to cause rock to fracture (e.g., Haeberli et al., 1997; Walder and Hallet, 1985; Draebing et al., 2014). These include (i) thermal processes resulting in permafrost degradation by increased thawing (Haeberli et al., 1997; Harris et al., 2001; Krautblatter et al., 2013), (ii) thermal stresses (Collins and Stock, 2016; Eppes et al., 2016), and (iii) cryogenic processes including frost shattering by volumetric expansion during freezing (Matsuoka, 1990; Matsuoka and Murton, 2008)~~,~~ and frost cracking by ice segregation (Murton et al., 2006; Walder and Hallet, 1985). The effectiveness of ~~the~~ cryogenic ~~se~~ processes is governed by volumetric expansion in response to diurnal and seasonal temperature variations ~~(Anderson, 1998) for volumetric expansion~~ (Matsuoka, 2008) and ice segregation (Anderson, 1998) respectively, and by temperature gradients in the bedrock (Hales and Roering, 2009; Matsuoka and Murton, 2008). Additionally the effectiveness particularly of cryogenic processes is strongly influenced by local water availability (Andersen et al., 2015; Anderson et al., 2013; Draebing et al., 2014; Sass, 2005), which conditions the formation of ice and thus the occurrence of rock falls mainly through the increase in local stresses as ice grows ~~-~~(Draebing and Krautblatter, 2019; Matsuoka, 2008). This requires, however, that the cooling of water and the formation of ice occurs rapidly, and that the pore space is saturated with water (Walder and Hallet, 1986). These conditions limit the effective expansion to a short time window (Davidson and Nye, 1985; Draebing and Krautblatter, 2019), which rarely occurs under natural conditions as recent studies have shown (Draebing et al., 2017b). Frost cracking from ice segregation is caused by the progressive ice growth in fractures at the freezing front (Hallet et al., 1991; Matsuoka and Murton, 2008; Walder and Hallet, 1985). This process requires the supply and thus the circulation of unfrozen water in bedrock (Andersen et al., 2015; Hales and Roering, 2009; Walder and Hallet, 1985). ~~These fracturing~~ Fracturing processes are additionally dependent on the variations in rock-type and -strength (Draebing and Krautblatter, 2012, 2019; Murton et al., 2016; Sanders et al., 2012), and they are influenced by discontinuities in the bedrock fabric (Draebing et al., 2014; Matsuoka, 2001). In ~~particular~~this context, it has been documented that the fabric of rock exerts a strong control on rock falls where a higher fracture density in bedrock promotes the occurrence of rock falls and rock slides (e.g., Amitrano et al., 2012; Anderson, 1998; Draebing et al., 2017b; Matsuoka, 1990). Thus, in addition to climatic conditions, bedrock pre-conditioning through faulting and folding exerts a significant control on the efficiency and scale of rock fall activity (Draebing et al., 2017b; Krautblatter and Moore, 2014; Sass and Wollny, 2001). ~~Furthermore~~As a final, closely related mechanism, it has been shown~~,~~ that paraglacial adjustment of the stress field in the local bedrock can induce rock fracturing and, as a consequence, ~~therefore~~ increase rock fall activity (McColl, 2012; McColl and Draebing, 2019), even up to millennia after ice degradation (Grämiger et al., 2017). Although these relationships are well understood, little is known on how rapid denudation of bedrock ~~headwall~~rockwalls has proceeded, and how denudation in these settings has responded to climatic changes particularly if longer time scales spanning millennia are considered (e.g., Gruber et al., 2004a; Krautblatter et al., 2013; Krautblatter and Moore, 2014).

Here, we study ~~combine concentrations of in-situ terrestrial cosmogenic nuclides (^{10}Be and ^{36}Cl), measured~~~~long-term~~the millennial--scale denudation ~~in depth profiles of a 1800 m-high~~ in vertical ~~bed~~rock-walls at ~~the~~ Mt. Eiger in the Swiss Alps (Fig. 1)~~,~~ in an effort to explore the mechanisms of denudation of this vertical headwall and the underlying controls.~~.~~ To achieve these goals, ~~with information on the bedrock fabric to quantify the long-term denudation of this mountain.~~ w~~W~~e ~~collect~~ collect data about the bedrock fabric of ~~from~~this mountain ~~the NW and SE faces of the Eiger~~, to illustrate how the high fracture density has preconditioned the headwall for rockfall processes to occur. We then present temperature and paleoclimate data to document that ~~, which~~ the NW and SE faces of the Eiger have experienced differences in insolation and thus ~~a~~ contrasting microclimatic conditions~~e~~. We ~~use~~complement this dataset with published information on ~~local~~in-situ rockwall denudation ~~information~~rates on both sites of the Eiger. Denudation rates at these sites have been derived from terrestrial cosmogenic nuclide (TCN) concentrations ~~along~~in bedrock depth profiles. ~~to understand spatial differences in denudation.~~ We finally combined this information into a simplified frost cracking model to explore ~~potential controls on rockwall denudation by analyzing~~how the local bedrock fabric- and temperature conditions ~~and comparing denudation rates and fabric to potential rock fall preparing factors. We aim at identifying the main~~have driven ~~driving processes of local rockwall~~the erosion of the headwalls of Mt. Eiger. ~~erosion and at understanding how it is related to changes in temperature. In order to do so, we field a simplified frost cracking model.~~~~We find that denudation rates are high on the SE side of the Eiger and at the foothill of the NW headwall, while denudation rates are up to four times lower on the upper part of the NW flank. We apply a simplified version of a frost cracking model to test whether the spatial pattern of denudation can be explained by the differences in microclimates around the Eiger Mountain. We find that the bedrock of the Eiger is highly fractured, which potentially promotes the occurrence of rock fall processes where dm-scale bedrock particles can be released at a high frequency. In addition, our results imply that frost cracking is effective where mean annual temperatures are slightly positive and where diurnal and annual temperature variations are large. This is particularly the case for the south side of the Eiger and also for the northern flank at its low-elevated footwall, where the denudation rates are high. We use these observations to propose that the denudation pattern of the Eiger is strongly controlled by insolation, and thus by temperature conditions.~~

2 Setting

~~2.1 Geomorphology and cosmogenic sampling sites~~

The Eiger Mountain (Fig. 1)~~, which is the focus of our study,~~ is characterized by a steep~~n over-steepened~~, ~~c~~approximately~~.~~ 1800 m-high NW face. This NW ~~flank~~rock face can be subdivided in an upper part that ranges in elevation between c. 3950 m a.s.l. and 2800 m a.s.l where the wall is > 50° steep ~~(> 50° slope angle) or~~and nearly vertical in some locations (Figs. 1b,2), and in a flatter ~~footwall~~ base segment (lower part), which continuously grades into grassland beneath an elevation of 2200 m a.s.l. ~~IOn~~On the opposite side, the~~ other side, the~~ SE ~~the flank~~rock face is a several hundred-meter yet equally steep rock wall (> 60° slope angle), and 2 small cirque glaciers feeding into a larger ~~, more distant~~ active glacier~~ active glaciers~~ further downslope (Figs. 1a,b)~~,~~ border the ~~footwall~~rockwall foot.

The morphology of the Alps largely records the response of glacial erosion during the Last Glacial Maximum (LGM) and previous glaciation (Schlunegger and Norton, 2013). For the region surrounding Mt. Eiger, the ~~glacial~~ history of glacial coverage and erosion ~~of the mountain~~ can ~~be~~only be inferred indirectly from reconstructions of previous ice extends, accomplished e.g., ~~from~~through the dating of moraines ~~dating~~ or the mapping of ice trim lines~~ mapping~~, since there is no ~~such~~geomorphic data available for ~~the~~Mt. Eiger ~~mountain~~itself that could be used to identify the glacial imprint on this mountain. ~~.~~ However, a ~~for the studied mountain~~reconstruction of the glacial coverage of the Alps during the LGM (Bini et al., 2009; Kelly et al., 2004) shows that the Alpine~~,~~ glaciers were large enough to cover the NW rock face even above 2800 m a.s.l.~~ were present for the last time during the Alpine Last Glacial Maximum (LGM; Bini et al., 2009; Kelly et al., 2004).~~ These ~~ice bodies~~glaciers disappeared shortly ~~in the central alps degraded~~ before c. 18 ka (Wirsig et al., 2016b, 2016a), and the NW rock face of the Mt. Eiger has been largely ice free since then. Exceptions are the small ice sheets on the uppermost part of the rock wall itself, ~~such~~ e.g., the so called ‘white spider’ (Weisse Spinne; Fig. 1). On the opposite side~~ SE, thereby constituting the last ice cover in the Eiger NW rock face. The~~the upper part of the ~~SE~~ rock face situated above 3000 m a.s.l. was not covered by ice since the at least the glacial advance ~~during~~during the Egesen Stadial of ~~, linked to~~ the Younger Drays, ~~not later than c.~~approximately 12 – 11 ka ago (Ivy-Ochs et al., 2009). This was thus the last time~~,~~ when ~~the~~ local glaciers ~~would~~could have ~~been able to amass enough ice to grow several tens of meters in thickness to~~ covered the rock wall above 3000 m elevation.

The denudation processes and rates operating on ~~the~~ Mt. Eiger ~~Mountain~~ have already been analyzed in a previous study, where concentrations of in-situ cosmogenic ^{36}Cl were measured in rock samples collected in ~~four~~ five depth profiles, of which four ~~could~~were diagnostic enough ~~befor used to~~ estimatinge denudation rates (Mair et al., 2019). The sites were situated on the SE (sites EM-01 and EM-02, Fig. 1) and on the NW bedrock ~~flank~~rock faces of the Eiger (sites EW-02 and EW-03; Fig. 1). On the NW ~~flank~~rock face, ~~the~~ site EW-03 ~~site~~ is located in the ~~footwall~~ base segment at an elevation of 2530 m.a.s.l, whereas site EW-02 is situated near the base of the upper, nearly vertical ~~segment~~ part at an elevation of 2803 m a.s.l. On the SE ~~flank~~rock face~~ of the Eiger~~, both ~~cosmogenic~~ depth profiles ~~sample sites~~ are located at c. 3100 m a.s.l. The results yielded generally high denudation rates, ranging between c. 45 cm kyr^{-1} ~~to~~ and c. 350 cm kyr^{-1} ~~for~~ over the last centuries to millennia (Table 1; Mair et al., 2019)~~)~~. On the NW ~~flank~~rock face, denudation rates are c. 350 cm kyr^{-1} at the ~~footwall~~ base of the Eiger (site EW-03) and c. 45 cm kyr^{-1} and thus substantially lower in the upper part of the rock wall (site EW-02). I~~O~~n the SW ~~side~~face, denudation rates range between 150 and 250 cm kyr^{-1} (sites EM-01 and EM-02). ~~Mair et al. (2019) used these rates together with the relatively large concentration of cosmogenic~~ ~~^{36}Cl at greater depths in the depth profiles to propose a model where denudation of the rock face has been accomplished by frequent, cm-scale rock fall processes together with chemical dissolution of limestone.~~ We ~~benefit from the results of this previous study and~~ complement ~~thate~~this denudation rate dataset with cosmogenic nuclide data of a further depth profile EW-01. This fifth section is situated at 2844 m a.s.l. (Swiss Coordinates ~~at point~~ site 643168/158980 ~~of the (Swiss Coordinates~~), near the base of the upper part of the NW face and thus ~~in~~ close ~~proximity~~ to site EW-02 (Table 1) for which ~~of the~~ Mair et al. (2019) ~~study~~ reported the lowest denudation rates of c. 45 cm kyr^{-1} (Figs. 1a, 1b). The bedrock at sites EM-01, EM-02 and EW-02 and EW-03 mainly comprises limestone, and this was also the reason why Mair et al. (2019) measured millennia denudation rates based on ^{36}Cl concentrations in depth profiles. ~~.~~ Since the bedrock at EW-01 ~~comprises~~ is a siliceous limestone and thus contains sufficient~~bedrock with high~~ quartz ~~content~~minerals, ~~This was also the reason why ^{36}Cl was the target cosmogenic nuclide (Mair et al., 2019). The new site EW-01, however, hosts bedrock with significant quartz content. This is the reason why for this site, we prepared samples for the analysis of~~we analyzed the bedrock for in-situ ^{10}Be instead. Similar to Mair et al. (2019), cosmogenic samples were taken ~~– within bedrock samples from~~ ~~instead. Similar to Mair et al. (2019), bedrock samples were collected along~~from a ~~the walls of a construction~~ tunnel that connects the Jungfraubahnen railway tunnel with the ~~headwall~~rockwall surface of the Eiger. These tunnels were used to depose material during tunnel construction between 1896 and 1905 AD. However, since the ^{10}Be concentrations of the cosmogenic samples are close to the detection limit of the Accelerator Mass Spectrometer (AMS), any inferences derived from this particular depth profile at EW-01 will be quite speculative. We therefore present all methodological details and the results for site EW-01 in ~~the Supplement~~Appendix A for the sake of completeness and transparency. ~~These tunnels were used to depose material during tunnel construction between 1896 and 1905 AD. All sample sites have a local slope of ≥ 50°, making snow cover over extended periods unlikely.~~

~~2.2 Climate and permafrost occurrence~~

~~The probability of permafrost occurrence in the Alps has been predicted based on ground surface temperature, air temperature and solar radiation. These information have been combined in a statistical model to reconstruct the Alpine-wide Permafrost Index Map (APIM) with a 30m resolution (Boeckli et al., 2012a, 2012b). For the NW face of the Eiger, the APIM data shows that all sites might be affected by permafrost. Whereas the sites EW-02 and EW-03 in the upper part of the north face show the highest tendency for permafrost occurrence (Fig. 2), the cosmogenic sampling sites on the SE facing flank are less likely to be affected by permafrost (Fig. 2).~~

~~2.3 Bedrock lithologies and fabrics~~

~~The region surrounding the Eiger is located at the geological contact between the crystalline rocks of the Aar massif, its sedimentary cover rocks and the Helvetic thrust nappes (Berger et al., 2017). The Eiger itself is mainly made up of micritic Jurassic and bioclastic Cretaceous limestone, with local chert layers and nodules, all of which were re-crystallized under lower greenschist facies conditions (c. 300°C; Mair et al., 2018; and references therin). During Alpine orogenesis, the bedrock was heavily deformed through multiple phases of folding and thrusting, which are recorded by a complex fabric in the exposed rock (Herwegh et al., 2017; Wehrens et al., 2017). At the cosmogenic sampling sites, the bedrock fabric is dominated by two generations of foliation and two sets of joints (Mair et al., 2018). The foliation that formed during the first deformation phase is oriented parallel to the sedimentary bedding and is associated with tight and isoclinal folds at the decimeter scale. The formation of this fabric was conditioned by micrometer-scale changes in sheet-silicate content during sedimentation. The second foliation is characterized by slip planes in micro shear zones, which display a large variation in the spacing between individual planes. This second foliation was considered to have formed at temperature conditions that were high enough for calcite minerals to deform in a ductile way (Mair et al., 2018). These structures are crosscut by two sets of brittle fault networks with steeply dipping fault planes. Age assignments on the formation of these structures are still a matter of debate (Mair et al., 2018).~~

3 Methods

~~We measured concentrations of cosmogenic ^{10}Be along depth profile EW-01 (Fig. 1) in order to extract information on denudation rate, exposure age and potential inheritance. The latter three variables are derived through Monte Carlo (MC) depth profile modelling techniques (Hidy et al., 2010).~~ We ~~then~~ aim to link the results of the cosmogenic nuclide analysis to the observations on the bedrock fabric, and we employ a frost cracking efficiency model to explore a potential dependency of denudation on bedrock and climate conditions. The range of methods thus includes field work to map the bedrock fabric and to determine the spacing between fractures and joints. We additionally compiled temperature data and combined these into a modeling framework on frost cracking processes where the model outputs will be constrained by previously published ^{36}Cl-based denudation rates for the Eiger north and south faces.

3.1 ~~Field data collection~~Investigations of bedrock fabric

Fieldwork, including bedrock sampling for TCN analysis (see Appendix A), took place in winter of 2016 and summer 2017. Bedrock fabric data was collected using a geological compass.~~ The mapping focused on the~~We mapped lithological contacts, the orientation of bedding and foliation planes and the geometries of~~, lithological contacts, foliation and~~ faults using~~ state of the art~~ techniques in structural geology. Upon mapping, we particularly focused on~~ and was designed to~~ investigatinge~~ the~~ crosscutting relationships between the structural fabrics, and on completing the ~~and structural~~ inventory of structures at the ~~on~~ outcrop scale (Mair et al., 2018). We determined mean values from o~~O~~rientation data using a spherical mean. These values were separately determined for the various structure categories that we identified in the field upon mapping ~~was analyzed for mean orientation of different, in the field identified structure categories, using a spherical mean~~ (Vollmer, 1995). Data visualization and stereo plot generation was done using the Orient 3.4.2 software (Vollmer, 2015). A ~~–and~~ handhold GPS was used to geo-reference the collected data. ~~in~~Digital and analogue topographic maps –were based on ~~combination with elevation information from~~ the 2m digital elevation model (SwissAlti3D, provided by the Federal office of Topopgraphy, swisstopo) for surface outcrops, and on a high-resolution elevation map of the Junfgfraubahnen railway tunnel for subsurface data.~~ The mapping focused on the orientation of bedding, lithological contacts, foliation and fault and was designed to investigate the crosscutting relation and structural inventory on outcrop scale (Mair et al., 2018). Orientation data was analyzed for mean orientation of different, in the field identified structure categories, using a spherical mean (Vollmer, 1995). Data visualization and stereo plot generation was done using the Orient 3.4.2 software (Vollmer, 2015).~~

~~3.1 Analysis of *in-situ* cosmogenic ^{10}Be~~

~~3.1.1 Collection of samples, extraction of Be and AMS measurements~~

~~We collected five bedrock samples within a depth profile at site EW-01 from quartz bearing recrystallized chert layers. The material was taken from a wall of a tunnel that connects the Jungfraubahnen railway tunnel with the headwall surface. Samples were quarried with a battery saw and chisel, thereby following standard sampling protocols (Dunai and Stuart, 2009). Each sample was 5 to 10 cm thick and consisted of 1 to 1.5 kg of rock material. Concentrations of cosmogenic ^{10}Be were measured on quartz grains that were extracted from these samples. Sample preparation followed the procedure of Akçar et al. (2012) and took place at the Institute of Geological Sciences, University of Bern. ^{10}Be/^{9}Be ratios were measured by accelerator mass spectrometry (AMS) at the AMS facility at ETH Zurich, and were normalized to internal standard S2007N (Christl et al., 2013). The measured ratios were corrected with a long-term, full process blank correction of 2.44 x 10^{-15}, which amounted to relative correction between 3 and <19 %.~~

~~3.1.2 Scaling and corrections for muogenic production~~

~~In-situ cosmogenic ^{10}Be is mainly produced through spallation and muon reactions on O and Si (Gosse and Phillips, 2001). Accordingly, the production needs a scaling to geographic position and elevation, and it needs a correction for shielding from secondary cosmic ray particles (Gosse and Phillips, 2001; Lal, 1991). Production rate scaling for spallation production was done using the method of Stone (2000), which is based on the work of Lal (1991). We updated these approaches using the recalibrated reference dataset of Borchers et al. (2016) for our scaling framework. For the consideration of muogenic production, we used the parametrization scheme by Balco et al. (2008), which is based on muogenic production systematics presented by Heisinger et al. (2002a,b). The experimental fit for muogenic production of these authors, however, is known to yield in an up to ~ 40% overestimation of muogenic ^{10}Be production (Borchers et al., 2016; Braucher et al., 2003, 2013). To account for this affect, an uncertainty of 40 % was assigned on the muogenic production during the MC modelling, which is~~

~~described below. We finally computed an open sky visibility on 1° azimuthal increments to account for headwall and bedrock specific geometry and shielding. This was done using a high resolution (2m) DEM provided by the Swiss Federal Office of Topography (Swisstopo) as basis. We used the combination of these constraints to calculate a total site-specific shielding factor (S_T) and apparent attenuation length ($\Lambda_{f,e}$) for spallogenic particles with the CRONUS Earth online Topographic Shielding Calculator v2.0 (Marrero et al., 2016). The shielding factor (S_T) was used to correct for both spallogenic and muogenic production, which is necessary due to the large height of the headwall (Mair et al., 2019). The site-specific apparent attenuation length for spallogenic particles ($\Lambda_{f,e}$) was used to correct for geometric effects (Dunne et al., 1999; Gosse and Phillips, 2001). A detailed discussion of the approach can be found in the supplement of Mair et al, (2019).~~

~~3.1.3 Depth profile modelling~~

~~We used the concentrations of cosmogenic ^{10}Be in the depth profile at EW-01 to estimate the local denudation history using a Monte Carlo randomization approach (Hidy et al., 2010) and considering nuclide production at depth (Anderson et al., 1996; Braucher et al., 2009). The modelling was done with a modified Mathcad™ code of Hidy et al. (2010). A MC approach for depth profile modelling requires initial constraints on the modelled quantities, i.e., exposure age, potential inheritance and denudation rate (Hidy et al., 2010). We selected a broad range for these values in an effort not to predetermine the solution space and thus not to bias the interpretation. We thus set a constraint of (i) 75 ka on the exposure age (which is an uppermost limit given the 20 ka for the LGM), (ii) the ^{10}Be concentration of the surface sample (i.e., 1.9×10^4 at g^{-1}) for inherited nuclides and (iii) a maximum rate of 1500 cm kyr^{-1} on the denudation variable and a maximum of 12, 15 and 20 m for the cumulative amount of denudation for up to 75 ka. These estimates are considered as conservative values because they represent uppermost bounds for a possible exposure age, denudation rate and an inherited concentration (for a full justification see method section of Mair et al., 2019). The main purpose of running three setups for the cumulative amount of denudation is to test the independence of the model results on the initial parameter constraints on denudation, which is the case here. We note that this approach is not applicable to extract exposure ages without independent denudation constraints (Anderson et al., 1996; Hidy et al., 2010).~~

~~The modelling of TCN profiles in bedrock requires the consideration of possible inherited nuclides from previous exposure. Since such an exposure can only occur through a removal of bedrock material, such an inheritance would have been produced by muons only (due to the position of the sample at significant depth) and would follow an exponential decrease with depth (Mair et al., 2019). To account for a potential inheritance, we modelled an inherited nuclide concentration for the surface sample (C_{inh}), which we used to parametrize inheritance at depth ($C_{inh,z}$) following~~

$$C_{inh,z} = C_{inh} \cdot e^{\left(-\frac{z}{\Lambda_{inh}}\right)}.$$

~~We used the value of a fitted muon attenuation length of 4852 g cm^{-2} for Λ_{inh}, which is in good agreement with published reconstructed muon attenuation lengths (Braucher et al., 2013). For rock density, we employed a uniform value of 2.68 ±~~

~~0.04 g cm^{-3} to account for the full density range between pure quartz (2.65 g cm^{-3}), the local limestone (2.68 ± 0.02 g cm^{-3} measured by Mair et al., 2019) and pure limestone (2.71 g cm^{-3}). This also includes density effects related to the occurrence of nodular chert, which was sampled for the purpose of this study. We ran the MC model until we obtained 10^5 profiles where the modeled concentrations fall within a 2σ confidence interval of the measured ^{10}Be concentrations (which corresponds to reduced χ^2 value < 3.09). All input parameters for the MC modelling are reported in Table 2. The documentation and raw results are provided in the supplement file.~~

3.2~~2~~ Temperature data and insolation

~~Fracturing of rock from frost damage and permafrost occurrence is related to local bedrock temperatures, with main parameters of interest being mean annual temperature (MAT), amplitude of annual temperature variation (dT_a) and mean amplitude of diurnal temperature variation (dT_d). We used these temperature variables to construct times series of temperature data as input for the frost cracking modelling, representing the conditions at sites EW-03, EW-01,-02 and EM-01,-02, respectively (Table 1).~~ Fracturing of rock from frost damage and permafrost occurrence ~~is related~~are both dependent on~~ to local~~ in-situ bedrock temperatures, ~~with main parameters of interest being~~ where the mean annual temperature (MAT), the amplitude of the annual temperature variation (dT_a) and the mean amplitude of the diurnal temperature variation (dT_d) constitute the main parameters of interest. We ~~used~~collected and constrained these temperature variables from various sources to construct times series of temperature data. We then used these data as input for the frost cracking modelling, representing the conditions at sites EW-03, EW-01,-02 and EM-01,-02, respectively (Table 1). In particular, p~~P~~resent temperature values for the sites EW-01 and EW-02 are based on near ground surface temperature (NGST) data at 10 cm depth ~~by Gruber et al. (2004b)~~ that were measured at the train stop Eigerfenster (643307, 159034, 2860 m; Gruber et al., 2004b). Data on near ground surface temperatures are also available ~~from~~ for the train station at Eismeer (643830, 158049, 3150 m) close to our cosmogenic nuclide sampling sites EM-01 and EM-02 on the SW ~~flank~~rock face of ~~the~~ Mt. Eiger (Gruber et al., 2004b). We ~~benefitted from this situation and~~ extracted information for constraining MAT, dT_a and dT_d from the dataset ~~spanning~~ comprising almost 15 years of daily averaged temperature data, available through the Swiss Permafrost Monitoring Network (PERMOS 2019; http://www.permos.ch/data.html). The MAT and dT_dvalues were then determined from the daily averaged temperature data, whereas dT_a was calculated from the monthly averaged values (Gruber et al., 2004b). We calculated MAT, dT_a and dT_d for the record between 2001 and 2014 AD and for the hydrological year 2002 separately. We used seven complete years of record for both the NW (Eigerfenster) and SE (Eismeer) ~~flank~~rock faces (Fig. 3). However, the data did not cover the same years for both sites.~~, F~~For the NW we therefore used the available data covering the hydrological years 2002, 2004 - 2008 and 2010.~~, whereas~~ F~~f~~or the SE ~~we used~~data for the hydrological years 2002, 2005 – 2007 and 2012 — 2014 were available, which we considered in this work accordingly (temperature data provided ~~in full~~ in the Supplement). For site EW-03 no such data was available. We~~,~~ therefore ~~we~~ scaled the available temperature data from the Eigerfenster train station to site EW-03 ~~, which is the closest location for which temperature data is available,~~ using an atmospheric temperature lapse rate of -6 °C km^{-1}, which is commonly used for alpine environments (e.g., Gruber et al., 2004b). ~~.~~In addition, also for site EW-03, we applied values of 9.0 ± 1.5 for dT_a and 7.0 ± 1 for dT_d. The values are higher than those we assigned for the higher locations EW-01,-02, mainly because EW03 receives more isolation~~that were slightly higher than for sites EW-01, 02. We chose these values, because of the~~~~we expect the~~ . ~~temperature in general to be similar to the upper NW sites, but overall warmer and more variable as the site receives more insolation than sites EW-01, -02 higher insolation due to southeast exposure.~~ These estimated temperatures were finally used to generate temperature curves (Anderesen et al., 2015) as input for the frost cracking modelling (Fig. 3).~~.~~

~~Past temperatures~~Temperatures for the last millennium were estimated using a lake record c. 45 km farther to the west (Seebergsee, ~~–~~46°370N, 7°280E). ~~In that~~For this lake, ~~lake,~~ Larocque-Tobler et al. (2012) ~~used~~ used chironomid taxa embedded within the sediments to reconstruct a temperature history for the most recent past. These provide estimates of how the mean temperatures during a distinct period in the past deviated from the modern ones representing the time span between 1961-1990 AD. The resulting differences ~~to the period~~are 0°C ~~1961-1990 AD~~ for the 19th century AD ~~(0°C)~~, -0.5°C for the L~~l~~ittle Ic~~ic~~e A~~a~~ge ~~(– 0.5 °C)~~ and +1.2°C for the ~~medieval~~ Medieval ~~climate~~ Climate ~~optimum~~ Optimum.~~(+ 1.2 °C).~~ ~~To test for temperature conditions further in the past w~~We additionally resorted to tree-ring based temperature reconstructions for Central Europe (Büntgen et al., 2011) ~~,~~and used these data as further constraint for the temperatures in the past. The tree ring data infer temperatures for the Central Alps, which are in good agreement ~~for~~with those from the lake record (Larocque-Tobler et al., 2012), at least for a shorter period ~~with temperature reconstructions for the Central Alps from tree-rings~~of a few centuries~~…..~~ (Büntgen et al., 2006)~~ and chironomid-derived record (Larocque-Tobler et al., 2012)~~. We therefore extracted temperature anomalies of~~∼~~ -1 °C for the migration period and + 0.5 °C for the period during the Roman climate optimum ~~period~~. We adjusted ~~these~~ all values to the 20th century AD warming (+ 0.8 °C) and calculated MATs for the corresponding periods under the assumption of a constant diurnal and annual temperature fluctuation. We inferred ~~and~~ no lag between the increase of mean air temperatures ~~warming~~ and the temperature adjustments on the rock surface ~~temperature response~~ (Table 1).

Maximum direct annual insolation was calculated using the 'Area Solar Radiation' tool of ESRI's ArcGIS Desktop 10.1 suite, which employs a hemispherical viewshed algorithm (Fu and Rich, 2002; and references therein). The calculation was done for 1 day and hourly intervals for a sky size of 512 cells for the whole year of 2015.

3.3~~3~~ Frost cracking modelling

Annual efficiency of frost cracking processes was computed using the ~~mechanistic~~ numerical model of Andersen et al. (2015), which builds on the approach of Anderson et al. (2013), Hales and Roering (2007) and Anderson (1998). The model propagates temperature changes into the ground by solving a one-dimensional heat flow equation (Hales and Roering, 2007). ~~The related expression~~It considers annual surface temperature as a sinusoidal function around the MAT and dT_a, ~~–~~and ~~is based on~~ a randomly superimposed sinusoidal ~~diurnal~~ function with an amplitude between 0 and dT_d (Andersen et al., 2015; Anderson et al., 2013). Whereas the Andersen et al. (2015) model is capable of incorporating a sediment layer of various thicknesses atop the bedrock, we used a setup without such a layer, ~~as~~ because field inspections have shown that ~~we considered~~ the local slope ~~as~~ is too steep to ~~accommodate~~ host a regolith layer (Table 1). The model calculates a frost cracking intensity (FCI) related to ice segregation, which is most effective where temperatures range within the so-called frost-cracking window (FCW; ~~between -8 to -3°C (~~Anderson, 1998; Walder and Hallet, 1985), and where water is available for ice to form (Andersen et al., 2015; Anderson et al., 2013; and references therein). The flow of water is influenced by the thermal gradient in the subsurface (Hales and Roering, 2007) and the distance to the freezing front (Anderson et al., 2013). The Andersen et al. (2015) model scales the FCI with both the thermal gradient and the occurrence of water along the path to the point of ice segregation. ~~This is accomplished using a penalty function that integrates the flow resistance (Anderson et al., 2013) for a mixture of frozen and unfrozen bedrock (Andersen et al., 2015).~~ Here, we~~We~~ employed the ‚standard model' of Andersen et al. (2015), which follows the concept ~~of~~where ~~limiting frost~~ cracking in the bedrock is limited, and thus controlled, by ~~with~~the distance to the water source and the water availability up to a critical threshold. This is accomplished by a penalty function that integrates the flow resistance (Anderson et al., 2013) for a mixture of frozen and unfrozen bedrock (Andersen et al., 2015). Aside from the water availability, the model ~~needs~~builds on a set of input variables and assumptions, where different ~~choices~~assignments of values and constraints might ~~change~~influence the results. ~~We~~The selected input variables (see ~~use the 'standard model' of Andersen et al. 82015) for the input variables (see~~ Appendix B) ~~for a list of variables),~~have indeed the potential to influence the outcome of the model results ~~of which the~~particularly for a FCW between ~~(~~-8 to -3°C and for the consideration of a~~)~~ ~~and the~~ thermal conductivity for bedrock~~ are the most relevant for our study~~. We therefore run sensitivity tests and varied the aforementioned quantities in order to explore how the results depend on the choice of input parameters. Because of the lithology dependency of FCW (Draebing and Krautblatter, 2019), we run test models with ~~To test the sensitivity of our results to the input choices, we varied the aforementioned quantities.~~ FCWs ~~are dependent ofbetweenof~~between -9.3 °C and -1.4°C, ~~-~~and between -4.5 °C to -1.8 °C. These values have been derived for paragneisses with high schistosity (~~by~~ Draebing et al., 2017b~~lithology and rock strength (Draebing and Krautblatter, 2019). In absence of FCW estimates for our limestone, we ran the model for two additional FCWs of -9.3 °C to -1.4°C and -4.5 °C to -1.8 °C, taken from Draebing et al. (2017b) to explore the sensitivity of the results on the FCW),~~. We ~~. These values were determined for paragneisses with high schistosity. a~~Additionally ~~, we~~ tested the model for a possible sensitivity to the thermal conductivity. We started with a standard conductivity of~~ aside from the~~ 3.0 W m^{-1} K^{-1} ~~of the~~(~~-~~Andersen et al., ~~(~~2015) ~~standard model~~and then considered upper and lower bounds compiled from various sources (see Appendix B for details and references).~~ Furthermore, W~~We also~~we~~ applied the material-specific standard model parameters of Andersen et al. (2015), which includes a general rock porosity of 2%. This value is in excellent agreement with the average porosity of 1.8 ± 0.5 % for the ~~local~~Eiger limestone, calculated from density measurements (Supplementary Notes S4 of Mair et al., 2019). The model assumes full water saturation for the bedrock. However, ~~the~~ for simplicity purposes, the model ~~also assumes~~considers ~~for simplicity~~ that heat transport ~~only~~ occurs ~~by~~through conduction only. ~~Thereby~~Accordingly, it fails to ~~it does not~~ capture bedrock anisotropies, i.e. cracks and foliations, which might facilitate the transport of heat by advection. Finally, the resulting diurnal depth-integrated $\overline{FCI}$ values are integrated over an entire year. We ran a series of models to account for variations in local temperature. We set the starting ~~Temperature~~ temperature (T_0) to the site-specific MAT, and the dT_a and dT_a to the mean, minimum, maximum and the average values of 2002, respectively, and we changed these conditions upon modelling. This setup does not necessarily provide an $\overline{FCI}$ envelope, as it is based on the assumption that changes in the MAT and daily temperature amplitude also affect changes in the annual temperature amplitude in the same way, i.e., lower MATs are likewise associated with damped changes in daily and annual temperatures.

4 Results

~~4.1 ^{10}Be concentrations and denudation rate~~

~~The 5 rock samples have ^{10}Be concentrations (Fig. 3) ranging from 1.9 x 10^4 at g^{-1} to 0.35 x 10^4 at g^{-1} (Table 3) that decrease with depth. The standard 1σ error (0.07 x 10^4 at g^{-1} to 0.24 x 10^4 at g^{-1}; Table 3) accounts for AMS reproducibility and counting statistics, with a relative uncertainty ranging from 11 % to 69 %. The resulting concentration profile allows for MC depth profile modelling (Fig. 3) and yields values on denudation rate, exposure age and potential nuclide inheritance. The MC simulation returned 10^5 profiles where the model concentrations are within a 2σ measurement confidence interval with minima at reduced χ^2 = 2.32. The MC simulation returns consistent values for inherited nuclides and denudation rate, where mean and median values are in good agreement and follow a well-defined Gaussian distribution (complete modelling results are provided in the Supplement). Thus, the MC simulation results are independent of the initial constraint on total denudation (Table 4). In detail, mean modelled inherited concentrations range from (2.4 ± 0.6) x 10^3 at g^{-1} to (2.6 ± 0.7) x 10^3 at g^{-1} ^{10}Be, accounting for 13 – 14% of the measured concentration for the surface sample. Mean denudation rate values range between (63.4 ± 13.5) cm kyr^{-1} and (64.7 ± 12.1) cm kyr^{-1}. Surface exposure ages cannot be estimated from the differing distributions for the model runs. However, the MC simulations yield agreeing minimum ages of 0.7 ka.~~

4.~~2~~1 Bedrock fabric

The Eiger itself consists of a suite of heavily fractured and re-crystallized~~,~~ micritic Jurassic and bioclastic Cretaceous limestones, with local chert layers and nodules. The foliation that formed during the first deformation phase is oriented parallel to the sedimentary bedding and is associated with tight and isoclinal folds at the decimeter scale. The formation of this fabric was conditioned by micrometer-scale changes in sheet-silicate content during sedimentation. The second foliation is characterized by slip planes in micro shear zones, which display a large variation in the spacing between individual planes. All studied sites expose bedrock with a strongly developed network of faults, fractures and foliations, especially close to the surface. The bedrock fabric at the SE ~~flank~~rock face (sites EM-01, -02) is dominated by small joints that developed along the NW dipping foliation planes of both foliation generations, here referred to as ~~(~~S1 and~~,~~ S~~3~~3 following Mair et al. (2018)~~;~~ (Fig. 4). Note that S2 foliations are only visibly close to the basement cover contact (Mair et al., 2018) and have thus not been mapped here. The joints are generally << 1 mm wide, but open and occasionally contain circulating water in summer, as was the case during sampling in summer of 2017~~ AD~~. The spacing between these joints varies, but generally measures between 2 and 10 cm. A second set of joints with a decimeter-wide spacing and 1 to 10 mm-wide cracks steeply dip to the SE. These joints are sometimes associated with preexisting calcite veins (Fig. 4b). The joints are generally open, but some calcite infill is also present. At the scale of an outcrop, both sets of joints are connected and regularly spaced. A third set of fractures, albeit with an irregular spacing, is found along up to several meter-broad brittle fault zones (Fig. 4c). These faults display open cracks at sub mm-scale. The spacing varies and some voids are filled with fault gauge.

A similar network of joints characterizes the sites within the NW ~~headwall~~rockwall at sites EW-01, -02, -03. Joints with openings between << 1mm and 1 mm are oriented parallel to the two generations of foliations (Fig. 5), which are gently SE dipping to flat lying. A set of SE dipping open joints with widths of up to 10 mm and a spacing of 10 cm is present at all sites (Fig. 5a). We additionally found steep and ~~headwall~~rockwall-parallel cracks with openings that are up to several cm wide (C2; Fig. 5d). We note that during sampling on Dec. 1st 2016, ice was present in these fractures (Fig. 5b,c).

4.~~3~~2 Temperature estimates and frost-cracking modelling

The near surface ground temperatures (Table 1) reconstructed from the available daily averaged records show that the sites EW-01 and EW-02 have experienced an average MAT of -0.5 ± 0.5 °C for the full year records between 2001 and 2014 AD. This is lower than the MAT average for the SE sites (EM-01, EM-02) where temperature ~~where the~~ values are 1.8 ± 0.8 °C for the same period, albeit not for the exact same years (see section 3.2). On the NW ~~flank~~rock face, also at sites EW-01 and EW-02, the annual temperature amplitude of dT_a = 8.1 ± 1.3 °C is smaller compared to the dT_a = 10.7 ± 1.7 °C i~~o~~n the other SE ~~side~~ face of ~~the~~ Mt. Eiger. A similar situation is observed for the mean diurnal temperature amplitude dT_d where the corresponding values are 6.1 ± 0.7 °C for the NW sites and 7.7 ± 0.9 °C for the SE sites. The temperature estimates for the hydrological year 2002 are similar to the mean values of the longer time period (Table 1). Temperatures for the lower NW site (EW-03) were estimated with a MAT of 1.5 ± 0.5 °C (using a constant lapse rate of , -6 °C km^{-1}), while values for dT_a of 9.0 °C and dT_d of 7.0 °C were ~~assumed~~ considered to be slightly higher than in the upper NW. Based on the recent t~~T~~emperature data and ~~historical reconstructions~~the reconstructed historical temperatures, we ~~allow to~~ exclude the occurrence of local permafrost conditions at the SE rockwall for all scenarios. For the upper NW headwall of Mt. Eiger, permafrost might occur ~~under~~at current conditions~~, while in the~~ and during the past when MATs were lower~~, permafrost occurrence is substantiated by the reconstructed temperatures.~~.

For the SE sites, the modelling of the annual frost cracking intensity ($\overline{FCI}$) returns values that range from 0.12 °C m for minimum conditions for modern dT_a, dT_d and MAT, to 0.25 °C m for the respective maximum conditions (Fig. 6, Table ~~5~~2). The consideration of mean values for temperature variations and MAT returns a $\overline{FCI}$ of 0.2 °C m, which is similar to the value of 0.17 °C m that results from the model where the 2002 temperatures are considered.

For site EW-03, situated at a relatively low elevation within the NW ~~headwall~~rockwall, the $\overline{FCI}$ modelling yields similar results as for the sites i~~o~~n the ~~other~~ opposite SE ~~side~~ face of ~~the~~ Mt. Eiger (Fig. 6), with intensities ranging from 0.10 °C m to 0.21 °C m. The mean MAT and mean temperature amplitude model run predicts an annual frost cracking intensity of 0.16 °C

m. For the sites EW-01 and EW-02, also situated on the NW ~~headwall~~rockwall but at higher elevations, the modelled minimum and maximum $\overline{FCI}$ values are lower and range from 0.07 °C m to 0.12 °C m. Also at these sites, the mean MAT and mean temperature amplitude model run returns a value of 0.094 °C m, which is very close to 0.089 °C m derived for the 2002 conditions. Accordingly, the model predicts a scenario where frost cracking processes at the upper NW sites (EW-02 and EW-01) are up to 50% less effective compared to the inferred frost cracking intensities at the ~~footwall~~ rockwall foot of the NW face~~side~~ (site EW-03; Fig.6) and on the SE locations (EM-01, -02).

5 Discussion

5.1 ~~Time scale of denudation rates~~Rockwall denudation from cosmogenic nuclide analysis

Denudation rates can be estimated from *in-situ* cosmogenic nuclide depth profile modelling (e.g, Hidy et al., 2010; Braucher et al., 2009). This method ~~can~~has been ~~be~~ applied for estimating the local denudation rates ~~estimation~~ in steep alpine rockwalls, and it has been very useful for extracting ~~and to infer~~ information on the ~~main~~mechanisms of denudation ~~mechanism~~, as shown in a recent ~~the pilot~~ study ~~with~~where denudation rates were measured with concentrations of cosmogenic ^{36}Cl in bedrock depth profiles at Mt. Eiger (Mair et al., 2019). We ~~tried to expand~~complemented the Mair et al. (2019) ~~the~~ denudation rate data-set by measuring concentrations of cosmogenic ^{10}Be ~~along~~for 5 samples in a bedrock depth profile at ~~(~~site EW-01 (~~;~~ Fig. 1), and we ~~and~~ modelled the local denudation rate over millennia (see Appendix A for details). The resulting ~~estimated~~rates ~~denudation~~ are ~~rate of~~ 63 ± 14 cm kyr^{-1}. ~~woul.~~ They are thus ~~d be~~ in good agreement with the results obtained for the close-by site EW-02 ~~of~~where the rates are 45 ± 9 cm kyr^{-1} (Mair et al., 2019). However, we note here that ~~due~~the ~~to~~ ^{10}Be concentrations are close to the blank background value, and that ~~and high~~the measurement uncertainties are high in some samples (up to 69 % for 1 σ). Therefore~~,~~ ~~different~~sample and measurement-specific blank corrections ~~approaches~~ would render the EW-01 samples non-~~un~~interpretable (see Appendix A).

Mair et al. (2019) measured relatively high ~~The cosmogenic nuclide depth profiles of Mair et al. (2019), i.e., by showing high concentrations at depth relative to the surface concentrations, were interpreted to preclude large rock fall events.~~ The concentrations of cosmogenic ^{36}Cl ~~nuclide depth profiles of Mair et al. (2019), i.e., by showing which most notably featured high concentrations~~ at depth relative to the surface ~~concentrations~~. These authors used this pattern~~, were~~~~and thus were interpreted~~ to preclude the occurrence of large rock fall events during the cosmogenic time scale, which in this case was several thousands of years. Instead, Mair et al. (2019) developed a scenario, based on Monte Carlo simulations, where ~~we interpret that~~ surface denudation has ~~should have~~ ~~has rather~~ been accomplished through multiple small-scale rock fall processes, where ~~dm~~cm-sized ~~large~~ bedrock particles have been removed at a high frequency from the ~~headwall~~rockwall surface. The episodic events have to occur on ~~a~~ spatial and temporal ~~small enough~~ scales that are small (< 1 cm to < 10 ~~d~~cm) and ~~over a~~ short enough ~~timescale~~ (< 1 yr), respectively, to be considered as a continuous erosional~~al~~ mechanism over ~~longer~~ time scales (> 10 yr) relevant for cosmogenic nuclide production. -We follow this interpretation and, ~~As~~ ~~as will be discussed in the next section~~consider that~~,~~ ~~and we explain~~ the small size of the particles involved in the rock fall processes are conditioned by the high density of fractures and faults (see next section). However, whereas the inferred mechanisms of denudation are likely to be the same across the entire Mt. Eiger, the erosional velocities are different. In particular, the denudation rates at sites EW-03 situated on the lower part of the NW ~~footwall~~~~base~~flank, and at sites EM01,-02 on the SE ~~flank~~rock face are > 150 cm kyr $^{-1}$, and thus 4 times ~~(45 ± 9 cm kyr^{-1}, Table 1)~~ ~~lower~~ higher than the denudation rates at sites EW-02 ~~a~~(45 ± 9 cm kyr^{-1}, Table 1) and EW-01, situated within the upper segment of the Eiger north face.~~,~~ As will be discussed in section 5.3~~ of this paper~~, we explain the spatial pattern of denudation rates by differences in frost shattering processes driven by the contrasts in insolation and temperature conditions. Please note that the modelled denudation rate estimates represent long-term, time-integrated values (e.g., Gosse and Phillips, 2001; Lal, 1991), most likely representative for the last millennium and possibly longer.

5.2 Preconditioning related to bedrock fabric

The rate of rock face denudation could be influenced by the bedrock fabric that affect rock failure in a complex and non-linear way (Krautblatter and Moore, 2014; Viles, 2013). Among these, fracture density and orientation has been considered as the most important variables as they positively correlate with rock wall denudation (Moore et al., 2009; Rapp, 1960; Terzaghi, 1962). In the context of rock fracturing by frost weathering processes, the permeability and porosity related to faults and fractures have been identified to significantly affect the boundaries of the frost cracking window (Draebing et al., 2017b; Matsuoka, 2001) and to limit water supply within the active layer of the bedrock (Andersen et al., 2015; Anderson et al., 2013; Rode et al., 2016; Sass, 2005). At ~~the~~ Mt. Eiger, the bedrock fabric, in both the NW and SE wall, is highly fractured along pre-existing structural weaknesses~~ (See section 4.2~~, which record the combined effect of stress and strain during Alpine orogenesis, and the differential responses of various bedrock lithologies to these conditions. In particular, ~~).~~ th~~Th~~e region surrounding ~~the~~Mt. Eiger is located at the geological contact between the crystalline rocks of the Aar massif, its sedimentary cover rocks and the Helvetic thrust nappes (Berger et al., 2017). During Alpine orogenesis, the bedrock was heavily deformed through multiple phases of folding and thrusting, which are recorded by a complex fabric in the exposed rock (Herwegh et al., 2017; Wehrens et al., 2017). At the cosmogenic sampling sites, the bedrock fabric is dominated by two generations of foliation and two sets of joints (Mair et al., 2018). Both foliations are considered to have formed at temperature conditions that were high enough for calcite minerals to deform in a ductile way (Mair et al., 2018). These structures are crosscut by two sets of brittle fault networks with steeply dipping fault planes, yielding a complex patter of fractures and foliations. ~~.~~Age assignments on the formation of these structures are still a matter of debate (Mair et al., 2018). ~~-~~We find that fractures are developed along foliation planes (S1, S3: Figs. 3 and 4) and are thus oriented parallel to weaknesses inherited from a tectonic stress field (e.g., Fig. 4b). Beside slight differences in the orientation of the foliations, there is little difference in the bedrock fabric between the SE and NW sides. These fractures effectively allow for the disintegration of bedrock into cm-~~ to dm-~~sized chips (e.g., Figs. 3a and 4a), which provides an explanation why there is no evidence in the cosmogenic dataset for the occurrence of large-scale rock fall processes (e.g., Mair et al., 2019). Instead, the production of small chips is most likely achieved by frost cracking and ice segregation growth as evidenced by the ice in the bedrock cracks during sampling in December 2016 (Figs. 4b,c). The ~~headwall~~rockwall parallel open joints (C2 in Fig. 5) in the NW and the large shear zones that dissect the mountain in NE – SW and SE - NW directions are suitable water pathways within the bedrock over large distances. Accordingly, the local bedrock fabric at all sites have the potential to allow for efficient bedrock weathering, and the large faults and shear zones are considered as suitable pathways for water to deeply penetrate through the mountain (Fig. 5e). However, while the high density of fractures and faults provides a suitable condition for the high-frequency occurrence of small-scale rock fall processes on both sites of the ~~Alps~~mountain, this variable alone is not capable of explaining the contrasts in denudation rates between the upper steep segment of the Eiger north face, and the other sites for which cosmogenic data is available.

~~-~~Another possible driver for rock fall activity could be ~~rock fracturing~~formation of sheeting joints in response to ~~from~~ paraglacial stress field adjustment after deglaciation (Grämiger et al., 2017; McColl, 2012; McColl and Draebing, 2019). However, we consider ~~sheeting joints in response to deglaciation~~this mechanism as unlikely to explain the differences in the denudation pattern because: 1) Suitable rockwall--parallel joints are only present in the NW (C2; Fig. 5), where they show a spacing of m to tens of meters. 2) The last possible glaciation was the LGM deglaciation period in the NW and the Younger Dryas in the SW, which would imply a response time of 9 ka or longer for sheeting joints to form~~ of 9 ka or longer~~. 3) Furthermore, the response time of stress release through sheeting ~~is related to~~depends on the rock quality (McColl, 2012). In highly fractured rock, as is the case for the limestone at Mt. Eiger, stress release should occur shortly after or during the deglaciation (McColl 2012; McColl and Draebing, 2019). The general likeliness of sheeting joints to form also depends on the pre-existing fracture density, where a high fracture density (as is the case at Mt. Eiger) better accommodates stresses during glaciation and deglaciation, which in turn hinders sheeting joints to form (McColl 2012). ~~However~~In summary, a reconfiguration of paraglacial stress might have been an important factor during the deglaciation and ~~sometime~~shortly thereafter, but we consider it unlikely as driving condition for the high-frequency release of cm- to dm-sized pieces of bedrock that we currently observe.~~.~~ As will be elaborated in the next sections, we rather relate the differences in denudation rates across the Eiger to the spatial pattern of frost cracking processes, which appears to be controlled by local insolation and temperature conditions.

5.3 ~~Headwall~~Rockwall temperature conditions and rock fracturing processes ~~and~~ efficiency

Variations in surface temperatures ~~-~~have been considered as one of the key variables driving mechanical disintegration of rock (e.g., Amitrano et al., 2012; Girard et al., 2013; Matsuoka, 2008). The instrumental record (Gruber et al., 2004b) of near ground surface temperatures (NGST; recorded at 10 cm bedrock depth) are a good proxy for the temperature conditions at the upper NW wall (sites EW-01,-02) and for the SE wall (sites EM-01,-02), as they have recorded ~~actual~~ in-situ rock temperatures (Allen et al., 2009), which vary~~ies~~ from air temperatures (Anderson, 1998). The individual sampling sites are close to the temperature logger sites, with differences in elevation of 16 m to 57 m for the sites in the NW wall and 28 m to 50 m for the sites in the SE wall, respectively. In addition, the logger sites are characterized by similar local aspect and slope as our cosmogenic sampling sites. A potential difference in local temperature variability of up to ~ 6 °C (Draebing et al., 2017a; Haberkorn et al., 2015) might arise from extended periods of sufficient snow cover. We cannot rule out the occurrence of snow cover for our cosmogenic sampling sites as snow might also accumulate on steep ~~headwall~~rockwalls as ~~the~~ Mt. Eiger (Draebing et al., 2017a; Haberkorn et al., 2015). However, due to the similar position, aspect and slope we do not consider that the logger sites experienced different conditions than the cosmogenic ~~nuclide~~ sampling sites. The calculated averages of temperatures, based on 7 full hydrological years between 2001 and 2014 each, are in good agreement with the temperature values for the hydrological year 2002 (Table 1). They show a large difference in MAT (~ 2 °C), mean annual and mean diurnal amplitude (~ 1.6 °C) ~~for~~ between the NW ~~headwall~~rockwall and the SE face, with the SE face experiencing higher and more variable temperatures, despite being at ~ 300 m higher elevation. We relate this difference to the effect of the mountain and ~~headwall~~rockwall geometry (Noetzli et al., 2007), which result in a strong insolation difference between the NW and SE walls (Fig. ~~7~~2). The processes that could be affected by this variable include permafrost degradation, thermal stresses, volumetric expansion of ice from freezing and thawing, or frost cracking from ice segregation. All of t~~T~~hese processes have the potential to weaken the bedrock trough fracturing, ~~and~~ thereby preconditioning the occurrence of rock fall processes. We first assess the general probability and potential effect of each process for the ~~the~~ Mt. Eiger ~~Mountain~~ sites before we discuss potential controls on the denudation efficiency.

Permafrost degradation has been shown to significantly reduce rock wall stability (Gruber et al., 2004a; Haeberli et al., 1997). For the cosmogenic sampling sites,~~ statistical permafrost models predict that permafrost is likely to have occurred at least for some time in the past (Boeckli et al., 2012b, 2012a), but is expected to be more widespread in the upper NW headwallrockwall than in the SE and the NW footwall rockwall foot (Fig. 2). However,~~ the relatively high temperatures (MAT = 1.8 °C; Table 1) rule out the occurrence of permafrost (Gruber et al., 2004b; Noetzli et al., 2007) particularly at the cosmogenic sites in the SE face, while lower MATs (< 0°C) potentially allow~~ing~~ for permafrost occurrence in the upper NW rockwall, at least during the past. Thus, degradation through permafrost alone seems an unlikely mechanism to explain the difference in denudation across the Eiger because it would affect the upper NW wall in an opposite way, which is not the case. However, despite the general ~~increasing~~increase ~~of~~in the number and the size of ~~cracking~~cracks at the freezing front ~~in~~under permafrost conditions (Murton et al., 2006), the occurrence of permanently frozen rock might limit the ~~availability~~ supply of water within the rock itself, especially at colder temperatures ~~without~~where ~~a~~ water reservoirs might be absent (e.g., Andersen et al., 2015; Anderson et al., 2013; Draebing et al., 2017b).

Thermal stresses and subsequent expansion and contraction from daily solar temperature fluctuations can weaken bedrock and cause the growth of subcritical fractures ~~growth~~ (Aldred et al., 2016; Eppes et al., 2016). The occurrence of cycles where cracks open and close on a daily basis has indeed been observed in rock slopes (Draebing et al., 2017b; Rode et al., 2016). This mechanism has been shown to lead to a progressive growth of cracks (Collins and Stock, 2016). Thermal-mechanical rock fracturing would especially affect the SE wall, as ~~it~~ this flank experiences significantly more direct insolation throughout a year (Fig. 2~~7~~). In a similar sense, volumetric expansion from freezing and thawing can also occur ~~under natural conditions~~ (Matsuoka, 2008), but ~~it~~ these processes are ~~is~~ limited by ice extrusion and require~~s~~ a high degree~~s~~ of water saturation and fast freezing (Davidson and Nye, 1985; Matsuoka and Murton, 2008). However, recent field (Draebing et al., 2017b) and laboratory experiments (Draebing and Krautblatter, 2019) ~~in similar environments~~ disclosed little evidence for significant frost cracking from volumetric expansion. Therefore, ~~(Draebing et al., 2017b) and cracking in lab environment (Draebing and Krautblatter, 2019). Thus,~~ we do not consider that this mechanism exerts a significant control on the denudation rates at our cosmogenic nuclide sampling sites.

Instead, we consider frost cracking from ice segregation and progressive growth of ice lenses (Walder and Hallet, 1985) as ~~the most~~a suitable mechanism that explains the denudation pattern we observe at ~~the~~ Mt. Eiger. Hallet et al. (1991) showed that t~~T~~hese processes ~~have supposedly~~ have the potential to generate large stresses up to 30 MPa in bedrock ~~(Hallet et al., 1991)~~. However, recent ~~findings~~experiments revealed ~~suggest~~ much lower stresses, which only allow for subcritical cracksing ~~to grow under subcriticasubcritical conditionsl crack growth~~ (Draebing and Krautblatter, 2019). Frost cracking has ~~been~~ often been ~~shown to be most effective~~associated within a frost cracking temperature window (FCW) ~~of~~ between -3 °C to -8 °C within the rock (Hales and Roering, 2007; Walder and Hallet, 1985), but this temperature window ~~might be~~is affected by ~~rock~~ the mechanical properties of the ~~rock~~bedrock itself (Draebing et al., 2017b; Draebing and Krautblatter, 2019; Matsuoka, 2001; Walder and Hallet, 1985). Theoretical modelling shows that ~~whereas~~ the lower boundary of ~~the~~ this window has no significant effect on the cracking efficiency.~~,~~ W~~w~~hile an upper FCW boundary of -3°C ~~should be considered to best capture the experimental results, particularly for limestone~~ was suggested by ~~(~~Hallet et al. (~~,~~1991) and~~;~~ Matsuoka (~~,~~2001) for limestone~~,).~~ Draebing and Krautblatter (2019) thought that experimental results are consistent with an upper FCW boundary of ~~However, recent findings found upper boundaries of~~ up to -0.64°C. Furthermore, these authors also~~C (Draebing and Krautblatter, 2019) and~~ suggested a strong dependency of the FCWe on lithology, crack geometry and fracture toughness (Rempel et al., 2016; Walder and Hallet, 1985). We tested the ~~sensitivity of our results to the~~dependency of the frost cracking intensity on the FCW ~~window~~ by applying values that were determined by Draebing et al. (2017b) for slaty gneiss (instead for limestone). ~~calculated for slaty gneiss from Draebing et al. (2017b). The results of these~~The model runs ~~indicate~~disclose two observations: First, ~~that~~ the general pattern of the annual cracking intensity in relation to the MAT ~~over MATs~~ remains the same ~~over~~for various FCW~~-MAT~~s. Second and most important, ~~and~~ the differences in~~t~~ intensities ~~for~~between the upper NW and the~~vs~~ lower NW and SE ~~conditions~~sites also remain the same (see Appendix B). However, the models also predict ~~predicted~~that the total fracture intensity increases with ~~(i)~~ the size and the upper boundary of the FCW (Fig. B1)~~, and (ii) higher~~ . ~~and the increase with changes in MATs.~~ ~~increase with the size and the upper boundary of the FCW (Fig. B1).~~ Thus, further studies on the lithology specific FCW is needed to compare our predicted cracking intensity ~~to~~with the results of other studies. ~~Furthermore~~

T~~, t~~he selection of values for the thermal conductivity of ~~the~~ bedrock ~~used in the model~~ might also affect the predicted fracture intensity~~results~~. In particular, while~~,~~ ~~as~~ lower conductivities (i.e., 1.2 W m^{-1} K^{-1}) tend to promote ~~increase the predicted~~the cracking processes~~-cracking intensity~~, ~~while~~ higher conductivities (i.e., ≥ 6.5 W m^{-1} K^{-1}) ~~decrease~~mitigate the occurrence of cracking ~~it~~ to the point ~~of~~where any frost cracking differences ~~completely erasing any significant difference with changes in MAT od~~ between the ~~different~~various sites at Mt. Eiger become undetectable~~non-measurable~~ (Fig. B2). However, the selected standard value of 3 W m^{-1} K^{-1} is in good agreement ~~for~~with ~~reported~~ values reported for limestone or sandstone where temperatures are close to 0 °C (Schön, 2015). Therefore, we do not consider that ~~we and thu~~our assigned values to the conductivity~~s, it does~~ introduce a bias in the ~~not distort the~~ model ~~predictions~~.

~~-~~In general, water needs to be available for continued and efficient cracking ~~Generally, frost cracking~~ from ice segregation, and the model employed in this study scales cracking intensity with the availability of liquid water~~-ability~~. ~~-~~For steep and bare bedrock ~~has~~ this has been related to two distinct temperature conditions: i) cold regions with negative MATs and ii) warm regions with positive MATs, where temperatures occasionally reach the frost cracking window (Andersen et al., 2015; Anderson et al., 2013; Delunel et al., 2010; Hales and Roering, 2007; Savi et al., 2015). ~~For the negative MAT case, water needs to be available for continued and efficient cracking.~~ Accordingly, in the absence of a regolith cover as a reservoir, bare bedrock might stay frozen over longer periods and therefore permafrost might reduce the ~~cracking efficiency~~water availability (Andersen et al., 2015; Draebing et al., 2017b). For ~~the~~ positive MATs~~ case~~, frost cracking ~~only~~ is predicted to only occur~~s~~ in winter~~,~~ when the surface is frozen and water is available from within the bedrock (Andersen et al., 2015; Anderson et al., 2013). ~~In winter, however, cracking intensity could be reduced through a regolith layer, which would prevent the bedrock from reaching the temperatures of the frost cracking window.~~ Extended snow cover could increase the frost cracking activity, since it has been shown to maintain the temperatures in the frost cracking window for a longer time interval, which facilitates the opening of fractures (Draebing et al., 2017b). For our ~~Eiger~~ sites at Mt. Eiger, the lower NW and the SE sites fall within the second temperature conditions favorable for frost cracking (Table 1), and water should be available through the network of faults within the bedrock (see Section 4.2). For the upper part of the north face, estimations of MATs ~~estimation~~ return ~~modern~~ values of -0.5 °C for the present (Table 1). For these conditions, ~~, which correspond to a condition for which~~ all models predict a limited cracking efficiency from ice segregation (Andersen et al., 2015; Anderson et al., 2013; Hales and Roering, 2007). ~~At these conditions~~In addition, predicted frost cracking occurs only at shallow depths, as the deeper rock is ~~completely~~ frozen without any water circulation particularly in winter. In summer, however, pore water is likely to be available, but bedrock temperatures are not reaching the FCI window. ~~As~~ As a result, all ~~modelled~~ models predict that in the SE wall and in the lower part of the NW flank, ~~annual $\overline{FCI}$s~~frost cracking processes are likely twice as efficient ~~predict that cracking in the SE and lower NW footwall section~~as in the upper part of the NW face ~~-is likely to be twice as efficient as in the upper segment of the north face~~ (Figs. 6, and 7~~8~~; Table 2~~5~~). In summary, we consider that frost cracking from ice segregation, potentially affected by permafrost, and thermal stress as the most important mechanisms for ~~the difference in rock fracturing~~the erosion of Mt. Eiger. The effectiveness of these processes is additionally enhanced by mechanical weaknesses in the bedrock due to faults~~, gauges~~ and foliations.

5.4 Past and future conditions

The modelled minimum exposure ages are 0.7 ka for EW-01, ~~are 0.7 ka~~ and 0.9 ka for EW-02 with apparent minimum exposure ages of up to 1.7 ka for EW-02 (Mair et al., 2019). This suggests ~~, which implies~~ that the denudation rates represent integrated averages for at least these time periods. Thus, conditions during these times might have changed. Modifications in local exposure geometry and ~~in~~ insolation could have only been achieved through the occurrence of bergsturz events (> 1 M m^3 rockfall volume).~~can be ruled out, which w~~We do not consider that this was the case because geological maps show that~~justify this through a lack of evidence for large rock fall~~~~suitable sediment deposits in local geological maps~~ are no voluminous scree deposits at the talus of Mt. Eiger (e.g., ~~(~~Günzler-Seifert and Wyss, 1938; Mair et al., 2018~~)~~) ~~events, which could have changed the local insolation conditions~~. Therefore, and because of the dependency of rock fracturing on temperatures, we consider variations in temperatures over the last two millennia~~um~~ as the only potential variable. However, $\overline{FCI}$ calculated for mean current temperatures ~~conditionss~~ are not exceeding the $\overline{FCI}$ estimated for maximum temperature excursions in the past. This is even the case for ~~,s~~ the medieval and Roman climate optimum, which was the warmest period with the largest temperature difference to the modern times~~and the~~~~even for the highest related variability difference during the warmest periods, which is are the medieval and Roman climate optimum~~ (Fig. 6). In contrast, colder conditions, which could have prevailed during the little ice age and the migration period, would have resulted in a lower efficiency of frost cracking at all cosmogenic sites (Table 1)~~s. This~~This reduction would have been ~~be~~ caused by a lower ~~reduced~~ water availability in the SE wall, and by temperatures ~~not~~that were too low to ~~being low enough to again~~ promote frost cracking ~~again~~ in the NW flank. ~~. However,~~ However, we note that the calculated differences in $\overline{FCI}$ between a warmer or a colder paleo-climate are lower than the contrasts in modern $\overline{FCI}$ between the upper sites in the NW ~~headwall~~rockwall and the lower location on the same face~~side~~ of ~~the~~ Mt. Eiger. They are also lower than the modern $\overline{FCI}$ contrasts between the upper NW and SE ~~headwall~~rockwall sites.

Temperatures are projected to increase during the 21st century up to 0.36°C per decade for the European Alps (emission scenario A1B; Gobiet et al., 2014). Mean annual air temperatures for Switzerland in 2100 AD could ~~be~~ increase by ~~between~~ 1.9 °C and ~~up to~~even 5.4 °C ~~higher than in~~compared with the period 1981-2010 (emission scenarios RCP2.6 and RCP 8.5, respectively; CH2018). These ~~projected~~ inferred differences in temperatures are larger than all~~the~~ reconstructed ~~variations~~ excursions for the past (Table 1~~Fig. 6~~). Such an increase in temperature could enhance the efficiency of frost cracking under similar diurnal and annual temperature amplitudes, especially in combination with permafrost degradation (Gruber and Haeberli, 2007), e.g., in the upper part of the NW ~~headwall~~rockwall. However, changes in precipitation and reduction of time spent in the frost cracking window might shift the overall controls on fracturing ~~control~~ to amplified thermal stresses, especially boosting rock fracturing on the SE face (Draebing et al., 2017b).

6 Conclusions

For our sites at ~~the~~ Mt. Eiger, ^{10}Be and ^{36}Cl nuclide inventories along depth profiles show that denudation on the SE wall and at the ~~footwall~~ base of the NW ~~flank~~rock face (Fig. 7~~8~~) are up to 4 times higher than the rates determined for the upper part of the NW ~~headwall~~rockwall. These conditions might have prevailed for several centuries to millennia. The difference in the long-term average denudation rates particularly between the upper ~~headwall~~rockwall of the Eiger north face~~,~~ and the ~~footwall~~ base, and the SE face~~side~~ of this mountain, can be related to different efficiencies of rock fracturing processes, which strongly depend on temperature conditions (Fig. 7~~8~~). Modelling indicates a strong contrast in frost cracking efficiency from ice segregation between the upper (relatively low) and lower sites on the NW wall (relatively large efficiency), but also between the upper site on the NW ~~flank~~rock face of ~~the~~ Mt. Eiger and the SE sites (also relatively large efficiency), which is caused by local temperature conditions. The contrast might be enhanced by permafrost in the upper NW wall. This could ~~, which would~~ potentially~~further~~ ~~could~~ reduce ~~water~~the availability of water and decrease ~~thereby reduce~~the cracking efficiency. Furthermore, thermal stresses from differences in insolation might additionally enhance rock fracturing in the SE rock faces. Throughout the last millennium, conditions have been very similar to the present temperatures in bedrock, yet ~~.~~ c~~C~~older temperatures during the little ice age might have slightly reduced frost cracking efficiency.

Appendix A: Denudation rate from *in-situ* cosmogenic ^{10}Be depth profile

We measured concentrations of cosmogenic ^{10}Be along a depth profile at site EW-01 (Fig. 1) to extract information on local bedrock denudation rate, and exposure age. These variables were derived through Monte Carlo (MC) depth profile modelling techniques (Hidy et al., 2010).

Sampling and ^{10}Be measurement

We collected five bedrock samples within a depth profile at site EW-01 (Fig. 01; Table 1) from quartz bearing recrystallized chert layers, from the wall of a tunnel that connects the Jungfraubahnen railway tunnel with the rockwall surface. The samples were collected ~~on~~from the intact, bare bedrock wall, while the surface sample was taken ~~on~~form the current bedrock face next to the tunnel opening. The bedrock material was quarried with a battery saw and chisel, thereby following standard sampling protocols (Dunai and Stuart, 2009). Each sample was 5 to 10 cm thick and consisted of 1 to 1.5 kg of rock material. Concentrations of cosmogenic ^{10}Be were measured on quartz grains that were extracted from these samples. Sample preparation followed the procedure of Akçar et al. (2012) and took place at the Institute of Geological Sciences, University of Bern. ^{10}Be/^{9}Be ratios were measured by accelerator mass spectrometry (AMS) at the AMS facility at ETH Zurich, and were normalized to internal standard S2007N (Christl et al., 2013). The measured ratios were corrected ~~with~~using a long-term, variance-weighted average, full process blank ratio ~~correction~~ of 2.48 x 10^{-15} with a relative weighted uncertainty of 18.8% (from 28 in-batch measured blanks from the same ^{35}Cl spike preparation over several ~~months time~~months' time). T~~he correction~~his amounted to a relative correction between 3 and < 19 %. We used the long-term average, as we consider the spike as main source of contamination of the blank and samples and thus, of stochastic nature. However, we note that the measured in-batch blank showed a ratio of (4.81 ± 1.12) x 10^{-15}. Using this value for correction would amount to relative blank corrections between 29% - 36% for samples EW-01-4, -5 and -6, which would render them uninterpretable, as concentrations would be too low to be considered as reliabl~~ye~~y detected. Thus, all subsequent steps in processing and interpretation on the ^{10}Be data rely on the validity of the long-term, variance-weighted average blank correction.

Nevertheless, the rock samples show ^{10}Be concentrations (Fig. A1) that range~~ing~~ from 1.9 x 10^4 at g^{-1} to 0.35 x 10^4 at g^{-1} (Table A1) and that decrease with depth. The standard 1σ error (ranging from 0.07 x 10^4 at g^{-1} to 0.24 x 10^4 at g^{-1}; Table A1), which accounts for AMS reproducibility and counting statistics, shows relative uncertainties~~y~~ ranging from 11 % to 69 %. These uncertainties are high, however, due to the low concentrations they still allow for a meaningful profile modelling.

Depth profile modelling

In-situ cosmogenic ^{10}Be is mainly produced through spallation and muon reactions on O and Si (Gosse and Phillips, 2001). Accordingly, the production needs a scaling to geographic position and elevation, and it needs a correction for shielding from secondary cosmic ray particles (Gosse and Phillips, 2001; Lal, 1991). Production rate scaling for spallation production was done using the method of Stone (2000), which is based on the work of Lal (1991). We updated these approaches using the recalibrated reference dataset of Borchers et al. (2016) for our scaling framework. For the consideration of muogenic production, we used the parametrization scheme by Balco et al. (2008), which is based on muogenic production systematics presented by Heisinger et al. (2002a,b). The experimental fit for muogenic production of these authors, however, is known to yield in an up to ~ 40% overestimation of muogenic ^{10}Be production (Borchers et al., 2016; Braucher et al., 2003, 2013). To account for this e~~a~~ffect, an uncertainty of 40 % was assigned on the muogenic production during the MC modelling, which is described below. We finally computed an open sky visibility ~~on~~over 1° azimuthal increments to account for rockwall and bedrock specific geometry and shielding. This was done using a high resolution (2m) DEM provided by the Swiss Federal Office of Topography (Swisstopo) as basis. We used the combination of these constraints to calculate a total site-specific shielding factor (S_T) and apparent attenuation length ($\Lambda_{f,e}$) for spallogenic production with the CRONUS Earth online Topographic Shielding Calculator v2.0 (Marrero et al., 2016). The shielding factor (S_T) was used to correct for both spallogenic and muogenic production, which is necessary due to the large height of the rockwall (Mair et al., 2019). The site-specific apparent attenuation length for spallogenic production ($\Lambda_{f,e}$) was used to correct for geometric effects (Dunne et al., 1999; Gosse and Phillips, 2001). A detailed discussion of the approach can be found in the supplement of Mair et al. (2019).

The modelling of TCN profiles in bedrock requires the consideration of possible inherited nuclides from previous exposure. For bedrock profiles, we explain the occurrence of inherited nuclides with a history where bedrock was previously exposed to cosmic rays. This could have been achieved in a scenario where the current exposure started with an erosion event that was too small to completely reset the TCN clock. Alternatively, inherited nuclides at depth can build up through a prolonged period during which the exposed surface has experienced a low denudation rate. Such a mechanism would allow for the accumulation of “excess nuclides” at depth. However, since such an exposure can only occur through a removal of bedrock material, such ~~an~~ a concentration of inherited nuclides would have been produced by muons only (due to the position of the sample at significant depth) and would follow an exponential decrease with depth (Mair et al., 2019). To account for excess nuclides, we modelled an inherited nuclide concentration for the surface sample (C_{inh}), which we used to parametrize potentially inherited nuclides at depth ($C_{inh,z}$) following

$$C_{inh,z} = C_{inh} \cdot e^{\left(-\frac{z}{\Lambda_{inh}}\right)}.$$

We used the value of a fitted muon attenuation length of 4852 g cm^{-2} for Λ_{inh}, which is in good agreement with published reconstructed muon attenuation lengths (Braucher et al., 2013).

In general, a MC approach for depth profile modelling requires initial ~~computational~~ boundaries for the modelled quantities, i.e., exposure age, potential inherited nuclides and denudation rate (Hidy et al., 2010). We selected a broad range for these values in an effort not to predetermine the solution space and thus not to bias the interpretation. We thus set a constraint of (i) 75 ka on the exposure age (which is an uppermost limit given the 20 ka for the LGM), (ii) the ^{10}Be concentration of the surface sample (i.e., 1.9 x 10^4 at g^{-1}) for inherited nuclides at depth and (iii) a maximum rate of 1500 cm kyr^{-1} on the denudation variable and thus a maximum of 12, 15 and 20 m for the cumulative amount of denudation for up to 75 ka. These estimates are considered as conservative values because they represent uppermost bounds for a possible exposure age, denudation rate and an inherited concentration (for a full justification see method section of Mair et al., 2019). We used these 3 values because the deepest samples were taken at depths close to or exceeding 7 m and consequently, the production of TCN has almost exclusively occurred by muon pathways. Muon attenuation scales exponentially, with reported muon attenuation lengths between ~4000 and 5300 ± 950 g cm^{-2} for 2.7 g cm^{-3} rock density (e.g., Braucher et al., 2013). This translates ~~to~~into muon attenuation depths of ~15 and ~19 m for 1 attenuation length, and ~30 to ~38 m for 2 attenuation lengths, which accounts for a reduction of muogenic production by ~63% and ~87%, respectively. This means that independent of the attenuation length, our deepest samples would have to be located at a depth of > 23 m at the start of the exposure to allow for more than 20 m of total erosion to occur. Any potential nuclides inherited from before would then have accumulated at this depth or even deeper (Mair et al., 2019). The main purpose of running three setups for the cumulative amount of denudation is to test whether ~~the independence of~~ the model results depend on the initial ~~parameter~~ constraints on denudation, which is not the case here (see next chapter). We note that this approach is not applicable to extract exposure ages without independent denudation constraints (Anderson et al., 1996; Hidy et al., 2010).

For rock density, we employed a uniform value of 2.68 ± 0.04 g cm^{-3} to account for the full density range between pure quartz (2.65 g cm^{-3}), the local limestone (2.68 ± 0.02 g cm^{-3} measured by Mair et al., 2019) and pure limestone (2.71 g cm^{-3}). This also includes density effects related to the occurrence of nodular chert, which was sampled for the purpose of this study. We ran the MC model until we obtained 10^5 profiles where the modeled concentrations fall within a 2σ-confidence interval of the measured ^{10}Be concentrations (which corresponds to reduced χ^2 value < 3.09). All input parameters for the MC modelling are reported in Table A2. The documentation and raw results are provided in the supplement file.

Model results

The MC simulation returned 10^5 profiles where the model concentrations are within a 2σ measurement confidence interval with a minimum ~~at~~of reduced χ^2 = 2.32, ~~which~~while χ^2 are lowest close to the mean and the estimates of ~~median~~ denudation rates ~~and inherited nuclide estimation~~. The MC simulation returns consistent values for inherited nuclides and denudation rate, where mean and median values are in good agreement and follow a well-defined Gaussian distribution (Fig. A~~3~~1; complete modelling results are provided in the Supplement). Thus, the MC simulation results are independent of the initial constraint on total denudation (Table A3). In detail, mean modelled inherited concentrations range from (2.4 ± 0.6) x 10^3 at g^{-1} to (2.6 ± 0.7) x 10^3 at g^{-1} ^{10}Be, accounting for 13 – 14% of the measured concentration for the surface sample. Mean denudation rate values range between (63.4 ± 13.5) cm kyr^{-1} and (64.7 ± 12.1) cm kyr^{-1}. Surface exposure ages cannot be estimated from ~~the differing distributions forof~~ the model run resultss. However, the MC simulations yield agreeing minimum ages of 0.7 ka.

Appendix B: Sensitivity of the frost cracking model

The frost cracking model of Andersen et al. (2015), which was employed in this paper, was run with the authors' standard setup, using the input values given in Table B1. The resulting annual $\overline{FCI}$ predictions are most sensitive to flow restrictions for water and to different FCW windows (Andersen et al., 2015). The former are discussed in detail by Andersen et al. (2015). These authors concluded that in case where no restrictions are set to water supply and water flow, then the cracking intensity is predicted to increase for positive MATs, but the relationships between MATs and the predicted $\overline{FCI}$s will remain. In contrast, in case where water supply is substantially restricted, then $\overline{FCI}$ values will increase for negative MATs (Andersen et al., 2013; 2015 see their Fig. 11). According to Anderson et al. (2015), only the predicted $\overline{FCI}$ pattern and intensity will only change significantly for the case where the FCW will be lowered to the window between -15 to -4 °C. However, the sensitivity analysis of these authors did not incorporate the range of recently reported FCW values for slaty gneisses (Draebing et al., 2017b), which are characterized by a significantly higher upper temperature threshold (i.e., -9.3 °C to -1.4°C) and a smaller temperature range (i.e., -4.5 to -1.8 °C). We used these values together with a FCW between -8 to -3 °C, which has been proposed for limestones (Matsuoka, 2001). With this setup, we aim to test the sensitivity of the model on the FCW. While the model predicts higher absolute $\overline{FCI}$ intensities for higher upper threshold temperatures, the relative relation with the MAT remains the same for all our settings and temperature regimes (Fig. B1). We further tested the sensitivity of the model for the thermal conductivity values that we employed in this paper, because thermal conductivities vary with bedrock type (e.g., Schön, 2015; and references therein). We did so by running the model with standard settings and bedrock thermal conductivity values of 1.2 and 6.5 W m^{-1} K^{-1}. This corresponds to the upper and lower bounds for gneisses and to the mean values for mono-mineralic quartz (Schön, 2015; and references therein). The results predict an absolute and relative increase in predicted $\overline{FCI}$ for positive MATs and for lower thermal conductivities. In contrast ,very high thermal conductivities would reduce $\overline{FCI}$ to a point, where no significant dependence on the MAT is present (Fig. B2). We note here that reported values for limestone at temperatures close to 0°C are close to the standard model value of 3.0 W m^{-1} K^{-1}.

Code availability

The code for the MC simulations is a modified version of the Mathcad™ file of Hidy et al. (2010), and provided in the supplement file. The code for the frost cracking model is available in the supplement of Andersen et al. (2015).

Data availability

Temperature data are online available through the Swiss Permafrost Monitoring Network, PERMOS (~~http://dx.doi.org/10.13093/permos-2016-01~~http://dx.doi.org/10.13093/permos-2016-01) and spreadsheet used for extraction can be found in the supplement file. Raw MC output is provided in the supplement file.

Author contributions

DM, FS and NA designed the study; DM and AL conducted the fieldwork. DM and SY processed the samples, whereas CV and MC were responsible for the AMS measurement. DM employed the frost cracking modelling and interpreted all data with additional scientific input from DT, RD and NA, and used the Monte Carlo code updated by DT. DM prepared the manuscript and figures with contributions from all co-authors.

Competing interests

The authors declare that they have no conflict of interest.

Acknowledgements

We thankfully acknowledge the logistic support and access to the railway tunnel from the “Jungfraubahnen” Railway Company and the High Altitude Research Stations Jungfraujoch and Gornergrat (HFSJG). This research was funded by the Swiss National Science Foundation through grant No 159299 awarded to Fritz Schlunegger.

References

Akçar, N., Deline, P., Ivy-Ochs, S., Alfimov, V., Hajdas, I., Kubik, P. W., Christl, M. and Schlüchter, C.: The AD 1717 rock avalanche deposits in the upper Ferret Valley (Italy): A dating approach with cosmogenic 10Be, J. Quat. Sci., 27, 383–392, doi:10.1002/jqs.1558, 2012.

Aldred, J., Eppes, M. C., Aquino, K., Deal, R., Garbini, J., Swami, S., Tuttle, A. and Xanthos, G.: The influence of solar-induced thermal stresses on the mechanical weathering of rocks in humid mid-latitudes, Earth Surf. Process. Landforms, 41, 603–614, doi:10.1002/esp.3849, 2016.

Allen, S. K., Gruber, S. and Owens, I. F.: Exploring steep bedrock permafrost and its relationship with recent slope failures in the Southern Alps of New Zealand, Permafr. Periglac. Process., 20, 345–356, doi:10.1002/ppp.658, 2009.

Amitrano, D., Gruber, S. and Girard, L.: Evidence of frost-cracking inferred from acoustic emissions in a high-alpine rock-wall, Earth Planet. Sci. Lett., 341–344, 86–93, doi:10.1016/j.epsl.2012.06.014, 2012.

Andersen, J. L., Egholm, D. L., Knudsen, M. F., Jansen, J. D. and Nielsen, S. B.: The periglacial engine of mountain erosion – Part 1: Rates of frost cracking and frost creep, Earth Surf. Dyn., 3, 447–462, doi:10.5194/esurf-3-447-2015, 2015.

Anderson, R. S.: Near-Surface Thermal Profiles in Alpine Bedrock: Implications for the Frost Weathering of Rock, Arct. Alp. Res., 30, 362, doi:10.2307/1552008, 1998.

Anderson, R. S., Repka, J. L. and Dick, G. S.: Explicit treatment of inheritance in dating depositional surfaces using in situ 10Be and 26Al, Geology, 24, 47, doi:10.1130/0091-7613(1996)024<0047:ETOIID>2.3.CO;2, 1996.

Anderson, R. S., Anderson, S. P. and Tucker, G. E.: Rock damage and regolith transport by frost: An example of climate modulation of the geomorphology of the critical zone, Earth Surf. Process. Landforms, 38, 299–316, doi:10.1002/esp.3330, 2013.

Balco, G., Stone, J. O., Lifton, N. A. and Dunai, T. J.: A complete and easily accessible means of calculating surface exposure ages or erosion rates from 10Be and 26Al measurements, Quat. Geochronol., 3, 174–195, doi:10.1016/j.quageo.2007.12.001, 2008.

Borchers, B., Marrero, S., Balco, G., Caffee, M., Goehring, B., Lifton, N., Nishiizumi, K., Phillips, F., Schaefer, J. and Stone, J.: Geological calibration of spallation production rates in the CRONUS-Earth project, Quat. Geochronol., 31, 188–198, doi:10.1016/j.quageo.2015.01.009, 2016.

Braucher, R., Brown, E. T., Bourlès, D. L. and Colin, F.: In situ produced 10Be measurements at great depths: Implications for production rates by fast muons, Earth Planet. Sci. Lett., 211, 251–258, doi:10.1016/S0012-821X(03)00205-X, 2003.

Braucher, R., Bourlès, D., Merchel, S., Vidal Romani, J., Fernadez-Mosquera, D., Marti, K., Léanni, L., Chauvet, F., Arnold, M., Aumaître, G. and Keddadouche, K.: Determination of muon attenuation lengths in depth profiles from in situ produced cosmogenic nuclides, Nucl. Instruments Methods Phys. Res. Sect. B Beam Interact. with Mater. Atoms, 294, 484–490, doi:10.1016/j.nimb.2012.05.023, 2013.

Büntgen, U., Frank, D. C., Nievergelt, D. and Esper, J.: Summer Temperature Variations in the European Alps, <scp>a.d.</scp> 755–2004, J. Clim., 19, 5606–5623, doi:10.1175/JCLI3917.1, 2006.

Büntgen, U., Tegel, W., Nicolussi, K., McCormick, M., Frank, D., Trouet, V., Kaplan, J. O., Herzig, F., Heussner, K.-U., Wanner, H., Luterbacher, J. and Esper, J.: 2500 Years of European Climate Variability and Human Susceptibility, Science (80-.)., 331, 578–582, doi:10.1126/science.1197175, 2011.

Christl, M., Vockenhuber, C., Kubik, P. W., Wacker, L., Lachner, J., Alfimov, V. and Synal, H. A.: The ETH Zurich AMS facilities: Performance parameters and reference materials, Nucl. Instruments Methods Phys. Res. Sect. B Beam Interact. with Mater. Atoms, 294, 29–38, doi:10.1016/j.nimb.2012.03.004, 2013.

CH2018 – Climate Scenarios for Switzerland, Technical Report, National Centre for Climate Services, Zurich, 2018.

Collins, B. D. and Stock, G. M.: Rockfall triggering by cyclic thermal stressing of exfoliation fractures, Nat. Geosci., 9, 395–400, doi:10.1038/ngeo2686, 2016.

Davidson, G. P. and Nye, J. F.: A photoelastic study of ice pressure in rock cracks, Cold Reg. Sci. Technol., 11, 141–153, doi:10.1016/0165-232X(85)90013-8, 1985.

Delunel, R., van der Beek, P. A., Carcaillet, J., Bourlès, D. L. and Valla, P. G.: Frost-cracking control on catchment denudation rates: Insights from in situ produced 10Be concentrations in stream sediments (Ecrins-Pelvoux massif, French Western Alps), Earth Planet. Sci. Lett., 293, 72–83, doi:10.1016/j.epsl.2010.02.020, 2010.

Draebing, D. and Krautblatter, M.: P-wave velocity changes in freezing hard low-porosity rocks: A laboratory-based time-average model, Cryosphere, 6, 1163–1174, doi:10.5194/tc-6-1163-2012, 2012.

Draebing, D. and Krautblatter, M.: The Efficacy of Frost Weathering Processes in Alpine Rockwalls, Geophys. Res. Lett., 46, 6516–6524, doi:10.1029/2019GL081981, 2019.

Draebing, D., Krautblatter, M. and Dikau, R.: Interaction of thermal and mechanical processes in steep permafrost rock walls: A conceptual approach, Geomorphology, 226, 226–235, doi:10.1016/j.geomorph.2014.08.009, 2014.

Draebing, D., Haberkorn, A., Krautblatter, M., Kenner, R. and Phillips, M.: Thermal and Mechanical Responses Resulting From Spatial and Temporal Snow Cover Variability in Permafrost Rock Slopes, Steintaelli, Swiss Alps, Permafr. Periglac. Process., 28, 140–157, doi:10.1002/ppp.1921, 2017a.

Draebing, D., Krautblatter, M. and Hoffmann, T.: Thermo-cryogenic controls of fracture kinematics in permafrost rockwalls, Geophys. Res. Lett., 44, 3535–3544, doi:10.1002/2016GL072050, 2017b.

Dunai, T. J. and Stuart, F. M.: Reporting of cosmogenic nuclide data for exposure age and erosion rate determinations, Quat. Geochronol., 4, 437–440, doi:10.1016/j.quageo.2009.04.003, 2009.

Dunne, J., Elmore, D. and Muzikar, P.: Scaling factors for the rates of production of cosmogenic nuclides for geometric shielding and attenuation at depth on sloped surfaces, Geomorphology, 27, 3–11, doi:10.1016/S0169-555X(98)00086-5, 1999.

Eppes, M. C., Magi, B., Hallet, B., Delmelle, E., Mackenzie-Helnwein, P., Warren, K. and Swami, S.: Deciphering the role of solar-induced thermal stresses in rock weathering, Bull. Geol. Soc. Am., 128, 1315–1338, doi:10.1130/B31422.1,

2016.
Fu, P. and Rich, P. M.: A geometric solar radiation model with applications in agriculture and forestry, Comput. Electron. Agric., 37, 25–35, doi:10.1016/S0168-1699(02)00115-1, 2002.
Girard, L., Gruber, S., Weber, S. and Beutel, J.: Environmental controls of frost cracking revealed through in situ acoustic emission measurements in steep bedrock, Geophys. Res. Lett., 40, 1748–1753, doi:10.1002/grl.50384, 2013.
Gobiet, A., Kotlarski, S., Beniston, M., Heinrich, G., Rajczak, J. and Stoffel, M.: 21st century climate change in the European Alps-A review, Sci. Total Environ., 493, 1138–1151, doi:10.1016/j.scitotenv.2013.07.050, 2014.
Gosse, J. C. and Phillips, F. M.: Terrestrial in situ cosmogenic nuclides: Theory and application, Quat. Sci. Rev., 20, 1475–1560, doi:10.1111/j.1755-0998.2010.02842.x, 2001.
Grämiger, L. M., Moore, J. R., Gischig, V. S., Ivy-Ochs, S. and Loew, S.: Beyond debuttressing: Mechanics of paraglacial rock slope damage during repeat glacial cycles, J. Geophys. Res. Earth Surf., 122, 1004–1036, doi:10.1002/2016JF003967, 2017.
Gruber, S. and Haeberli, W.: Permafrost in steep bedrock slopes and its temperatures-related destabilization following climate change, J. Geophys. Res. Earth Surf., 112, 1–10, doi:10.1029/2006JF000547, 2007.
Gruber, S., Hoelzle, M. and Haeberli, W.: Permafrost thaw and destabilization of Alpine rock walls in the hot summer of 2003, Geophys. Res. Lett., 31, 1–4, doi:10.1029/2004GL020051, 2004a.
Gruber, S., Hoelzle, M. and Haeberli, W.: Rock-wall temperatures in the Alps: Modelling their topographic distribution and regional differences, Permafr. Periglac. Process., 15, 299–307, doi:10.1002/ppp.501, 2004b.
Günzler-Seifert, H. and Wyss, R.: Erläuterungen zum Kartenblatt Grindelwald, Geol. Kommision der schweiz. Naturforsch. Gesellschaft, 1938.
Haberkorn, A., Hoelzle, M., Phillips, M. and Kenner, R.: Snow as a driving factor of rock surface temperatures in steep rough rock walls, Cold Reg. Sci. Technol., 118, 64–75, doi:10.1016/j.coldregions.2015.06.013, 2015.
Haeberli, W., Wegmann, M. and Mühll, D. V.: Slope stability problems related to glacier shrinkage and permafrost degradation in the Alps, Eclogae Geol. Helv., 90, 407–414, 1997.
Hales, T. C. and Roering, J. J.: Climatic controls on frost cracking and implications for the evolution of bedrock landscapes, J. Geophys. Res. Earth Surf., 112, 1–14, doi:10.1029/2006JF000616, 2007.
Hales, T. C. and Roering, J. J.: A frost “buzzsaw” mechanism for erosion of the eastern Southern Alps, New Zealand, Geomorphology, 107, 241–253, doi:10.1016/j.geomorph.2008.12.012, 2009.
Hallet, B., Walder, J. S. and Stubbs, C. W.: Weathering by segregation ice growth in microcracks at sustained subzero temperatures: Verification from an experimental study using acoustic emissions, Permafr. Periglac. Process., 2, 283–300, doi:10.1002/ppp.3430020404, 1991.
Harris, C., Haeberli, W., Vonder Mühll, D. and King, L.: Permafrost monitoring in the high mountains of Europe: the PACE Project in its global context, Permafr. Periglac. Process., 12, 3–11, doi:10.1002/ppp.377, 2001.
Heisinger, B., Lal, D., Jull, A. J. T., Kubik, P., Ivy-Ochs, S., Neumaier, S., Knie, K., Lazarev, V. and Nolte, E.: Production

of selected cosmogenic radionuclides by muons: 1. Fast muons, Earth Planet. Sci. Lett., 200, 345–355, doi:10.1016/S0012-821X(02)00640-4, 2002a.

Heisinger, B., Lal, D., Jull, A. J. T., Kubik, P., Ivy-Ochs, S., Knie, K. and Nolte, E.: Production of selected cosmogenic radionuclides by muons: 2. Capture of negative muons, Earth Planet. Sci. Lett., 200, 357–369, doi:10.1016/S0012-821X(02)00641-6, 2002b.

Herwegh, M., Berger, A., Baumberger, R., Wehrens, P. and Kissling, E.: Large-Scale Crustal-Block-Extrusion During Late Alpine Collision, Sci. Rep., 7, 1–10, doi:10.1038/s41598-017-00440-0, 2017.

Hidy, A. J., Gosse, J. C., Pederson, J. L., Mattern, J. P. and Finkel, R. C.: A geologically constrained Monte Carlo approach to modeling exposure ages from profiles of cosmogenic nuclides: An example from Lees Ferry, Arizona, Geochemistry, Geophys. Geosystems, 11, doi:10.1029/2010GC003084, 2010.

Ivy-Ochs, S., Kerschner, H., Maisch, M., Christl, M., Kubik, P. W. and Schlüchter, C.: Latest Pleistocene and Holocene glacier variations in the European Alps, Quat. Sci. Rev., 28, 2137–2149, doi:10.1016/j.quascirev.2009.03.009, 2009.

Kelly, M. A., Buoncristiani, J. F. and Schlüchter, C.: A reconstruction of the last glacial maximum (LGM) ice-surface geometry in the western Swiss Alps and contiguous Alpine regions in Italy and France, Eclogae Geol. Helv., 97, 57–75, doi:10.1007/s00015-004-1109-6, 2004.

Krautblatter, M. and Moore, J. R.: Rock slope instability and erosion: Toward improved process understanding, Earth Surf. Process. Landforms, 39, 1273–1278, doi:10.1002/esp.3578, 2014.

Krautblatter, M., Moser, M., Schrott, L., Wolf, J. and Morche, D.: Significance of rockfall magnitude and carbonate dissolution for rock slope erosion and geomorphic work on Alpine limestone cliffs (Reintal, German Alps), Geomorphology, 167–168, 21–34, doi:10.1016/j.geomorph.2012.04.007, 2012.

Krautblatter, M., Funk, D. and Günzel, F. K.: Why permafrost rocks become unstable: A rock-ice-mechanical model in time and space, Earth Surf. Process. Landforms, 38, 876–887, doi:10.1002/esp.3374, 2013.

Lal, D.: Cosmic ray labeling of erosion surfaces: in situ nuclide production rates and erosion models, Earth Planet. Sci. Lett., 104, 424–439, doi:10.1016/0012-821X(91)90220-C, 1991.

Mair, D., Lechmann, A., Herwegh, M., Nibourel, L. and Schlunegger, F.: Linking Alpine deformation in the Aar Massif basement and its cover units - The case of the Jungfrau-Eiger mountains (Central Alps, Switzerland), Solid Earth, 9, 1099–1122, doi:10.5194/se-9-1099-2018, 2018.

Mair, D., Lechmann, A., Yesilyurt, S., Tikhomirov, D., Delunel, R., Vockenhuber, C., Akçar, N. and Schlunegger, F.: Fast long-term denudation rate of steep alpine headwalls inferred from cosmogenic 36Cl depth profiles, Sci. Rep., 9, 11023, doi:10.1038/s41598-019-46969-0, 2019.

Marrero, S. M., Phillips, F. M., Borchers, B., Lifton, N., Aumer, R. and Balco, G.: Cosmogenic nuclide systematics and the CRONUScalc program, Quat. Geochronol., 31, 160–187, doi:10.1016/j.quageo.2015.09.005, 2016.

Matsuoka, N.: The rate of bedrock weathering by frost action: Field measurements and a predictive model, Earth Surf. Process. Landforms, 15, 73–90, doi:10.1002/esp.3290150108, 1990.

Matsuoka, N.: Microgelivation versus macrogelivation: towards bridging the gap between laboratory and field frost weathering, Permafr. Periglac. Process., 12, 299–313, doi:10.1002/ppp.393, 2001.

Matsuoka, N.: Frost weathering and rockwall erosion in the southeastern Swiss Alps: Long-term (1994-2006) observations, Geomorphology, 99, 353–368, doi:10.1016/j.geomorph.2007.11.013, 2008.

Matsuoka, N. and Murton, J.: Frost weathering: recent advances and future directions, Permafr. Periglac. Process., 19, 195–210, doi:10.1002/ppp.620, 2008.

McColl, S. T.: Paraglacial rock-slope stability, Geomorphology, 153–154, 1–16, doi:10.1016/j.geomorph.2012.02.015, 2012.

McColl, S. T. and Draebing, D.: Rock Slope Instability in the Proglacial Zone: State of the Art, , 119–141, doi:10.1007/978-3-319-94184-4_8, 2019.

Moore, J. R., Sanders, J. W., Dietrich, W. E. and Glaser, S. D.: Influence of rock mass strength on the erosion rate of alpine cliffs, Earth Surf. Process. Landforms, 34, 1339–1352, doi:10.1002/esp.1821, 2009.

Murton, J. B., Peterson, R. and Ozouf, J. C.: Bedrock fracture by ice segregation in cold regions, Science (80-.)., 314, 1127–1129, doi:10.1126/science.1132127, 2006.

Murton, J. B., Ozouf, J. C. and Peterson, R.: Heave, settlement and fracture of chalk during physical modelling experiments with temperature cycling above and below 0 °C, Geomorphology, 270, 71–87, doi:10.1016/j.geomorph.2016.07.016, 2016.

Noetzli, J., Gruber, S., Kohl, T., Salzmann, N. and Haeberli, W.: Three-dimensional distribution and evolution of permafrost temperatures in idealized high-mountain topography, J. Geophys. Res., 112, F02S13, doi:10.1029/2006JF000545, 2007.

PERMOS 2019. PERMOS Database. Swiss Permafrost Monitoring Network, Fribourg and Davos, Switzerland. DOI:10.13093/permos-2019-01.

Rapp, A.: Recent Development of Mountain Slopes in Kärkevagge and Surroundings, Northern Scandinavia, Geogr. Ann., 42, 65, doi:10.2307/520126, 1960.

Rempel, A. W., Marshall, J. A. and Roering, J. J.: Modeling relative frost weathering rates at geomorphic scales, Earth Planet. Sci. Lett., 453, 87–95, doi:10.1016/j.epsl.2016.08.019, 2016.

Rode, M., Schnepfleitner, H. and Sass, O.: Simulation of moisture content in alpine rockwalls during freeze–thaw events, Earth Surf. Process. Landforms, 41, 1937–1950, doi:10.1002/esp.3961, 2016.

Sanders, J. W., Cuffey, K. M., Moore, J. R., MacGregor, K. R. and Kavanaugh, J. L.: Periglacial weathering and headwall erosion in cirque glacier bergschrunds, Geology, 40, 779–782, doi:10.1130/G33330.1, 2012.

Sass, O.: Rock moisture measurements: Techniques, results, and implications for weathering, Earth Surf. Process. Landforms, 30, 359–374, doi:10.1002/esp.1214, 2005.

Sass, O. and Wollny, K.: Investigations regarding Alpine talus slopes using ground-penetrating radar (GPR) in the Bavarian Alps, Germany, Earth Surf. Process. Landforms, 26, 1071–1086, doi:10.1002/esp.254, 2001.

Savi, S., Delunel, R. and Schlunegger, F.: Efficiency of frost-cracking processes through space and time: An example from the eastern Italian Alps, Geomorphology, 232, 248–260, doi:10.1016/j.geomorph.2015.01.009, 2015.

Schlunegger, F. and Norton, K. P.: Water versus ice: The competing roles of modern climate and Pleistocene glacial erosion in the Central Alps of Switzerland, Tectonophysics, 602, 370–381, doi:10.1016/j.tecto.2013.03.027, 2013.

Stone, J. O.: Air pressure and cosmogenic isotope production, J. Geophys. Res. Solid Earth, 105, 23753–23759, doi:10.1029/2000JB900181, 2000.

Terzaghi, K.: Stability of Steep Slopes on Hard Unweathered Rock, Géotechnique, 12, 251–270, doi:10.1680/geot.1962.12.4.251, 1962.

Viles, H. A.: Linking weathering and rock slope instability: Non-linear perspectives, Earth Surf. Process. Landforms, 38, 62–70, doi:10.1002/esp.3294, 2013.

Vollmer, F. W.: C program for automatic contouring of spherical orientation data using a modified Kamb method, Comput. Geosci., 21, 31–49, doi:10.1016/0098-3004(94)00058-3, 1995.

Vollmer, F. W.: Orient 3: A new integrated software program for orientation data analysis, kinematic analysis, spherical projections, and Schmidt plots, Abstr. with Programs - Geol. Soc. Am., 47, 49 [online] Available from: http://login.ezproxy.library.ualberta.ca/login?url=http://search.ebscohost.com/login.aspx?direct=true&db=geh&AN=2016-009202&site=ehost-live&scope=site, 2015.

Walder, J. S. and Hallet, B.: Geological Society of America Bulletin A theoretical model of the fracture of rock during freezin, GSA Bull., 96, 336–346, doi:10.1130/0016-7606(1985)96<336, 1985.

Walder, J. S. and Hallet, B.: The Physical Basis of Frost Weathering: Toward a More Fundamental and Unified Perspective, Arct. Alp. Res., 18, 27, doi:10.2307/1551211, 1986.

Wehrens, P., Baumberger, R., Berger, A. and Herwegh, M.: How is strain localized in a meta-granitoid, mid-crustal basement section? Spatial distribution of deformation in the central Aar massif (Switzerland), J. Struct. Geol., 94, 47–67, doi:10.1016/j.jsg.2016.11.004, 2017.

Wirsig, C., Zasadni, J., Ivy-Ochs, S., Christl, M., Kober, F. and Schlüchter, C.: A deglaciation model of the Oberhasli, Switzerland, J. Quat. Sci., 31, 46–59, doi:10.1002/jqs.2831, 2016a.

Wirsig, C., Zasadni, J., Christl, M., Akçar, N. and Ivy-Ochs, S.: Dating the onset of LGM ice surface lowering in the High Alps, Quat. Sci. Rev., 143, 37–50, doi:10.1016/j.quascirev.2016.05.001, 2016b.

Figures

985

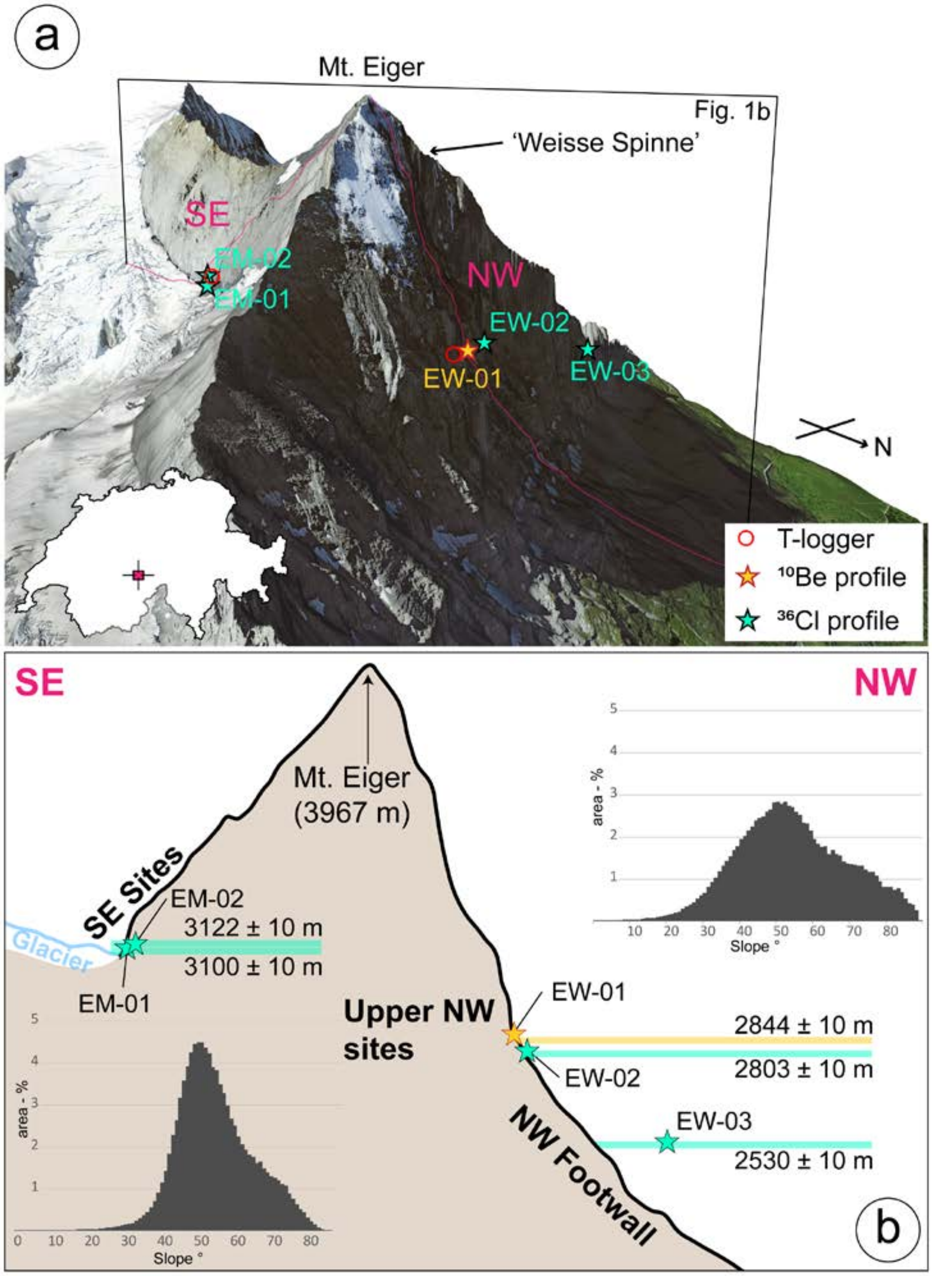

Figure 1: Mt. Eiger in the Central Swiss Alps (insert) is characterized by steep SE and NW rockwalls (a); Sites for denudation rate estimations with cosmogenic nuclides and temperature loggers from Gruber et al. (2004b) are indicated. (b) Schematic section along trace highlighted in panel (a); Cosmogenic sampling sites (stars) are projected into the section, and elevation of sample sites are also indicated. The area used for slope angle distribution is indicated in Fig. 2b.

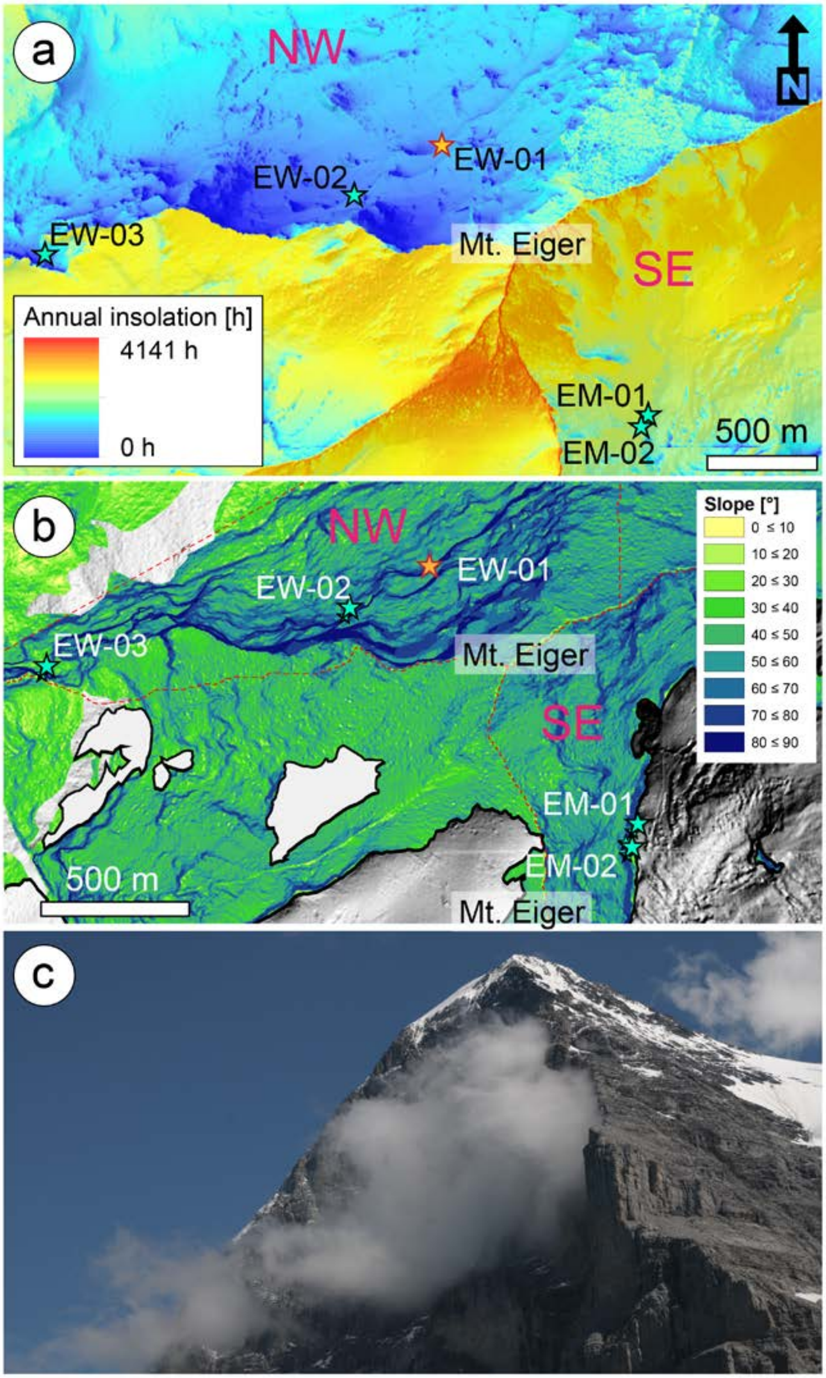

Figure 2: Differences in local temperature conditions between the NW and the SE face. (a) Potential annual solar insolation in hours over a year (2015), calculated using the hemispherical viewshed algorithm included in ESRIs ArcGIS^{TM} (Fu and Rich, 2002). (b) Slope angle map calculated from a high-resolution DEM (Swiss Alti3D 2m, 2015; provided by the Federal office of topography, swisstopo) for the NW and SE of Mt. Eiger. (c) Field photograph of the NW wall, taken in the summer of 2017 AD, with local clouds illustrating the potential difference in microclimatic conditions.

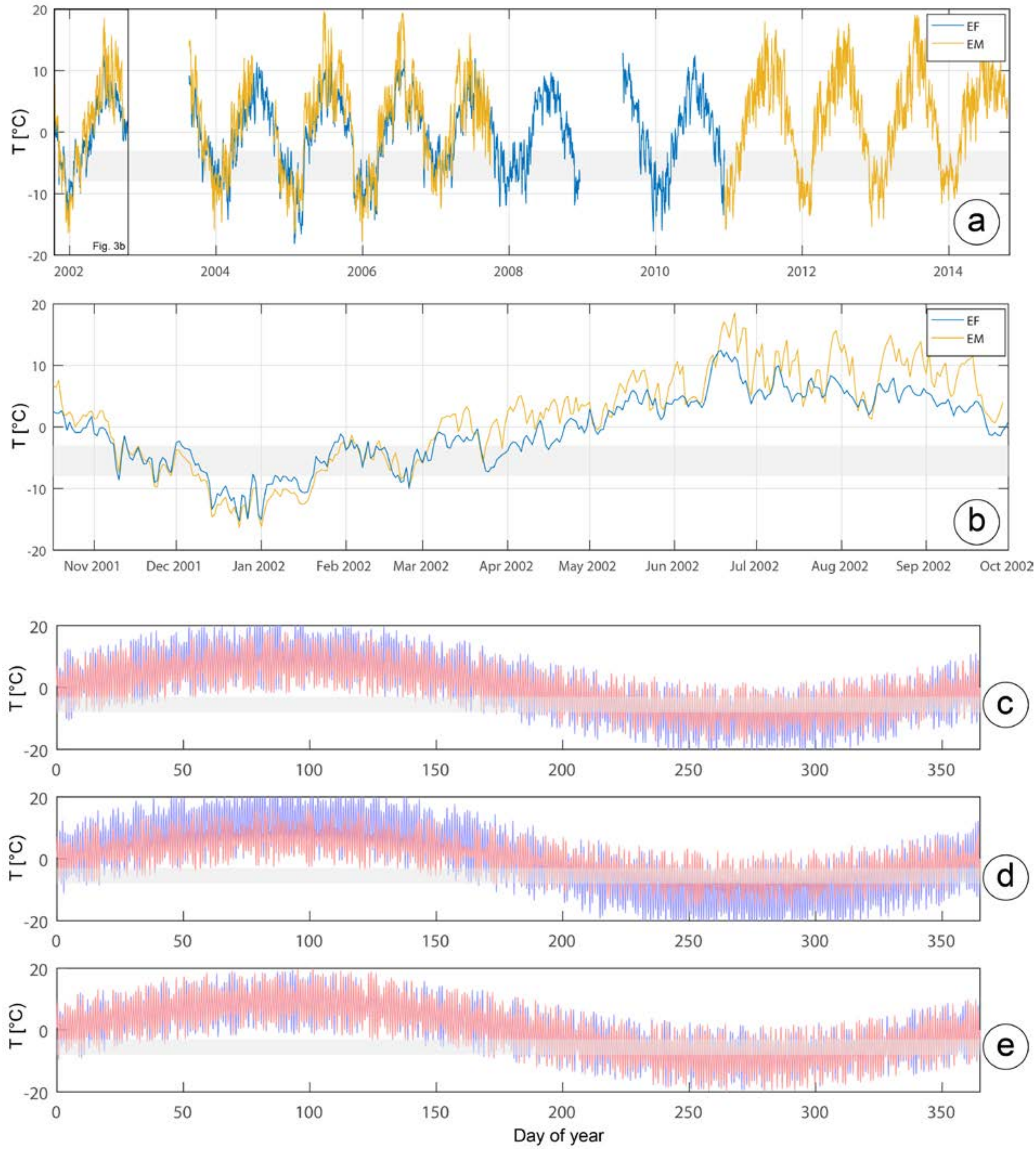

Figure 3: (a) Complete daily averaged PERMOS (2019) temperature data for the upper NW (EF) and the SE sites (EM). (b) Daily averaged hydrological year 2002, which were used in this study ~~for the study~~ to estimate $\boldsymbol{dT_a}$ and $\boldsymbol{dT_d}$. For modern min, mean and max estimations only complete years were used. Synthetic temperature curves which were used for the frost cracking model for the upper NW (blue) and SE (red) sites for modern mean (c), modern minimum (d) and modern maximum conditions (e). Shaded area corresponds to the frost cracking window of -3 to -8 °C. See text for discussion.

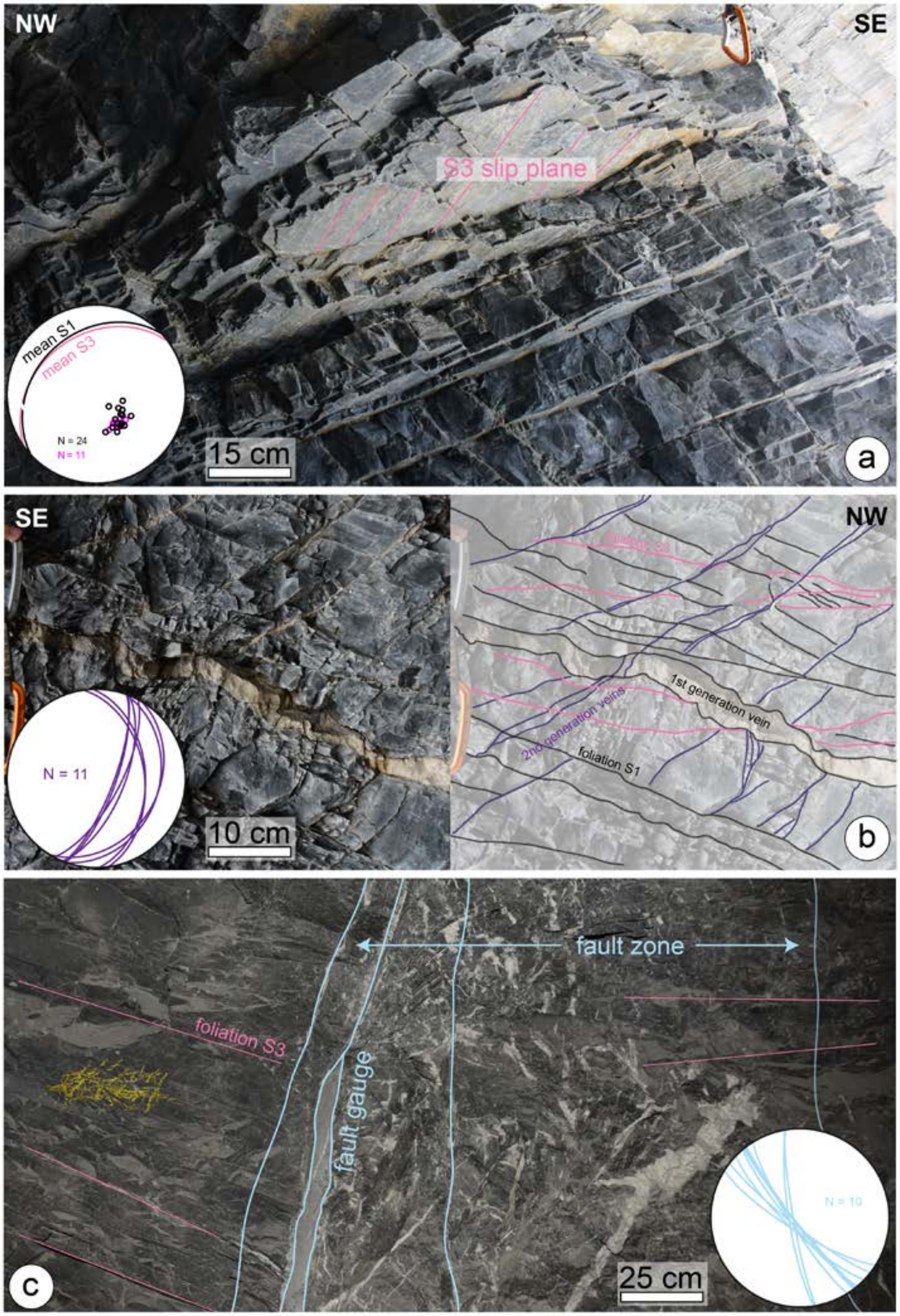

Figure 4: Bedrock fabric and discontinuity network at sample sites EM-01 and EM-02 at the SE sides. (a) Bedrock at current surface close to EM-01 highlighting the weathering paths along preexisting weaknesses. (b) Details of the bedrock fabric at site EM-02 with structural interpretation in the right panel. (c) Fault zone near the sampling sites that deeply penetrate the Eiger (based on Appendix image from Mair et al., 2018). Structural orientation data partly based on Mair et al. (2018).

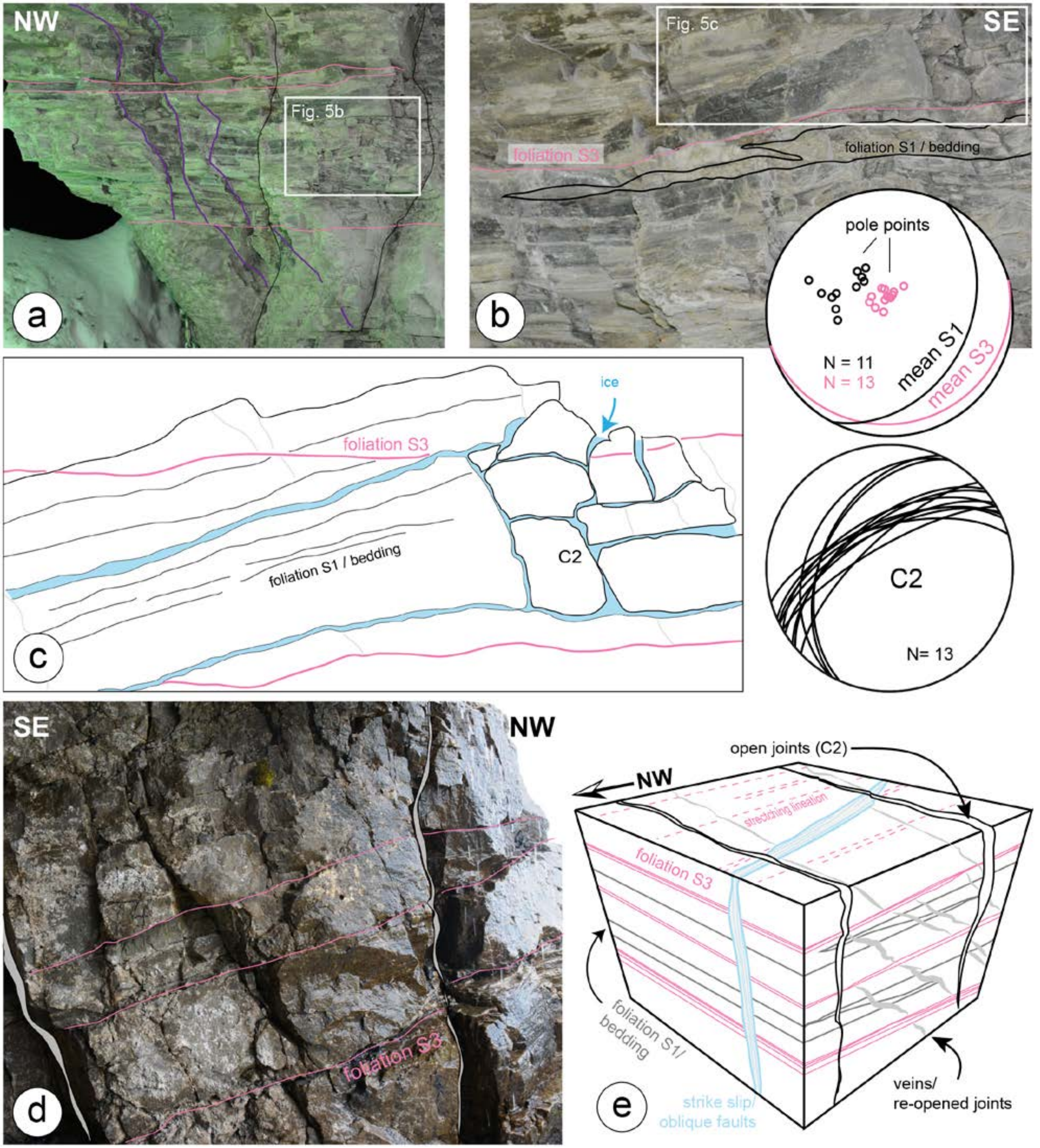

1010 **Figure 5:** Bedrock fabric from cosmogenic sites within the NW face, at site EW-02 (a). (b,c) Details with ice lenses present during sampling on Dec. 1st 2016 AD, highlighting the relation of fractures with the pre-existing structures. (d) Structures at sampling sites EW-01. (e) Bedrock discontinuities relevant for bedrock fracturing, synthesized for the NW ~~headwall~~rockwall.

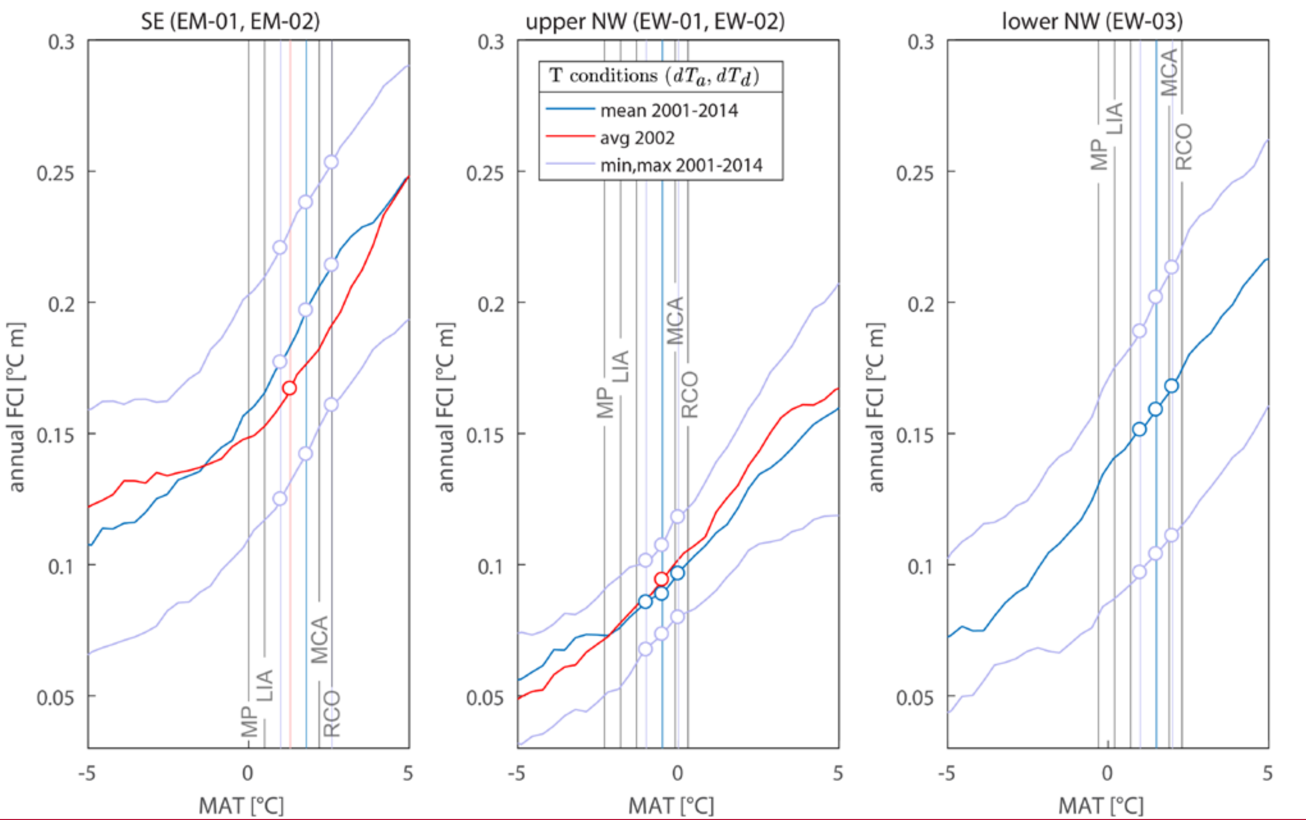

Figure 6: Modelled annual frost cracking intensity ($\overline{\boldsymbol{FCI}}$) for the individual sites and the different thermal regimes. For the site-specific model run conditions (min, max, mean and 2002) see Table 1 and Section 3.2. Resulting $\overline{\boldsymbol{FCI}}$ values for the indicated circles are presented in Table 4. MAT = mean annual temperature, LIA = little ice age, MCA = medieval climate optimum, MP = migration period, Roman climatic optimum.~~.~~

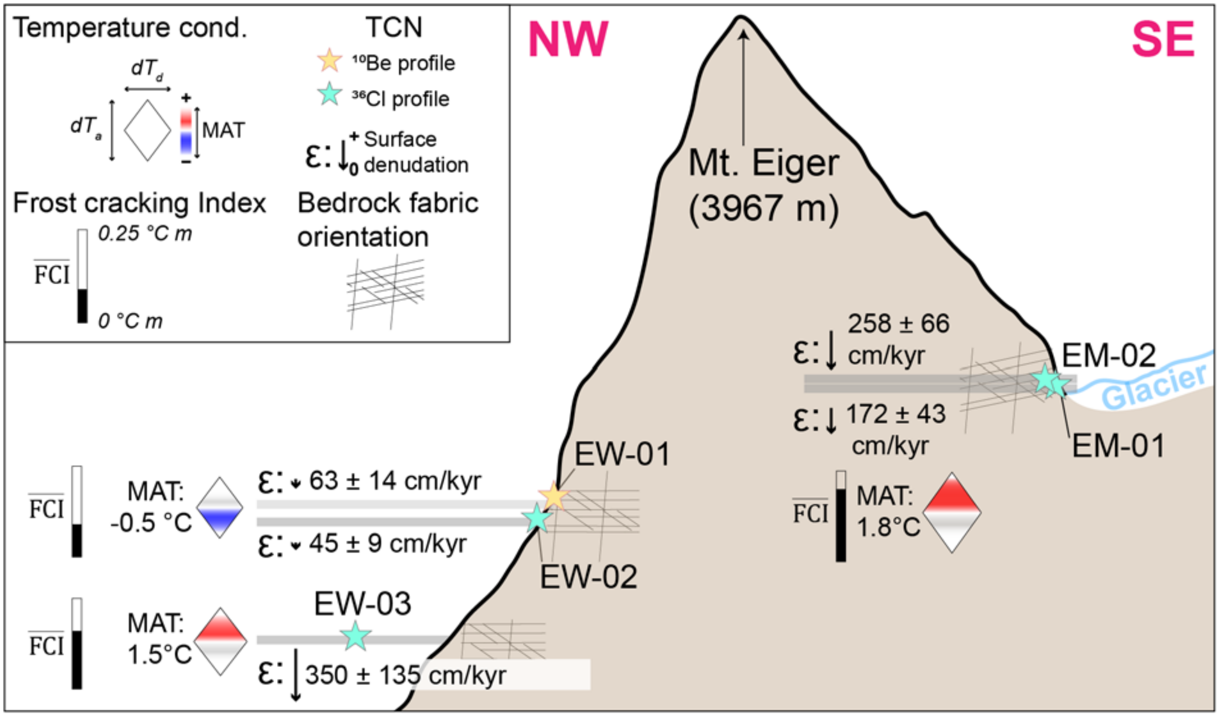

Figure 7~~8~~: Schematic section (for trace see Fig. 1) with main findings~~ indicated~~. MAT = mean annual temperature, $\boldsymbol{\overline{FCI}}$ = annual frost cracking intensity index, ε = denudation rate. $\boldsymbol{\overline{FCI}}$ symbols represent mean modern temperature conditions (Table 4), MAT symbols represent mean modern temperature conditions color-coded with symbol size representing mean annual, diurnal amplitude (Table 1); see text for discussion.

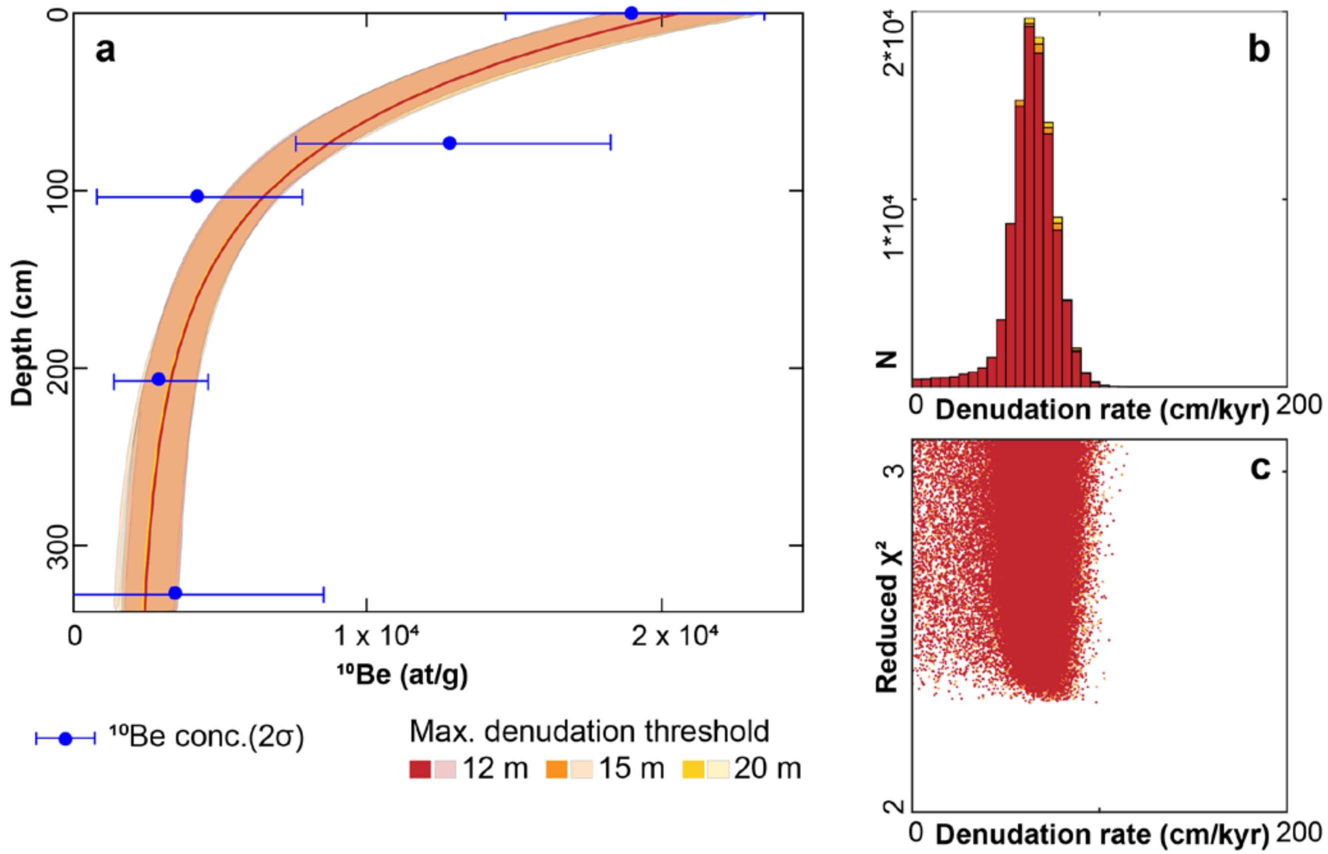

1025 **Figure A1:** ~~Results for~~Analysis of cosmogenic ^{10}Be ~~analysis~~ at site EW-01. (a) Measured ^{10}Be concentrations plotted against the Monte Carlo (MC) solution space (light colors) and the best-fit profiles. (b) Denudation rate histogram from the MC modelling for 10^5 model profiles and (c) ~~with~~ corresponding reduced chi-square (χ^2) values~~ showing (c)~~. Different model setup results are superimposed (for discussion see text).

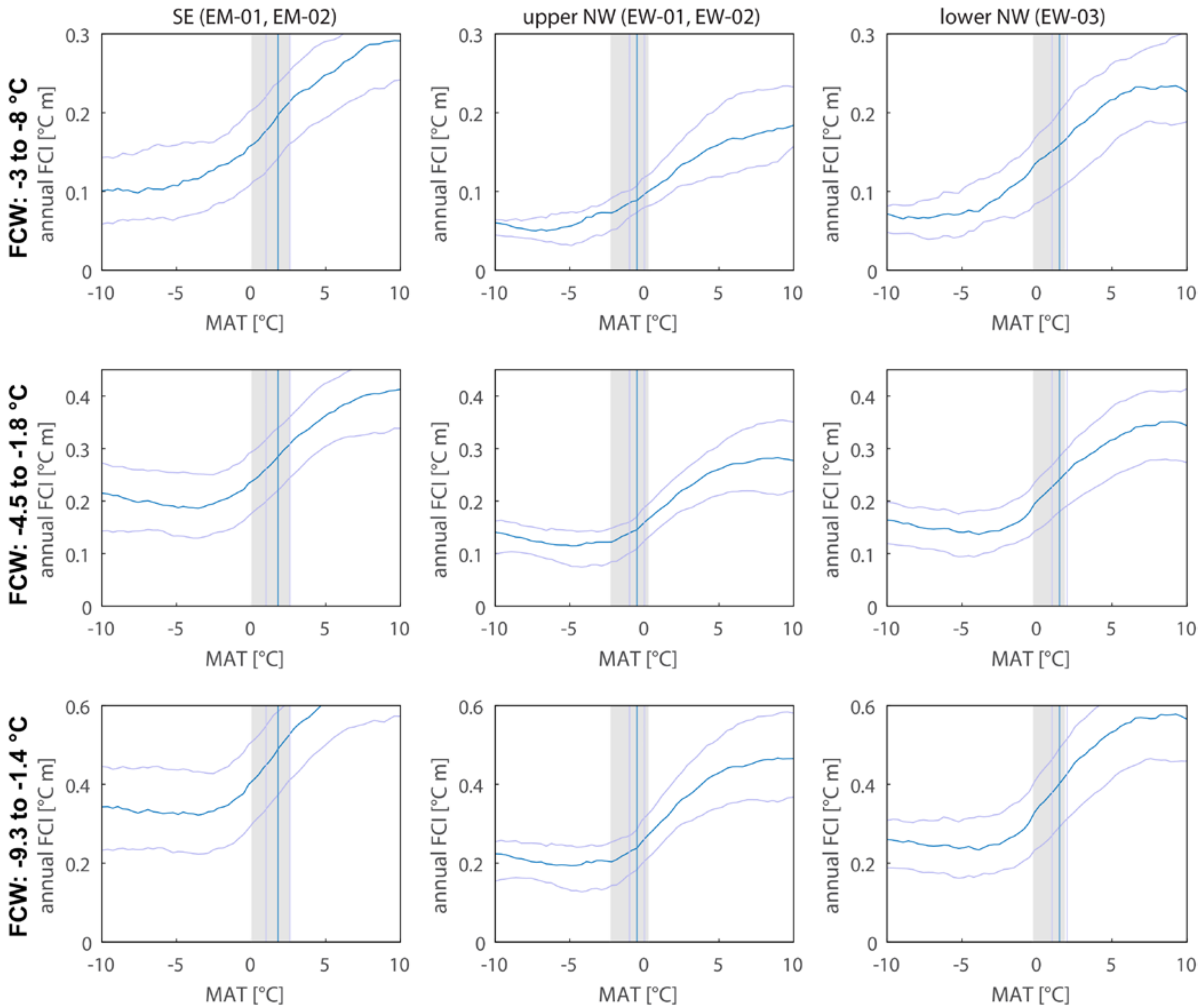

1030 **Figure B1:** $\overline{FCI}$ sensitivity to different frost cracking windows (FCW) for the frost cracking model, with standard model inputs from Andersen et al. (2015) in the upper row, and two windows from Draebing et al. (2017b) in the middle and lower row, respectively. These are dependent on the mechanical bedrock properties and were originally calculated for anisotropic slaty paragneisses. Shaded area corresponds to reconstructed historical temperature range; vertical bars indicate modern mean, min. and max. MAT conditions and curves represent the corresponding dT_a and dT_d conditions. Note the different y-axis scale for the $\overline{FCI}$ of each row.

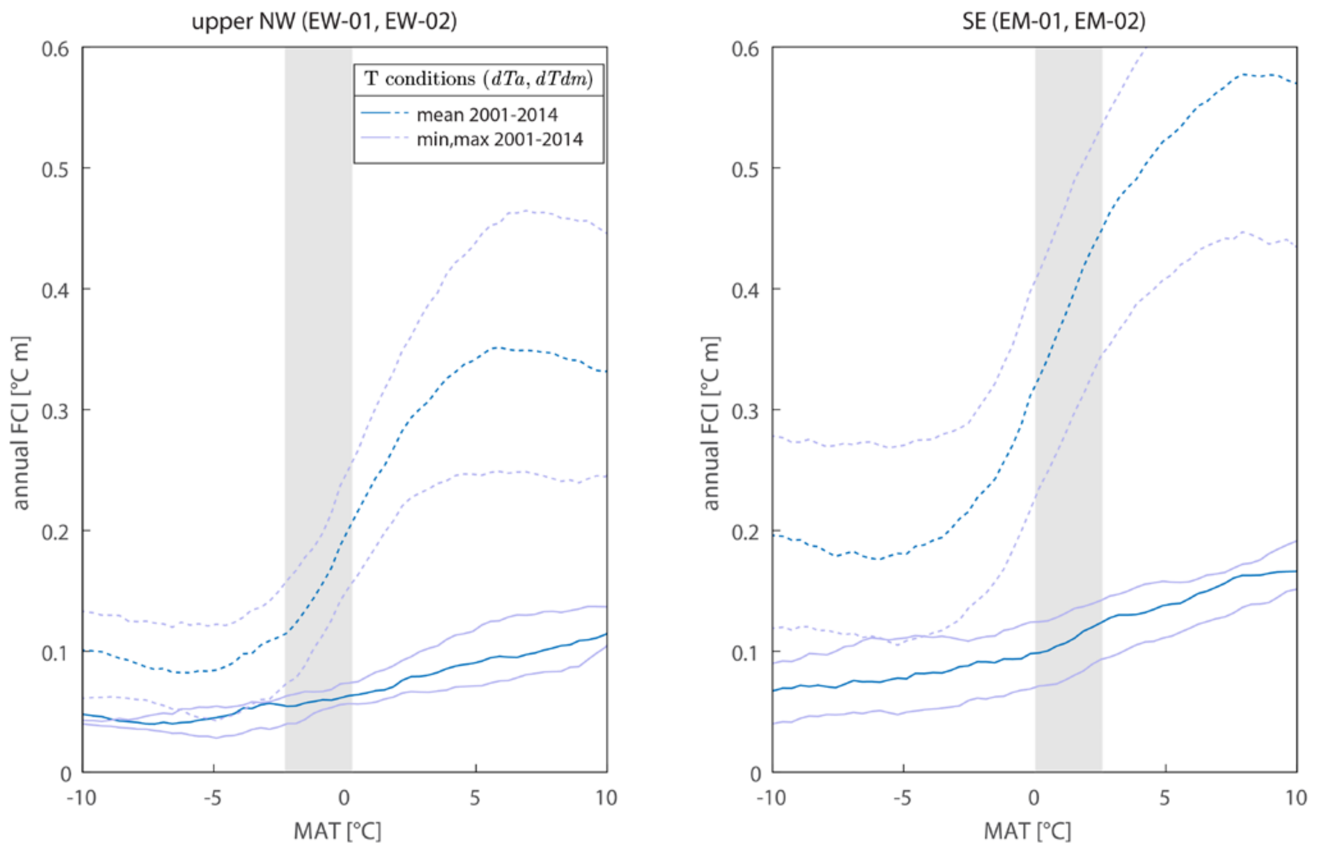

Figure B2: $\overline{\boldsymbol{FCI}}$ sensitivity to thermal conductivity of bedrock (kr). Modelled results for $\overline{\boldsymbol{FCI}}$ results with kr = 1.2 W m−1 K−1 (dashed lines) and kr = 6.5 W m−1 K−1 (solid lines), representing upper and lower thresholds for thermal conductivities compiled for various lithologies (Schön, 2015). Model set up to standard conditions of Andersen et al. (2015) for all other input variables. The shaded area corresponds to the reconstructed historic temperature range.

Tables

TCN Site	EW-01	EW-02	EW-03	EM-01	EM-02
Elevation [m]	2844	2803	2530	3100	3122
Slope [°]	50	53	83	75	75
Aspect [°]	370	298	7	96	111
Denudation rate [cm kyr^{-1}]	63~~.4~~ ± 14~~[3.5]~~[a]	45.4 ± ~~9[a]~~9[b]	350.1 ± 135~~[a]~~[b]	172.0 ± ~~43[a]~~43[b]	258 ± ~~66[a]~~66[b]

	Upper NW	Lower NW	SE
Temperature regime		**NGST 2002**	
MAT [° C]	-0.5	n/a	1.3
dT_a [° C]	8.1	n/a	10.3
dT_d [° C]	5.8	n/a	7.8
		NGST Present (2001 - 2014)	
MAT [° C]	-0.5 ± 0.5	(1.5 ± 0.5)[ǂ]	1.8 ± 0.8
dT_a [° C]	8.1 ± 1.3	(9.0 ± 1.5)[*]	10.7 ± 1.7
dT_d [° C]	6.1 ± 0.7	(7.0 ± 1)[*]	7.7 ± 0.9
		19th century AD	
MAT [° C]	-1.3	0.7	1.0
		LIA	
MAT [° C]	-1.8	0.2	0.5
		MCA	
MAT [° C]	-0.1	1.9	2.2
		Migration period	
MAT [° C]	-2.3	-0.3	0
		Roman climate optimum	
MAT [° C]	0.3	2.3	2.6

Table 1: Study site parameters and reconstructed temperature values. NGST sites from Gruber et al. (2004b); temperature data available at ~~**http://www.permos.ch/data.html**~~**http://www.permos.ch/data.html** (PERMOS 2019). For used record, see method section. [a] rate dependent on ^{10}Be blank correction (see Appendix A), ~~[a]~~ [b] data from Mair et al. (201~~8~~9), [ǂ] scaled from the Eigerfenster site (Gruber et al., 2004b), [*] values assumed (see section 3.2 for details). TCN = terrestrial cosmogenic nuclide, NGST = near ground surface temperatures at a depth of 10cm, LIA = little ice age, MCA = medieval climate optimum, MAT = mean annual temperature, $\boldsymbol{dT_a}$ = amplitude of annual temperature variation, $\boldsymbol{dT_d}$ = mean amplitude of diurnal variation; n/a = not available.

T regime	Model setups (dT_a and dT_d)	$\overline{FCI}$ min. MAT [°C m]	$\overline{FCI}$ mean MAT [°C m]	$\overline{FCI}$ max. MAT [°C m]	$\overline{FCI}$ 2002 MAT [°C m]
	Min 2001- 2014	0.12	0.14	0.16	n/a
SE	Mean 2001- 2014	0.18	0.20	0.21	0.17
	Max 2001- 2014	0.22	0.24	0.25	n/a
	Min 2001- 2014	0.07	0.07	0.08	n/a
NW	Mean 2001- 2014	0.09	0.09	0.10	0.09
	Max 2001- 2014	0.10	0.11	0.12	n/a
	Min 2001- 2014	0.10	0.10	0.11	n/a
Lower NW (EW-03)	Mean 2001- 2014	0.15	0.16	0.17	n/a
	Max 2001- 2014	0.19	0.20	0.21	n/a

Table 2~~5~~: Selected annually integrated frost cracking efficiencies ($\overline{FCI}$) for the studied temperature regimes, and the different model runs with the respective mean annual temperatures (MAT). T = temperature, n/a = not available.

Sample	Depth [cm]	Dissolved Qtz [g]	~~^{10}~~^{9}Be spike [mg]	^{10}Be/^{9}Be measured [10^{-14}]			^{10}Be measured concentration [10^{4} at/g]		
EW-01-1	0.0	50.01830	0.1991	7.39	±	0.8	1.90	±	0.21
EW-01-3	73.3	50.07070	0.1988	5.08	±	0.96	1.28	±	0.26
EW-01-4	103.5	44.37640	0.1988	1.66	±	0.56	0.42~~4.23~~	±	0.17
EW-01-5	207.0	50.12830	0.1991	1.35	±	0.27	0.29~~2.92~~	±	0.07
EW-01-6	327.8	50.20810	0.1990	1.56	±	0.9	0.35~~3.48~~	±	0.24

Table A1: Measured ^{10}Be/^{9}Be ratios and ^{10}Be concentrations for samples of depth profile EW-01. ^{10}Be concentrations were adjusted using a weighted long-term average blank ratio of 2.48 x 10^{-15}, amounting to corrections of between 3 and <19 % (see discussion in text).

Parameter	Value
Elevation [m]	2844
Latitude [degree]	46.58070
Longitude [degree]	8.00181
Slope [°]	50
Strike [°]	227.2
Shielding factor S_T	0.55
Cover correction	1
Reference production rate [at g^{-1} a^{-1}]	4.01
Local spall. production rate [at g^{-1} a^{-1}]	19.84 ± 1.98
Uncertainty of ^{10}Be half-life [%]	5
Depth of muon fit [m]	30
Density [g cm^{-3}]	2.68 ± 0.04
Error on muogenic production rate [%]	40
Apparent attenuation length $\Lambda_{f,e}$ [g cm^{-2}]	153.2 ± 15.3
χ^2 cut-off	3.09
Min. age [a]	0
Max. age [a]	75000
Min. denudation rate [cm kyr^{-1}]	0
Max. denudation rate [cm kyr^{-1}]	1500
Min. total denudation [cm]	0
Max. total denudation [cm]	1200, 1500, 2000
Min. ~~inheritance~~ inherited nuclides [at g^{-1}]	0
Max. inherited nuclides~~tance~~ [at g^{-1}]	19012

Table A2: Input parameters for the modified Monte Carlo (MC) simulation code of Hidy et al. (2010).

	Age [ka]	**ε [cm/kyr]**	**Inh. [10^3 at/g]**	**Age [ka]**	**ε [cm/kyr]**	**Inh. [10^3 at/g]**	**Age [ka]**	**ε [cm/kyr]**	**Inh. [10^3 at/g]**
	12 m max. denudation			15 m max. denudation			20 m max. denudation		
MEAN	9.3	63.4	2.6	11.6	64.0	2.5	15.4	64.7	2.4
STD	5.4	13.5	0.7	6.8	12.8	0.7	9.1	12.1	0.8
MEDIAN	9.0	64.3	2.6	11.3	64.6	2.6	15.1	65.0	2.4
MODE	1.1	64.3	3.0	1.2	63.0	3.0	1.2	62.8	2.0
Min	0.7	0.0	0.0	0.7	0.0	0.0	0.7	0.1	0.0
lowest χ^2	6.8	98.5	2.2	21.1	63.4	1.9	21.1	63.4	1.9
Max	29.9	114.9	4.5	37.3	113.3	4.7	54.3	114.9	4.9

Table A3: Result statistics for Monte Carlo (MC) depth profile modelling of profile EW-01.

Parameter	**Value**
Flow restriction in warm bedrock [m^{-1}]	2.0
Flow restriction in cold bedrock [m^{-1}]	4.0
Critical water volume [m]	0.04
Porosity bedrock	0.02
Basal heat flow [$W\ m^{-2}$]	0.05
Thermal conductivity water [$W\ m^{-1}\ K^{-1}$]	0.56
Thermal conductivity ice [$W\ m^{-1}\ K^{-1}$]	2.14
Thermal conductivity bedrock [$W\ m^{-1}\ K^{-1}$]	3.0
Volumetric heat capacity water [$kJm^{-3}\ K^{-1}$]	4210
Volumetric heat capacity ice [$kJm^{-3}\ K^{-1}$]	1879
Volumetric heat capacity bedrock [$kJm^{-3}\ K^{-1}$]	2094
Specific latent heat of water [$J\ kg^{-1}$]	333.6
Density of water [$kg\ m^{-3}$]	1000

Table B1: Model parameters for the frost cracking model of Andersen et al. (2015) used and not already given in Section 3 of the main text.